Negative Feedback and Competition in the Yeast Polarity Establishment Circuit

by

Chi-Fang Wu

University Program in Genetics and Genomics
Duke University

Date:_____

Approved:

_____
Daniel Lew, Supervisor

_____
Patrick Brennwald

_____
Steve Haase

_____
David Sherwood

_____
Raphael Valdivia

Dissertation submitted in partial fulfillment of
the requirements for the degree of Doctor
of Philosophy in the University Program in
Genetics and Genomics
of Duke University

2013

ABSTRACT

Negative Feedback and Competition in the Yeast Polarity Establishment Circuit

by

Chi-Fang Wu

University Program in Genetics and Genomics
Duke University

Date:_____

Approved:

_____
Daniel Lew, Supervisor

_____
Patrick Brennwald

_____
Steve Haase

_____
David Sherwood

_____
Raphael Valdivia

An abstract of a dissertation submitted in partial
fulfillment of the requirements for the degree
of Doctor of Philosophy in the University Program in
Genetics and Genomics of
Duke University

2013

Abstract

Many cells spontaneously establish a polarity axis even in the absence of directional cues, a process called symmetry breaking. A central question concerns how cells polarize towards one, and only one, randomly oriented "front". The conserved Rho-type GTPase Cdc42p is an essential factor for both directed and spontaneous polarization in various organisms, whose local activation is thought to define the cell's front. We previously proposed that in yeast cells, a small stochastic cluster of GTP-Cdc42p at a random site on the cortex can grow into a large, dominating cluster via a positive feedback loop involving the scaffold protein Bem1p. As stochastic Cdc42p clusters could presumably arise at many sites, why does only one site become the dominating "front"? We speculated that competition between growing clusters for limiting factors would lead to growth of a single winning "front" at the expense of the others. Utilizing time-lapse imaging with high spatiotemporal resolution, we now document initiation of multiple polarized clusters that competed rapidly to resolve a winning cluster. Such multicluster intermediates are observed in wild-type yeast cells with functional directional cues, but the locations where they are initiated are biased by the spatial cues. In addition, we detected an unexpected oscillatory polarization in a majority of the cells breaking symmetry, in which polarity factors initially concentrated very brightly and then dimmed in an oscillatory manner, dampening down to a final intermediate level after 2-3 peaks. Dampened oscillation suggests that the polarity circuit contains an in-built negative

feedback loop. Mathematical modeling predicts that negative feedback would confer robustness to the polarity circuit and make the kinetics of competition between polarity factor clusters relatively insensitive to polarity factor concentration.

We are trying to understand how competition between clusters occurs. We find that the yeast guanine-nucleotide dissociation inhibitor (GDI), Rdi1p, is needed for rapid competition between clusters. In the absence of Rdi1p the initial clustering of polarity factors is slowed, and competition is also much slower: in some cases cells still have two clusters at the time of bud emergence and they form two buds. We suggest that in the absence of Rdi1p, the clusters compete for a limiting pool of Cdc42p, and that slow exchange of Cdc42p on and off the membrane in *rdi1Δ* cells leads to slow competition.

Contents

List of Tables

List of Figures

Acknowledgements

Joining the Lew lab and being mentored by Danny was one of the best choices I've ever made. Five year ago, my fear of being thousand miles away from family and friends were overcome by my passion on research, driving me to pursue my graduate study in the US. At that time, I was a master graduate with some experimental skills, but not with well-trained brains. I was hoping to meet a mentor who could teach me how to ask good questions and think critically. Danny has been the one who helped me grow academically and shaped who I am today. He could patiently spend hours answering my questions or explaining a concept to me. He could always immediately point out the flaw of my thinking process and at the same time challenge me to come up with caveats or alternative hypotheses. He has spent efforts polishing my writings and presentations, teaching me the clear and effective ways to tell a story. Being a stutterer, I've been struggling to communicate with people in a language I'm not familiar with. I feel very grateful that Danny gave me enormous encouragement and support throughout these years and always have faith in me. If it were not for him, I would have quitted science few years ago. He is the mentor and scientist I will respect forever.

I would like to thank Audrey Howell, who is like my big sister in science. Everything I know about live-cell microscopy was generously taught by her. She gave me precious advice to deal with the ups and downs in graduate school and still cares about

me till today. I would like to thank our awesome technicians, Trevin Zyla and Michelle Jin, who helped me tremendously on cloning and strain construction. I would not have gone this far on my projects without their assistance. I would like to thank two great modelers, Meng Jin and Natasha Savage. Their collaborative works strengthened my stories and constantly provided me with new directions on my projects. I would like to thank my committee members, Patrick Brennwald, Steve Haase, David Sherwood and Raphael Valdivia, who always gave me constructive suggestions and perspectives which helped me improve my projects greatly. I would like to thank Sam Johnson and Yasheng Gao from Duke Light Microscopy Core Facility for their technical support all these years.

I'm so lucky to have a group of dear Taiwanese friends in Durham, especially Yi-Shan, Ming-Shan, Linda, Chia-Yu, Nai-Jia and Ming-Feng. Life is much more interesting and full of laughter with their company. I would like to thank my volleyball teammates. Every practice and every game with them have become the highlights of the past five years. I would like to thank my best friends of all times, Yu-Lun and Su-Ya, who are far away in Taiwan. They have more confidence in me than I do and the warm words they sent me had the magic power to cheer me up instantly.

Last but not least, I have the best parents in the world. No one will ever know me better than they do. Even though they really wanted to persuade me to stay in Taiwan, they respected and supported my dreams, letting me pursue my graduate study on the other side of the earth. During the dark time when I thought of quitting graduate school, it was them who encouraged me to keep trying because they deeply knew that I would

regret if I did so. I feel so thankful of their insistence and would like to dedicate this thesis work to them.

1. Introduction

Establishing an axis of polarity is of fundamental importance of many aspects of cell and developmental biology in various cell types, ranging from chemotaxis of neutrophils, generation of specialized functional domains in differentiated epithelial cells, to proliferation of budding yeast. In most cases, polarized cells usually establish a "front" and a "back." In order for the front of the cell to be functional, it needs to be the only one. That is, the cell must ensure that only a single polarity axis is established (here referred to as singularity). There are usually spatial cues, either extrinsic (e.g. chemotaxing cells) or intrinsic (e.g. budding yeast), in place to determine where the front will be. However, in the absence of all apparent spatial cues, many cells are still capable of establishing a single axis of polarity through a process called symmetry breaking (Wedlich-Soldner and Li, 2003). The ability of cells to break symmetry and maintain singularity indicates that there is a core polarization mechanism in cells that can be biased by spatial cues. Unraveling the intrinsic mechanism for spontaneous polarization can help us to understand the fundamental of cellular morphogenesis.

1.1 Establishing cell polarity

1.1.1 Theoretical models for polarity establishment

Cell polarization has been widely documented, but the underlying mechanisms are not well understood. How do cells transition from a non-polarized state with

homogeneous distribution of polarity factors to a polarized state with asymmetric protein distribution? Theorists have proposed a number of potential models to address this question. One of the most influential models that predicted pattern formation in biological system was first proposed by Alan Turing in 1952 (Turing, 1952) and later elaborated by Gierer and Meinhardt (Gierer and Meinhardt, 1972; Meinhardt and Gierer, 1974). In Turing's model, the first key assumption that leads to spontaneous pattern formation is the production of an activator is autocatalytic. The activator starts with a homogeneous steady state but it is not stable. Any slight local but not uniform deviation from the steady state could be amplified by autocatalysis and induce pattern formation. However, if such amplification process keeps going on (assuming there are sufficient reservoirs of activators), eventually the cluster will grow too large or overwhelm the entire field. An antagonizing process, therefore, is needed to restrict the local activating process. Based on Turing's equations, the activator not only catalyzes its own production but also triggers the production of the inhibitor. The second key assumption is that the diffusion of the inhibitor is faster than the activator. Due to its fast diffusion, the inhibitor diffuses away from the activator peak, so the peak will decrease a little bit but is not completely destroyed by the inhibitor. Therefore, a small local elevation of the activator will grow further, leading to a polarized state. The basic concepts in the Gierer-Meinhardt model are similar to the Turing model, but the key features of local autocatalysis and lateral inhibition (long-ranging inhibition) are further formulated. The activator has a nonlinear positive feedback on its own production, which is required to generate a stable steady state. The lateral inhibition is achieved by either the production of an inhibitor

triggered by the activator or the depletion of a fast-diffusing substrate, which is consumed by the activation process. As mentioned above, lateral inhibition will not destroy the activation peak; however, the activator in the vicinity of the peak will be antagonized by lateral inhibition, thereby preventing the formation of a second peak. If the size of a given field exceeds the range of inhibitor, a second peak of high activator concentration can occur. In some cases of pattern formation, a new activation peak will arise at a distance of the initial activating area and eventually forms periodic or regularly-spaced patters.

The Turing and Gierer-Meinhardt models were initially proposed to explain morphogenesis of some developmental processes such as tissue formation, but they can also apply to the polarization event within a single cell. Clusters of polarity factors could arise from an initially homogeneous condition through the local amplification of stochastic noise, such as fluctuations in protein concentrations or stochastic receptor occupancy. A self-reinforcing positive feedback mechanism amplifies local fluctuations into a larger asymmetry. Although amplification of stochastic clusters of polarity factors can explain how large asymmetries can develop in initially symmetric cells, positive feedback alone does not explain why many cells display only one dominating asymmetry. Theoretically, positive feedback could amplify multiple clusters in a cell at once, so how do cells ensure singularity? In the Gierer-Meinhardt model, a fast-diffusing inhibitor could block the amplification of additional polarization sites, leaving a single axis of polarity. In the yeast polarization model proposed by Goryachev and Pokhilko, they further elaborated this idea and showed that competition between multiple amplifying

clusters for a limiting pool of polarity factors could, in theory, guarantee singularity without the need of an inhibitor (Goryachev and Pokhilko, 2008; Howell et al., 2009).

1.1.2 Local accumulation of active GTPases is the key to polarization

What are the molecular regulators of polarity establishment? The models presented above typically assume the local activation process involves slow-diffusing, membrane-bound proteins, whereas the inhibitor is assumed to be fast-diffusing, cytosolic molecules (Onsum and Rao, 2009). However, in many cases, the molecular components predicted by the models, such as the putative inhibitors, have yet to be discovered. Geneticists have attempted to discover polarity factors through genetic screens for mutants that exhibit polarity defects.

Several conserved molecular mechanisms involving in polarity establishment have emerged from studies in different organisms and cell types. The Rho-type GTPases, including Cdc42, Rac and Rop, play a central role in cell polarity establishment in many eukaryotes. The key to the specification of the "front" of a cell during polarity establishment usually involves local accumulation of the active, GTP-bound form of the GTPases (Etienne-Manneville, 2004; Johnson et al., 2011; Yang and Lavagi). The importance of Cdc42 in controlling polarity was first discovered in a genetic screening in *Saccharomyces cerevisiae*, in which a temperature sensitive mutant defective in *CDC42* (*cdc42-1*^{ts}) abolished polarized secretion and budding at restrictive temperature (Adams et al., 1990). Yeast cells proliferate by budding, which depends on polarized actin cytoskeleton for secretion and cell-surface deposition to the new bud (Adams and Pringle, 1984; Kilmartin and Adams, 1984; Novick and Botstein, 1985). The first key step in

yeast polarization is the local recruitment and activation of Cdc42 at the presumptive bud site, where it subsequently recruits its downstream effectors that eventually reorient actin cytoskeleton toward the bud site. In the absence of Cdc42, actin does not become polarized, resulting in the isotropic cell growth and accumulation of large, unbudded cells (Adams et al., 1990).

Cdc42 is not only responsible for polarized growth in yeast, but also plays a central role in polarity establishment in multicellular organisms during cell migration and morphogenesis. In multicellular organisms, cell polarity is primarily determined by external stimuli, such as cell-cell or cell-extracellular matrix contacts via cell adhesion molecules, or by gradient of soluble chemoattractants. These cues lead to localized recruitment and activation of Cdc42, which in turn regulates the reorganization of actin cytoskeleton (Hall, 1998; Tapon and Hall, 1997) and polarization of microtubule-organizing center (MTOC) toward the front (Watanabe et al., 2005). The evidence that directly links localized Cdc42 activation and polarity establishment in mammalian system was from the work done by Castellano et al (Castellano et al., 1999). They generated a system where GTP-locked Cdc42 could be recruited to a synthetic transmembrane receptor via adding rapamycin. The addition of antibody-coupled beads clustered these receptors and thus the bound GTP-Cdc42 at random sites on the plasma membrane without the need of other stimuli and subsequent signaling factors. Induced clustering of active Cdc42 at the membrane led to the polymerization of actin cytoskeleton and the formation of protrusions, providing a direct link between GTP-Cdc42 clustering and polarity establishment (Castellano et al., 1999).

Microtubules are not involved in yeast cell polarity, but microtubule reorganization is a key polarization event in many eukaryotic cell types. In the first few cell divisions of *Caenorhabditis elegans* embryo, the uneven pulling forces on the anterior and posterior poles lead to asymmetric positioning of the microtubule spindle and subsequent asymmetric cell division (Grill et al., 2001). This process is regulated by the conserved PAR (partitioning-defective) proteins, which were identified through screens in *C. elegans* for mutants defective in anterior-posterior patterning (Nance and Zallen, 2011). PAR-6 and PAR-3 proteins polarize at the anterior pole of the embryo and form a complex with the atypical protein kinase C PKC3 (Hung and Kemphues, 1999). On the other hand, PAR-2 protein is recruited to the posterior pole (Boyd et al., 1996), leading to two non-overlapping and independent anterior and posterior cortical domains. The asymmetrical localization of the PAR-6-Par-3-PKC3 complex and PAR-2 is required for the positioning of the microtubule spindle for asymmetric cell divisions. This conserved PAR complex is also involved in the polarization of microtubule cytoskeleton in epithelial cells and migrating astrocytes (Etienne-Manneville and Hall, 2003). Further investigation of PAR-6 revealed that it is an effector of Cdc42p. GTP-Cdc42p binds to PAR-6 and induces a conformational change of PAR-6 that activates PKC3 in the complex (Garrard et al., 2003). Knockdown of Cdc42p expression disrupts polarized localization of Par6p and leads to partitioning defects in *C. elegans* embryos (Gotta et al., 2001; Kay and Hunter, 2001).

Cdc42 is highly conserved in many eukaryotes, with yeast and human Cdc42 sharing 80% sequence identity (Munemitsu et al., 1990; Shinjo et al., 1990). This thesis

will focus on Cdc42p-mediated polarity establishment in budding yeast *Saccharomyces cerevisiae*.

1.2 Yeast polarity establishment

1.2.1 Polarized growth during yeast cell cycle

S. cerevisiae proliferates by budding. The morphogenesis of budding yeast is temporally linked to cell cycle progression. Bud formation is initiated by the passage through a regulatory point in late G1 termed START (Hartwell et al., 1974). Passage through START and the progression through the rest of the cell cycle are controlled by the master regulator cyclin-dependent kinase (CDK, Cdc28 in *S. cerevisiae*), which is activated when bound to its regulators cyclins. In early G1 phase of haploid cells, the Cdc42-directed GEF Cdc24 is sequestered in the nucleus by Far1. Upon entry into the cell cycle, the activation of G1-CDK triggers the phosphorylation and degradation of Far1, resulting in the nuclear export of Cdc24 to cytoplasm (Nern and Arkowitz, 2000; Shimada et al., 2000). Cdc24 is then recruited to the presumptive bud site and catalyzes the localized activation of Cdc42 at the pre-bud site. Through interacting with its downstream effectors, GTP-Cdc42 is responsible for polarizing both actin and septin cytoskeletons. Cdc42 and the actin cytoskeleton stay polarized to the tip of the growing bud until G2, when cells are ready to enter mitosis. In early G2 phase, cells switch from apical growth, in which the cell mainly continues growing at the tip of the bud, to isotropic growth, where the actin cytoskeleton is less polarized and the bud generally increases in size (Lew and Reed, 1993). Following mitotic exit, an actomyosin ring forms

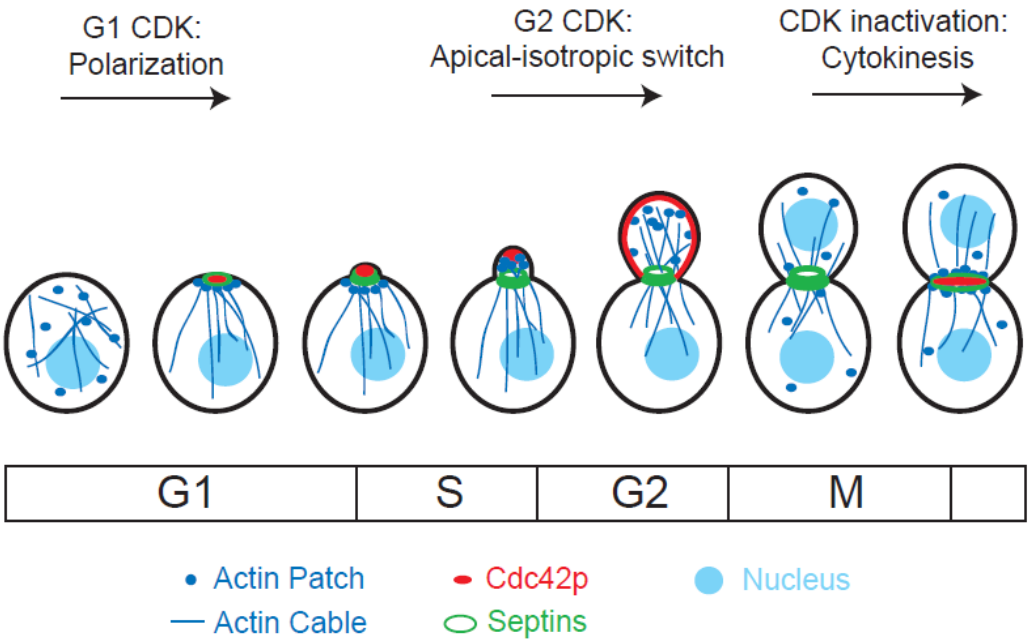

Figure 1.1 Yeast polarized growth

In response to cyclin/CDK activity, yeast cells polarize Cdc42p and reorient actin cytoskeleton.

at the bud neck to aid in cytokinesis. Cdc42 and actin cytoskeleton also repolarize to the bud neck to help septum formation. Fluorescent microscopy analysis showed that GFP-Cdc42 localizes around the entire cell periphery and internal membranes at all stages of the cell cycle but concentrates to polarized growth sites, including the pre-bud sites, bud tips, sides of large buds and mother-daughter neck regions (Richman et al., 2002; Ziman et al., 1993).

The yeast actin cytoskeleton is required for polarized growth in budding and for shmoo formation during mating. This thesis will focus on the budding process. There are two kinds of actin structures responsible for bud growth: cables and patches. GTP-Cdc42 activates formins that nucleate the polymerization of actin filaments, which are then assembled into actin cables pointing toward the pre-bud site (Pruyne et al., 2004). Type V myosin Myo2 delivers secretory vesicles, which carry the materials for bud growth and cell wall synthesis, to the pre-bud site along the actin cables (Johnston et al., 1991; Schott et al., 1999). Immunofluorescence of Myo2 and a vesicle marker Sec4 (a Rab GTPase required for the fusion of vesicles with the plasma membrane) revealed that they are polarized at the pre-bud site (Lillie and Brown, 1994; Walch-Solimena et al., 1997). The loss of actin cables in a *tpm1-2 tpm2Δ* (isoforms of yeast tropomyosin) mutant or the loss of Myo2 motor activity in *myo2-66* mutant stop vesicle delivery and lead to enlarged, unbudded cells (Pruyne et al., 1998; Schott et al., 1999). Once reaching at the pre-bud site, secretory vesicles are docked and fused to the plasma membrane with the help of t-SNAREs and the exocyst complex (Finger and Novick, 1998). Cdc42 not only polarizes actin cables, it also plays a role in the docking and fusion of secretory vesicles during

exocytosis (Adamo et al., 2001; Wu et al., 2010).

Actin patches are punctate cortical structures that polarize at the pre-bud site (Adams and Pringle, 1984). In *cdc42* mutants, actin patches still assemble but distribute randomly at the cell cortex, suggesting Cdc42 is required for the polarization of actin patches, not their assembly (Adams et al., 1990). In budding yeast, actin patches function in endocytosis. Most of the proteins involved in endocytic internalization partially or fully colocalize with cortical actin patches (Engqvist-Goldstein and Drubin, 2003). Endocytosis is important for regulation of cell wall assembly and the recycling of secreted proteins and lipids. Proper cell wall assembly not only depends on the actin-cable-dependent polarized delivery of synthetic enzymes (e.g. chitin and glucan synthases), but also requires the re-internalization of these proteins. Defects in actin patch components do not block polarized growth but fail to clear cell wall synthesis enzymes from the cell surface after growth is redirected, leading to the formation of multiple layers of cell walls in the mother cells (Ayscough et al., 1999; Mulholland et al., 1997; Ziman et al., 1996).

In addition to actin cytoskeleton, GTP-Cdc42 is responsible for the recruitment and polarization of septins, which are a conserved family of filament-forming proteins that play a role in cytokinesis in fungi and animal cells (Gladfelter et al., 2001). Septin recruitment depends on GTP-Cdc42p and two Cdc42 effectors, Gic1 and Gic2 (Cid et al., 2001; Iwase et al., 2006). Septins are assembled into a ring before bud emergence and remain as a collar subjacent to the plasma membrane at the mother-daughter neck for most of the cell cycle (Kim et al., 1991). The initial septin ring assembly requires Cdc42

to cycle between the GDP- and GTP-bound states (Gladfelter et al., 2002). Upon bud emergence the septins rearrange into a hourglass structure at the mother-bud neck (Gladfelter et al., 2001). Although not required for bud emergence, the septins act as a scaffold to concentrate a variety of signaling molecules, aid in shaping the bud and strengthening the cell wall at the division site, and may be a diffusion barrier partitioning the mother and bud plasma membranes (Barral et al., 2000; Luedeke et al., 2005; Shcheprova et al., 2008; Takizawa et al., 2000).

1.2.2 Polarization of Cdc42 in response to intrinsic landmark cues

During the mating process, yeast cells of the opposite mating types sense the external pheromone cues and perform chemotropism (growth navigated by chemical stimulus) to grow toward each other. In contrast, during the budding process, the direction of bud growth is determined by the internal "landmark" cues (Bi and Park, 2012). Yeast cells adopt a cell-type-specific budding pattern. Haploid **a** and α cells bud in an axial pattern in which the new bud site is immediately adjacent to the previous division site. The diploid **a**/α cells bud in a bipolar pattern: the mother cells bud either next to their division site or on the opposite end of the cell, whereas the daughter cells mostly bud away from their division site (Chant and Pringle, 1995). The budding pattern is guided by three different groups of landmark proteins (Bi and Park, 2012). The first group of proteins is responsible for the axial pattern. One of the members Axl2 localizes to the bud neck in medium and large budded cells and following cytokinesis, remains as a ring marking the division site (Halme et al., 1996). The second group, including Bud7, Bud8, Bud9, Rax1, and Rax2, are specifically required for the bipolar pattern. Bud8 and

Bud9 mark the poles distal and proximal to the birth pole of a daughter cell, respectively (Harkins et al., 2001; Zahner et al., 1996). Rax1 and Rax2 localize to both poles of the cell and appear to function as long-term markers of previous division sites in diploids (Kang et al., 2004). The third group, including Rsr1/Bud1, Bud2, and Bud5, are required for both budding patterns. Rsr1, a Ras family GTPase, is activated by its GEF Bud5 (Bender, 1993; Chant et al., 1991) and inactivated by its GAP Bud2p (Park et al., 1993). It has been proposed that Bud5 is the key player that interacts with landmark proteins and recruits and activates Rsr1 at the chosen site (Kang et al., 2010). Rsr1-GTP directly interacts with Cdc42-directed GEF, Cdc24, and GDP-Cdc42, thereby linking the bud-site-selection machinery to the polarity establishment machinery (Kozminski et al., 2003; Park et al., 1997; Zheng et al., 1995) and leading to localized activation of Cdc42 at the predetermined bud site.

1.2.3 Cdc42 regulators and effectors

Like other GTPases, Cdc42 cycles between the active GTP-bound and inactive GDP-bound forms. The GDP-GTP cycling is required for the functions of Cdc42 (Gladfelter et al., 2002; Irazoqui et al., 2003; Ziman et al., 1991). The switching between different nucleotide-bound states is regulated by two kinds of molecules: guanine nucleotide exchange factors (GEFs) activate Cdc42 by stimulating the release of GDP, allowing the binding of GTP; GTPase activating proteins (GAPs) catalyze the hydrolysis of GTP and inactivate Cdc42. Membrane localization of Cdc42 is of equal importance to its activation status and is regulated by a third class of regulator, guanine nucleotide dissociation inhibitors (GDIs). Through these regulators, the concentration and

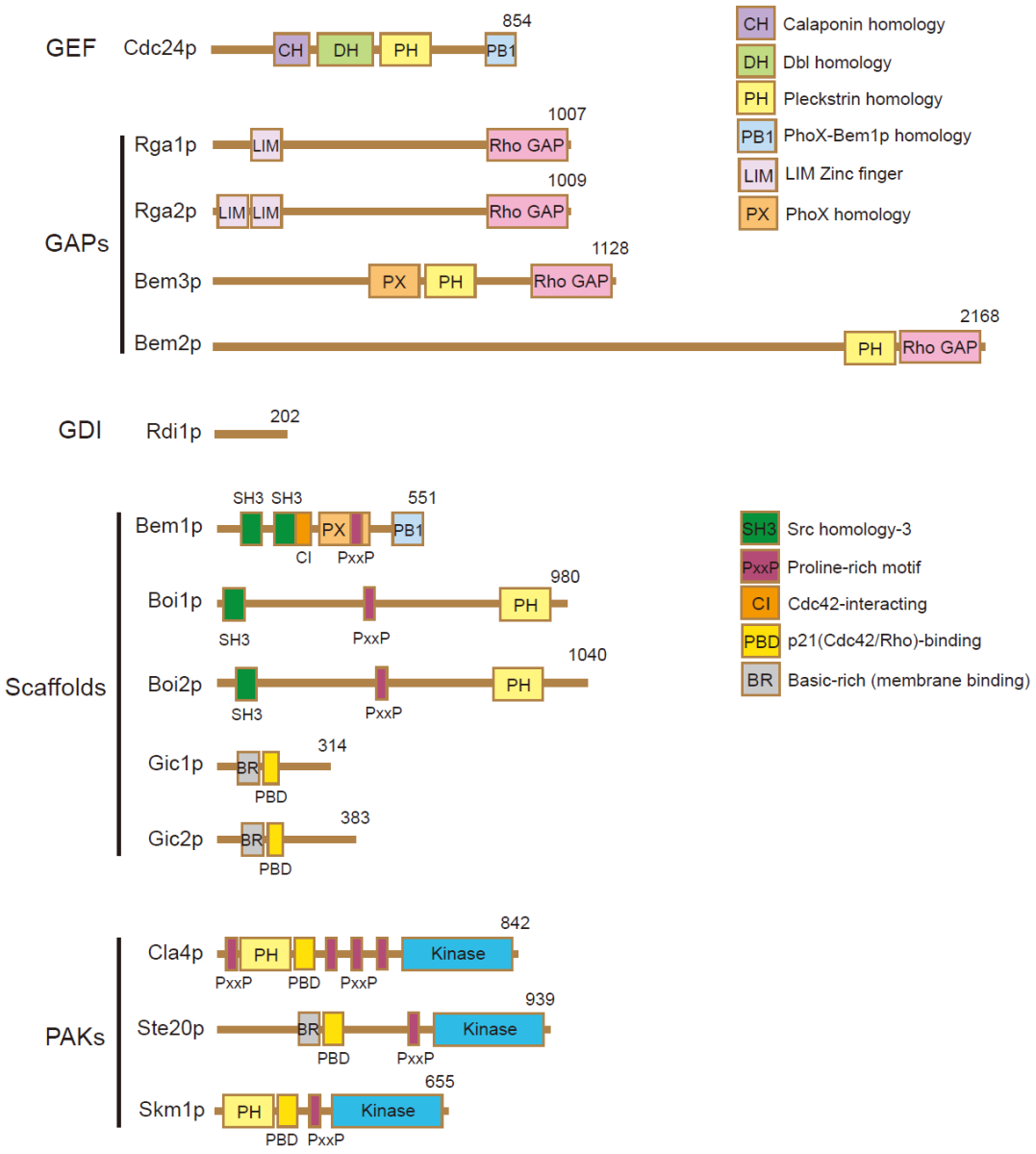

Figure 1.2 Regulators and effectors of Cdc42p

Schematic of domains in regulators and effectors of yeast Cdc42p.

localization of GTP-Cdc42 available to interact with effectors can be precisely controlled.

GEF: *S. cerevisiae* has a single essential Cdc42p-directed GEF, Cdc24. The role of Cdc24p in polarity establishment was discovered in genetic screens that *cdc24* temperature sensitive mutants were defective in budding (Sloat et al., 1981; Sloat and Pringle, 1978). Loss of Cdc24 resembles loss of Cdc42 in cells, suggesting that Cdc24 is dedicated to the activation of Cdc42p (Zheng et al., 1994). Without Cdc24, cells also fail to polarize the actin cytoskeleton.

GAPs: Budding yeast has four redundant Cdc42-directed GAPs: Rga1 (Stevenson et al., 1995), Rga2 (Smith et al., 2002), Bem2 (Marquitz et al., 2002), and Bem3 (Zheng et al., 1994). All of them have a conserved Rho-GAP domain at the C terminus that carries out the GAP activity. Careful examination of budding patterns revealed that Rga1 appears to block formation of a bud within the previous division site by creating an exclusion zone for GTP-Cdc42p within the division site (Tong et al., 2007). Unlike Cdc24, no single GAP is essential and the exact roles they play in polarity establishment are unclear.

GDI: The CAAX motif at the C terminus of Cdc42 provides a modification site for geranylgeranylation that is necessary for its membrane anchorage (Ziman et al., 1991). A polybasic domain preceding the prenylation site also contributes to membrane association. GDI is able to form a 1:1 complex with Cdc42 by binding to the geranylgeranyl group and extract Cdc42 from the membrane to the cytoplasm (Leonard et al., 1992). Given these properties, GDI has been considered acting as a negative regulator of Cdc42 (keeping Cdc4p in a cytoplasmic inactive state), a chaperone for Cdc42

(Boulter et al., 2010), and a vehicle to shuttle Cdc42 between different membrane compartments (Lin et al., 2003). Budding yeast has a sole GDI, Rdi1 (Masuda et al., 1994). Part of this thesis work focuses on GDI, so the function of GDI in polarity establishment will be discussed in detail in the next section.

p21-activated kinases (PAKs): There are three PAKs, Cla4, Ste20, and Skm1 in budding yeast. The PAKs each contain a CRIB (for "Cdc42/Rac Interactive Binding") domain (also known as the "p21-Binding Domain", or PBD) that specifically interacts with GTP-Cdc42. Ste20 and Cla4 localize to sites of polarized growth and have proposed roles in both actin and septin organization (Cvrckova et al., 1995; Holly and Blumer, 1999; Peter et al., 1996; Weiss et al., 2000); however, the role of Skm1 remains unclear. Cla4 plays a role in septin ring assembly (Dobbelaere et al., 2003; Longtine et al., 2000; Versele and Thorner, 2004) and also phosphorylates Cdc24, presumably to regulate the GEF activity (Bose et al., 2001; Gulli et al., 2000). Ste20 and Cla4 appear to be partially redundant. *ste20Δ* and *cla4Δ* single deletions are viable but the *ste20Δ cla4Δ* double deletion is dead, due to severe cytokinesis defects (Cvrckova et al., 1995).

Scaffolds: *BEM1* is not an essential gene in budding yeast, but *bem1Δ* cells have severe polarization defects, becoming large, round and multinucleated (Bender and Pringle, 1991). Bem1 binds to GTP-Cdc42 through its second Src homology3 (SH3-2) domain and a CI (Cdc42p interacting) domain distinct from the CRIB domain described above (Yamaguchi et al., 2007). In addition to GTP-Cdc42, Bem1 binds to Cdc24 through its C-terminal PB1 domain (Ito et al., 2001; Peterson et al., 1994), and to the PAKs Cla4 and Ste20 through the SH3-2 domain (Bose et al., 2001; Winters and Pryciak,

2005). Based on analysis of point mutations and protein fusions, the role of Bem1 in polarity establishment appears to bring Cdc24 in association with a PAK to help generate more localized GTP-Cdc42 (Kozubowski et al., 2008).

Two putative Cdc42 effectors, Boi1 and Boi2, were identified based on their ability to bind the second SH3-2 domain of Bem1 (Bender et al., 1996; Matsui et al., 1996). This Bem1-binding ability is mediated by the proline-rich (PxxP) domain (Bender et al., 1996). Although Boi1 and Boi2 do not have a CRIB domain like the PAKs, they appear to be able to bind to GTP-Cdc42 through the C-terminal pleckstrin homology (PH) domain (Bender et al., 1996). Boi1 and Boi2 are functionally redundant. Deletion of both *BOI1* and *BOI2* leads to large round cells, displaying defects in bud formation and polarity maintenance. However, their function in polarity establishment is unclear.

Gic1 and Gic2 were identified as Cdc42 effectors based on the presence of CRIB domains. Gic1 and Gic2 colocalize with Cdc42 at the polarization site, and the deletion of both genes leads to defects in actin polarization at high temperatures as seen in *cdc42* mutants (Brown et al., 1997; Chen et al., 1997). A recent study showed that Gic2 mediates the interaction between GTP-Cdc42 and the actin-nucleating protein Bni1, promoting the polarization of actin cytoskeleton (Chen et al., 2012). Gic1 and Gic2 also appear to help recruit septins to the incipient bud site, presumably via direct interaction with the septin component Cdc12 (Iwase et al., 2006).

1.2.4 The role of GDI in polarity establishment

As its name implies, GDI was originally characterized because of its ability to inhibit the dissociation of GDP from Rho GTPases, including Rho, Rac and Cdc42

(Fukumoto et al., 1990; Leonard et al., 1992; Ueda et al., 1990). It was subsequently shown that GDI is capable of blocking both intrinsic and GAP-stimulated GTP hydrolysis of Rho GTPases (Hancock and Hall, 1993; Hart et al., 1992). These findings indicated that GDI is able to interact with both GDP- and GTP-bound forms of Rho GTPases and inhibits their GDP/GTP cycling. Deletion of GDI in yeast and depletion of GDI in mammalian cells cause the misfolding and degradation of cytoplasmic Rho GTPases, indicating that GDI also acts as a chaperone to stabilize Rho GTPases when they are not associated with membranes (Boulter et al., 2010). The stable pool of inactive, cytoplasmic Rho GTPases maintained by GDI presumably acts as a reservoir, allowing rapid translocation of Rho GTPases to any membrane for activation in response to signals (Garcia-Mata et al., 2011). Therefore, GDI is involved in spatial regulation of Rho GTPases, shuttling them between cytosol and membranes. For example, GDI is suggested as a transporter of a lipid kinase complex containing Rac1, PtdInsP 5'-kinase and diacylglycerol kinase (DGK). GDI interacts with Rac1 and sequesters this complex in the cytosol. Upon stimulation, this preformed complex is shuttled to the membrane where it is in proximity to its substrates and released from GDI (Tolias et al., 1998).

The negative regulatory role of GDI was shown in several early studies that overexpression or microinjection of GDI in mammalian cells caused defects involving actin cytoskeleton reorganization, including morphology change accompanied by the disappearance of stress fibers (Miura et al., 1993) and loss of motility (Takaishi et al., 1993). However, overexpression of GDI can greatly affect the stoichiometry between GDI and its binding partners and cause misleading interpretation of the phenotypes. The

ability of GDI to inhibit GTP hydrolysis and thus prevent the inactivation of Rho GTPases also makes the role of GDI ambiguous. On the contrary, several studies revealed the positive regulatory role of GDI on other Rho GTPases. For example, Rac1/GDI complex was firstly identified as one of the active components required for NADPH oxidase activation in phagocytes, which is required to produce reduced oxygen species important in killing microorganisms (Abo et al., 1991). Rac1 mutants unable to interact with GDI lost their ability to activate NADPH oxidase, indicating that GDI binding is required for Rac1 activity (Di-Poi et al., 2001). Introduction of the GDI binding-defective mutation R66A within a fast-exchanging Cdc42(F28L) mutant background abolished the ability of the Cdc42(F28L) allele to transform NIH 3T3 fibroblasts, strongly suggesting that Cdc42-GDI interaction is required for Cdc42p-mediated cellular transformation (Lin et al., 2003).

Biochemical and fluorescent assays confirmed that GDI is able to extract Cdc42 from the membrane, suggesting that GDI plays a role in shuttling Cdc42 between different cellular compartments (Leonard et al., 1992; Nomanbhoy et al., 1999). The mobility of Cdc42 in yeast is severely crippled when the sole GDI, Rdi1, is deleted, supporting the role of GDI in Cdc42 trafficking (Slaughter et al., 2009a). When the GDI-Cdc42 complex was first characterized, biochemical data suggested that the ability of GDI to bind GDP- or GTP-bound form of Cdc42 was not obviously different (Leonard et al., 1992). Another fluorescence spectroscopic assay also showed that GDI had similar K_d values interacting with either form of Cdc42 in solution (Nomanbhoy and Cerione, 1996). However, it was later found out that membrane plays a previously unappreciated role in

helping GDI to distinguish between GDP and GTP-bound Cdc42 (Johnson et al., 2009). Around 10-fold greater amount of GDI was necessary to dissociate GTP-Cdc42 from the membrane with similar efficiency compared to extracting GDP-Cdc42, indicating that GDI has a much higher affinity to GDP-Cdc42 when they interact along the membrane surface (Freisinger et al., 2013; Johnson et al., 2009). A mathematical model of yeast polarity establishment proposed by Goryachev and Pokhilko introduced the idea that GDI acts as a vehicle to transport Cdc42 and that it only extract GDP-Cdc42 from the membrane (Goryachev and Pokhilko, 2008). Their model suggests that GDI-mediated differential extraction of Cdc42 and shuttling is one of the keys that contribute to symmetry breaking polarization in yeast.

1.3 Symmetry breaking

Wild-type yeast cells utilize landmark proteins to polarize and bud at predetermined sites. However, in the absence of these internal cues (e.g. *rsr1Δ, bud2Δ, bud5Δ*), yeast cells are fully capable of polarizing at a single, random site with unaffected budding efficiency, a process called symmetry breaking (Bender, 1993; Bender and Pringle, 1989; Chant et al., 1991; Park et al., 1993). Therefore yeast cells must contain some core polarity establishment mechanism that can polarize the cell independent of positional cues. The Turing-type models of symmetry breaking polarization require a positive feedback loop to amplify stochastic fluctuations of polarity factors. Several studies combining biochemistry, live-cell imaging and mathematical modeling have

proposed different positive feedback mechanisms to explain how yeast cells break symmetry.

1.3.1 Bem1 complex-mediated symmetry breaking

What is the molecular basis for the positive feedback loop in yeast? A possible mechanism for the positive feedback loop required for symmetry breaking relies on the formation of a Bem1p complex (Kozubowski et al., 2008). *BEM1* is not essential in wild-type yeast cells even though its absence causes severe polarization defects. However, the essential role of *BEM1* in symmetry breaking was revealed in a genetic screen that *bem1Δ* is synthetic lethal with *rsr1Δ*, which disrupts the positional cue (Irazoqui et al., 2003). Specifically, the binding of the GEF Cdc24 to the PB1 domain and a PAK kinase to the SH3-2 domain of the same Bem1 molecule is required for symmetry breaking (Bose et al., 2001; Gulli et al., 2000; Irazoqui et al., 2003; Kozubowski et al., 2008). This Bem1-Cdc24-PAK complex could be recruited to a stochastic cluster of GTP-Cdc42 through the interaction with the PAK CRIB domain. The GEF on the same complex then convert more neighboring GDP-Cdc42 to GTP-Cdc42, which in turn recruits more Bem1p complexes in a positive feedback loop to generate a larger GFP-Cdc42 cluster (Kozubowski et al., 2008).

Scaffold proteins with similar domain organization like Bem1 are present in many fungi (Endo et al., 2003). Although mammalian cells lack a Bem1 homolog, a number of mammalian Cdc24-related GEFs have one or more SH3 domains, many of which interact with PAKs (Feng et al., 2002; Schiller et al., 2006). It is likely that through the direct interaction of the GEF and the PAK, mammalian cells have evolved to bypass the need of

a scaffold protein to bring these two molecules together. Interestingly, mimicking the mammalian GEF architecture by fusing Cdc24 and the PAK or generating an artificial SH3 domain-containing Cdc24p able to bind PAKs could bypass the need of Bem1 in symmetry breaking polarization in yeast (Kozubowski et al., 2008).

The Bem1 complex-based positive feedback mechanism can initially generate a local GTP-Cdc42 gradient but it can dissipate by membrane diffusion if Cdc42 is not further delivered and concentrated at the polarization site. Given the much faster cytoplasmic diffusion rate of GDI-Cdc42 complex than the Cdc42 membrane diffusion rate, it has been suggested in a Turing-type modeling that GDI-mediated cytoplasmic flux of Cdc42 can counteract the diffusive spread of the polarized cluster (Goryachev and Pokhilko, 2008). As mentioned earlier, GDI preferentially extracts GDP-Cdc42. GDI extracts GDP-Cdc42 from and puts it back to random places on the membrane; however, quick conversion of Cdc42 to GTP-bound form at the polarization site makes it unable to be plucked off the membrane by GDI, leading to the local buildup of a GTP-Cdc42 cluster.

1.3.2 Actin-mediated symmetry breaking

An alternative positive feedback mechanism relying on actin-mediated trafficking and recycling has been proposed to be functioning in yeast. Overexpression of GTP-locked $Cdc42^{Q61L}$ could promote polarization at random sites in cells arrested in G1 phase (Wedlich-Soldner et al., 2003), although the higher levels of protein needed to induce spontaneous polarization also resulted in cell death (Irazoqui et al., 2003). Symmetry breaking by $Cdc42^{Q61L}$ required a polymerized actin cytoskeleton and myosin-mediated

vesicular trafficking (Wedlich-Soldner et al., 2003). The authors proposed that clusters of $Cdc42^{Q61L}$ grow via a positive feedback loop in which $Cdc42^{Q61L}$ nucleates actin cables, which then deliver more $Cdc42^{Q61L}$ on secretory vesicles. Sustained polarization required retrieval of $Cdc42^{Q61L}$ by endocytosis before it diffused too far from the cluster (Marco et al., 2007).

Although the actin-mediated positive feedback loop was first described in a highly artificial system, Wedlich-Soldner and colleagues proposed that an actin-mediated positive feedback mechanism polarizes wild-type Cdc42p as well. Releasing G1-arrested cells in the presence of actin depolymerizing drug Latrunculin A (Lat A) could delay the polarization of Cdc24-GFP and GFP-Cdc42 (Wedlich-Soldner et al., 2004). A similar delay was observed in *bem1Δ* cells following release from arrest. Furthermore, disruption of both putative feedback loops (by adding Lat A to *bem1Δ* cells) abolished the polarization of Cdc24-GFP and GFP-Cdc42p. These observations lead the authors to conclude that an actin-mediated positive feedback loop normally functions in parallel to the Bem1p complex-mediated feedback loop.

Based on the contradictory results from experiments and modeling, the role of actin cytoskeleton in cell polarization has been under debate. It has been reported a while ago that Cdc42 polarization does not require polymerized actin either during wild type polarization in response to positional cues (Ayscough et al., 1997) or during symmetry breaking (Irazoqui et al., 2003), suggesting that actin does not play a central role in yeast polarity establishment. Additionally, actin cytoskeleton has been suggested to play a negative impact on yeast symmetry breaking. Ozbudak and colleagues found that the

polarized cluster of GTP-Cdc42 (visualized by PBD probe) was not stable in *rsr1Δ* cells, displaying a wave-live movement. Such movement was decreased when actin polymerization was inhibited (Ozbudak et al., 2005). They proposed that there is a delayed actin-mediated negative feedback loop that destabilizes the polarization site, possibly through endocytic dispersal of polarity factor by actin patches, or delivery of Cdc42 GAPs on secretory vesicles along the polarized actin cables. One caveat of this study is that the period between polarization to budding was more than 50 min, significantly longer than the approximately 10 min period reported in other studies. Therefore it remains unclear whether the motile polarization cluster was an experimental artifact captured under non-physiological conditions.

Mathematical models centering on actin-mediated positive feedback mechanism treated Cdc42 traffic as a direct protein flux without considering the membranes that carry Cdc42. However, if the membrane flux was taken into account, such actin-mediated Cdc42 recycling was not able to establish and maintain a polarized steady state under the condition that vesicular Cdc42 concentration is the same as the donor membrane (Layton et al., 2011). The polarization of some integral transmembrane proteins like v-SNAREs depends on actin-mediated transport and recycling, but it requires the proteins being concentrated in both exocytic and endocytic vesicles (Valdez-Taubas and Pelham, 2003). Although not know for Cdc42 in vivo, concentrating Cdc42 in both vesicles in the same mathematical simulation still failed to sustain a polarized steady state, owing to the faster membrane diffusion of Cdc42p compared to v-SNARE (Layton et al., 2011). Another simulation combining both Bem1 complex- and actin-mediated positive feedback

mechanisms revealed almost identical outcomes no matter the vesicles carry Cdc42 or not, arguing that the Bem1-based positive feedback and GDI-mediated Cdc42 recycling are the dominant mechanism for Cdc42 polarization (Savage et al., 2012).

1.3.3 Other potential mechanisms involved in yeast symmetry breaking

By incorporating the membranes as the vesicular carriers in their model, Layton et al. suggested that actin-mediated vesicle trafficking has no effect or even dilutes Cdc42p at the polarization cluster, depending on the relative Cdc42p concentrations in the donor and target membranes (Layton et al., 2011). Slaughter et al. recently proposed that non-uniform membrane diffusion at the sites of exocytosis and endocytosis could maintain polarization via actin-mediated vesicle trafficking. All of their experiments were performed in *rdi1Δ* cells to solely focus on actin-mediated Cdc42p trafficking. Using high-resolution confocal imaging and single-photon detector, they showed that exocytosis and endocytosis spatially happen at different domains on the plasma membrane (Slaughter et al., 2013). The sites of active exocytosis (marked by Bni1p-GFP) correlate with microdomains of higher concentration and slow diffusion of Cdc42p, whereas endocytosis (marked by Myo5p-mCherry) happens at sites with lower concentration and fast diffusion of Cdc42p. By incorporating two different diffusion rate constants to their model (which lacks the GDI-mediated trafficking), a stable polar cap could be generated and stably maintained. They concluded that the presence of microdomains with different membrane diffusion rates plays a critical role in actin-mediated cell polarization. One potential problem of this mechanism is that the uneven membrane diffusion and disproportional delivery versus recycling of Cdc42p could lead to the over-accumulation

of Cdc42p on the plasma membrane, generating a large polarized cluster or even overwhelming the cell cortex. However, *rdi1Δ* cells do not seem to have broader polarized clusters than wild-type cells (Slaughter et al., 2009b).

Smith et al. recently isolated viable *rsr1Δ bem1Δ* strains, which were previously reported dead because of the synthetic lethality, and found that they were able to polarize and bud. Suspecting that Rsr1p might play an unidentified role in symmetry breaking, they generated another strain that broke symmetry by deleting *AXL2*, *RAX1* and *RAX2* in combination with *bem1Δ*. The resulting strains were also viable and able to polarize GFP-Cdc42 and Cdc24-GFP, presumably by Rsr1 (Smith et al., 2013). In contrast, their *rsr1Δ bem1Δ* strains were able to polarize Cdc42 but not Cdc24. These data argued that Bem1 complex-mediated positive feedback is not required for symmetry breaking as previously reported (Irazoqui et al., 2003). They suggested that the role of Bem1p in symmetry breaking is to boosts the GEF activity of Cdc24. Combining with modeling, they proposed that in the absence of actin-mediated trafficking, cells require GDI-mediated Cdc42 trafficking to polarize. With lower but uniform GEF activity all over the cortex, stochastic activation of Cdc42 could lead to the delivery of more Cdc42 from the cytoplasmic GDI-Cdc42 pool in a positive feedback, eventually leading to symmetry breaking. This study provides a new perspective on the mechanism of yeast symmetry breaking.

1.3.4 Singularity in polarity establishment

If symmetry breaking depends on an initial stochastic activation event, one can

imagine that several polarization clusters could be amplified through the positive feedback mechanisms. How do yeast cells ensure singularity? Is singularity in budding an intrinsic characteristic of the amplification mechanism, or is there a global inhibitor that acts to prevent multiple polarization sites from forming? Yeast geneticists have been looking for mutants that violate singularity. *cdc42-22* was isolated from a genetic screen for *cdc42* mutants that generate multiple buds per cell cycle at restrictive temperature (Caviston et al., 2002). Time-lapse imaging showed that multiple buds emerged sequentially within a short period of time or in some rare cases emerged simultaneously in *cdc42-22* cells, which is different from another mutant $cdc42^{D38E}$ that consecutively initiated buds in a cell cycle without affecting singularity of budding at any given time (Richman and Johnson, 2000). Further characterization revealed that the mutation of *cdc42-22* occurred at the domain required for GTP binding and hydrolysis and thus made *cdc42-22* hyperactive, suggesting Cdc42 activity could affect singularity. Another study on Cdc42-directed GAPs supported this view. Deletion of *BEM2*, which resulted in a higher GTP-Cdc42 level in the cells, also caused the formation of multiple buds (Knaus et al., 2007). Even though *bem2Δ* cells could accumulate Cdc24-GFP at multiple sites at a time, we recently showed that most, if not all, *bem2Δ* cells generated multiple buds sequentially (unpublished data).

Another interesting finding from *cdc42-22* was that it could bypass the need of Cdc24p to polarize a cell, indicating that *cdc42-22* cells no longer use Bem1p-Cdc24p-PAK complex for cell polarization (Caviston et al., 2002). This result raised the possibility that singularity is intrinsic to the Cdc42p amplification mechanism. Consistent

with this hypothesis, the mathematical model proposed by Goryachev and Pokhilko predicted that singularity is guaranteed by competition between polarization sites for limiting Bem1p complex (Goryachev and Pokhilko, 2008). In order to ask whether altering specific amplification mechanism would impact singularity, Howell et al. fused Bem1p to v-SNARE Snc2p, rewiring the cells to employ only the actin-mediated mechanism for polarization. Multiple polarized Bem1p clusters could be detected in rewired cells and they competed with each other, resolving a winning cluster that became the bud. In a small percentage of rewired cells, the multiple clusters failed to complete competition before bud emergence, thereby generating two buds (Howell et al., 2009). Such multicluster intermediates could also be detected in normal cells but the competition occurred much more rapidly than in the rewired cells. Slowing down competition by overexpressing Bem1p in normal cells could also lead to the simultaneous growth of two buds (Howell et al., 2009). These results indicated that singularity is enforced by the Bem1p-mediated positive feedback mechanism that allows rapid competition between polarized clusters.

1.4 Thesis objectives

A polarized cell usually has a single axis of polarity no matter the positional cues are present or not. The fact that yeast cells are able to polarize to one and only one front has been a mystery. Studies utilizing time-lapse imaging and mathematical modeling have provided evidence that yeast polarity machinery may have an intrinsic competition property built into the amplification mechanism to ensure singularity. The competition

hypothesis predicts that polarity establishment should frequently proceed via a transient intermediate stage with more than one polarity cluster, and it is important to understand the mechanism of competition. There was limited experimental evidence for such multicluster intermediates, as only rare, fleeting two-cluster instances were identified in cells breaking symmetry. Using imaging with improved spatiotemporal resolution, we hoped to capture more multicluster intermediates, as predicted if competition is a frequent process to guarantee singularity. Also, we hoped to visualize the competition process in more details, helping us to unravel how competition works.

It is conceivable that multiple clusters could be amplified from stochastic noise in the absence of directional cues. What about wild-type yeast cells with predetermined bud sites? In the presence of landmark cues, is singularity guaranteed by generating only one polarized cluster without the need of competition? Or competition still happens but is biased to where the landmarks are located? We will test these two hypotheses using time-lapse imaging.

A recent study by Freisinger et al. showed that *rdi1Δ* cells occasionally violate singularity and form two buds (Freisinger et al., 2013), suggesting that Rdi1 may be involved in singularity. There are limited reports about the role of Rdi1 on polarity establishment and maintenance. Through characterizing the polarization dynamics and behaviors in *rdi1Δ* cells, we wished to understand how the absence of Rdi1p impacts competition and singularity and by what mechanism Rdi1p ensures singularity.

2. Negative Feedback in Yeast Polarity Circuit

Published as Howell et al. 2012 *Cell* 149(2):322-33.

This chapter is a result of collaborative work. The author contributed to the experimental part of this work. Mathematical modeling was done by Meng Jin.

2.1 Introduction

Polarity establishment employs an evolutionarily conserved machinery centered around the Rho-family GTPase Cdc42. During polarity establishment, active GTP-Cdc42p gets concentrated at the "front" of the cell and leads to the reorganization of actin cytoskeleton that is required for morphogenesis. In response to cell cycle cues, wild-type yeast cells follow the bud-site selection rule to polarize Cdc42p at one of several predetermined sites dictated by landmark proteins (Park and Bi, 2007). In the absence of landmark cues (e.g. in *rsr1Δ* mutant), however, yeast cells are able to polarize Cdc42p to random, yet unique site (Bender and Pringle, 1989; Chant and Herskowitz, 1991). Such "symmetry breaking" polarization depends on an autocatalytic amplification mechanism involving a scaffold protein Bem1p, which brings Cdc42p-directed GEF, Cdc24p, and a Cdc42p effector, p21-activating kinase (PAK), together to form a cytoplasmic three-way complex (Bose et al., 2001; Gulli et al., 2000; Irazoqui et al., 2003; Kozubowski et al., 2008). This complex is thought to amplify stochastic GTP-Cdc42p blips in a positive feedback loop, enabling them to grow into polarized clusters (Kozubowski et al., 2008). A diffusion-mediated amplification model suggested that molecular noise was sufficient to induce spontaneous Cdc42p cluster formation by the Bem1p-Cdc42p complexes

(Goryachev and Pokhilko, 2008). In the absence of spatial cues, stochastic activation of Cdc42p could happen randomly at more than one site, potentially leading to the amplification of multiple clusters. Mathematical modeling predicted that such amplification events could occur at multiple sites; however, the clusters competed with each other for the limiting cytoplasmic pool of Bem1p complex and only one mature cluster emerged eventually (Goryachev and Pokhilko, 2008; Howell et al., 2009).

If the competition hypothesis is correct, transient multiple-cluster intermediates should be caught during the polarization process by time-lapse imaging. Two-cluster intermediates have been detected in *rsr1Δ* yeast cells, but they happened rarely and usually resolved to a single cluster within 1.5 min (Howell et al., 2009). Besides this report, no other experimental evidence has been documented. It is possible that competition between polarity clusters occurs very rapidly so that it is difficult to catch the intermediates with previous imaging resolution.

Phototoxicity has been the major obstacle for high-resolution live cell imaging in yeast cells. High intensity of excitation light could arrest or even kill yeast cells with little or no cell division (Carlton et al., 2010). The images of two-cluster intermediates reported by Howell et al. were taken at 15 Z stacks every 1.5 min, which was the fastest time-lapse rate that did not cause phototoxicity (Howell et al., 2009). In order to image cell with improved resolution yet avoid phototoxicity, we reasoned that synchronizing cells prior to imaging could shorten the imaging time, thereby reducing light exposure. We tested several synchrony protocol and found that cells synchronized by hydroxyurea (HU) arrest/release were more resistant to excitation light than unsynchronized cells,

allowing us to image our cells with 4-fold light exposure without causing noticeable phototoxicity.

With higher spatiotemporal resolution, we found the multiple-cluster intermediates formed frequently during symmetry breaking polarization in *rsr1Δ* cells, supporting the competition hypothesis. Rapid filming also revealed unexpected oscillatory clustering of polarity factors, indicating the existence of a negative feedback loop in yeast polarity circuit. Mathematical modeling suggested the negative feedback loop confers robustness to yeast polarization and ensures rapid competition between polarity clusters even with increased polarity factor concentrations. These predictions were confirmed experimentally.

2.2 Results

2.2.1 Fast imaging revealed competition between multiple polarity clusters

The HU arrest/release synchrony allowed us to film yeast cells with 30 Z stacks every 45 sec, which was a 4-fold increase in resolution compared to previous filming conditions (15 Z stacks every 1.5 min). The strains used in all the following imaging experiments were pretreated with HU unless otherwise specified. In diploid cells breaking symmetry, we detected two or three Bem1-GFP clusters in 28% of cells (n = 67) (Fig. 2.1A). In the majority of cells forming multiple clusters, one of the clusters grew in size and/or GFP intensity while the other(s) shrunk, which is indicative of competition. Merging of Bem1p-GFP clusters happened in the rest of cells where clusters are closer to each other. In most of the competition cases the bigger/brighter cluster had the advantage

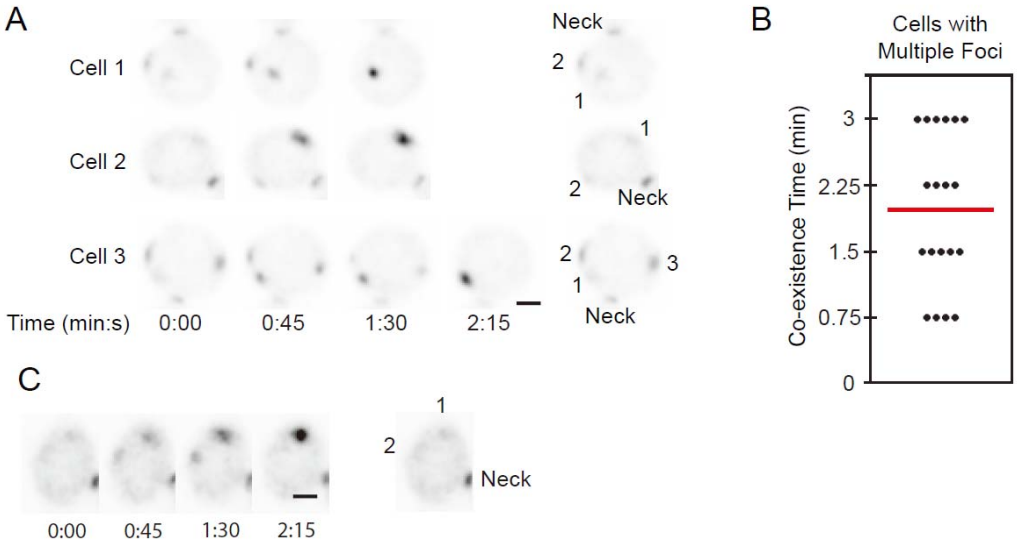

Figure 2.1 Competition between Bem1p-GFP clusters in *rsr1Δ* cells

(A) Growth and competition between multiple clusters (numbered in the key at right) in *rsr1Δ/rsr1Δ* diploid cells (DLY9200) synchronized with HU. Bem1p-GFP also localizes to the old neck (marked as "Neck" in the key) from the previous cell cycle. Images are deconvolved, cropped and inverted (dark spots indicate the accumulation of Bem1p-GFP) from maximum projections of 30 Z stacks (0.24 µm per Z step). t = 0 indicates the first detection of multiple clusters. Scale bar, 2 µm. **(B)** Coexistence time between the first detection of multiple clusters and the first frame showing the resolution to a single cluster. Each dot indicates an individual cell (n = 19). The red line is the average coexistence time. **(C)** Growth of multiple clusters and resolution to a single cluster in asynchronous *rsr1Δ/rsr1Δ* diploid cells. Scale bar, 2 µm.

for competition and usually became the winning cluster; however, in few cases the smaller/dimmer one won the competition eventually (e.g. cell 1 and 3 in Fig. 2.1A). In all cases, competition and merging occurred rapidly and efficiently to resolve a winning cluster that became the incipient bud site. Growth of the clusters and resolution of a single cluster occurred within 2 min on average (Fig. 2.1B). This may explain why multiple-cluster intermediates were rarely detected with 1.5 min filming intervals.

To make sure the competition we observed in synchronized cells was not just a byproduct of HU treatment, we imaged asynchronous *rsr1Δ* cells with the same microscopy settings but only documented cells that polarized during the first 30 min of filming, avoiding adverse effect caused by phototoxicity after extensive light exposure. Even though the signal was weaker (potentially due to the smaller cell size and lower amount of polarity factors), multiple-cluster intermediates were detected in asynchronous cells and the duration of competition was similar to that in synchronized cells (Fig. 2.1C).

2.2.2 Oscillations in polarity factor concentration within the polarized cluster

Fast filming also revealed an unexpected oscillatory behavior of Bem1-GFP concentration at the polarity cluster (Fig. 2.2A). Bem1p-GFP initially accumulated at the cluster rapidly but was then rapidly dispersed. Such behavior was generally followed by one or two more cycles of clustering and dispersal, often with lower amplitude, before bud emergence (Fig. 2.2B). Similar but less dramatic oscillation occurred in asynchronous cells (Fig. 2.2C). The initial clustering of Bem1-GFP was also slower in asynchronous cells. Since the entry into cell cycle in budding yeast requires a threshold cell size (Hartwell and Unger, 1977; Johnston et al., 1977), we speculate that

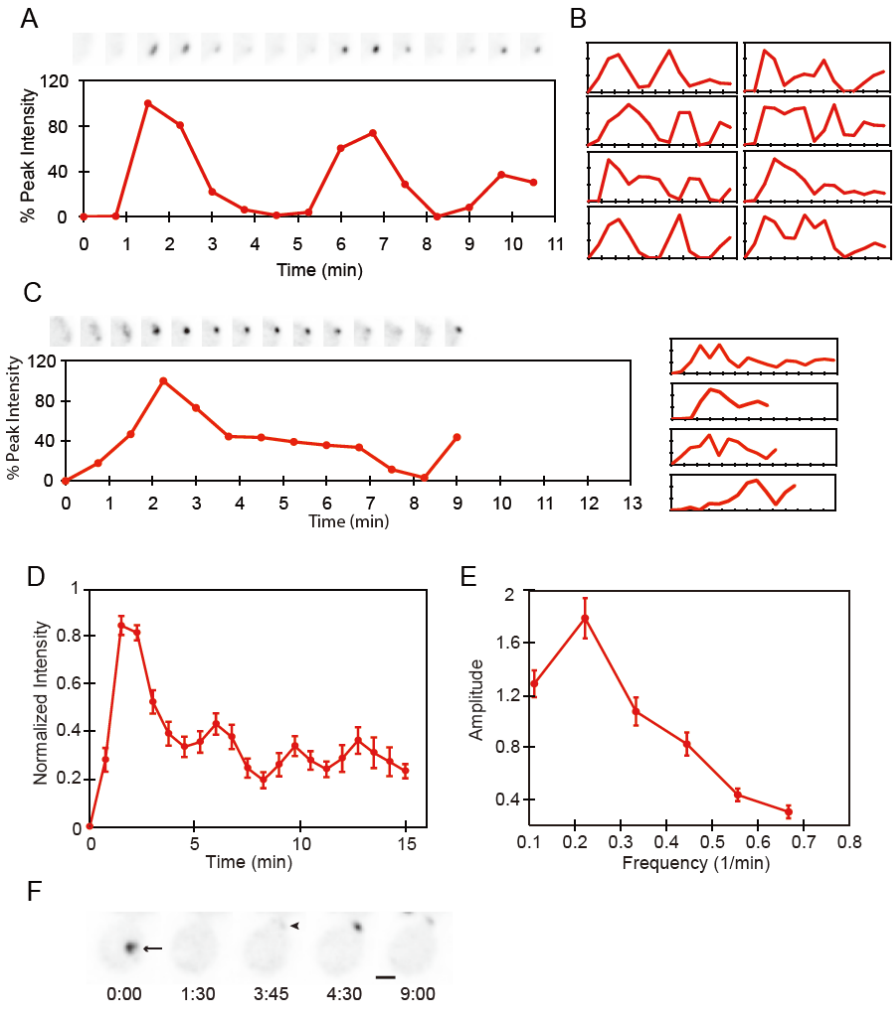

Figure 2.2 Oscillation and relocation of the Bem1-GFP cluster

(A) Oscillatory clustering of Bem1p-GFP in *rsr1Δ/rsr1Δ* diploid cells (DLY9200) pre-treated with HU. Top panel is the cropped images of the polarized cluster at 45 sec intervals. Bottom panel represents the changes of Bem1p-GFP sum intensity at the polarized cluster. t = 0 is 45 sec before the first detection of polarized signal. The trace ends at bud emergence. **(B)** Bem1p-GFP clustering in another eight cells. **(C)** Bem1p-GFP clustering in asynchronous *rsr1Δ* diploid cells. **(D)** Averaged trace from 36 HU-treated cells aligned with the first peak. **(E)** Power spectrum analysis of 12 cells with the longest traces. **(F)** Relocating Bem1p-GFP cluster. An initial cluster (arrow) disappears and shows up at another location (arrowhead), which becomes the bud site. Scale bar, 2 μm. Error bars in (E) and (F) represent SEM.

G1cyclin/CDK activity (which triggers polarization (Gulli et al., 2000) may rise more slowly in asynchronous cells than in HU-treated cells, which are much larger. CDK activation may influence the initial growth of the cluster. In cells with multiple clusters, the oscillation happened after the clusters had resolved to a single cluster. Despite cell-to-cell variability, oscillation was still apparent in the averaged traces from 36 cells aligned with the first peak (Fig. 2.2D). Power spectrum analysis suggested a dominant oscillation frequency of 0.22/min (Fig. 2.2E). In 15% of cells that formed a single cluster, the initial polarized cluster was completely dispersed and a new cluster appeared at a different site (usually at the previous cytokinesis site, Fig. 2.2F). Such relocation phenotype and the oscillatory behavior of Bem1p-GFP clusters suggest the existence of some form of negative feedback that antagonizes the initial clustering of Bem1p.

We next did two-color filming to ask whether the oscillation and relocation behaviors are shared by other core polarity factors. The oscillating signal of the Cdc42p-directed GEF, Cdc24p, paralleled that of Bem1p-GFP (Fig. 2.3A). Probes detecting GTP-Cdc42p (PBD probe, Fig. 2.3B) and total Cdc42p (Fig. 2.3C) also showed similar oscillation behaviors with Bem1p-GFP. The relocation and competition behaviors were observed with all other probes (Fig. 2.3D-G). Although sometimes the two probes within a strain had a slight time difference reaching the oscillatory peak or relocating at another location, the overall behaviors are generally in concert.

2.2.3 Problems of GFP-Cdc42p and PBD probes

Even though GFP-Cdc42p probes have been commonly used in several studies, we noticed that they are not fully functional and somewhat toxic. Most published data on

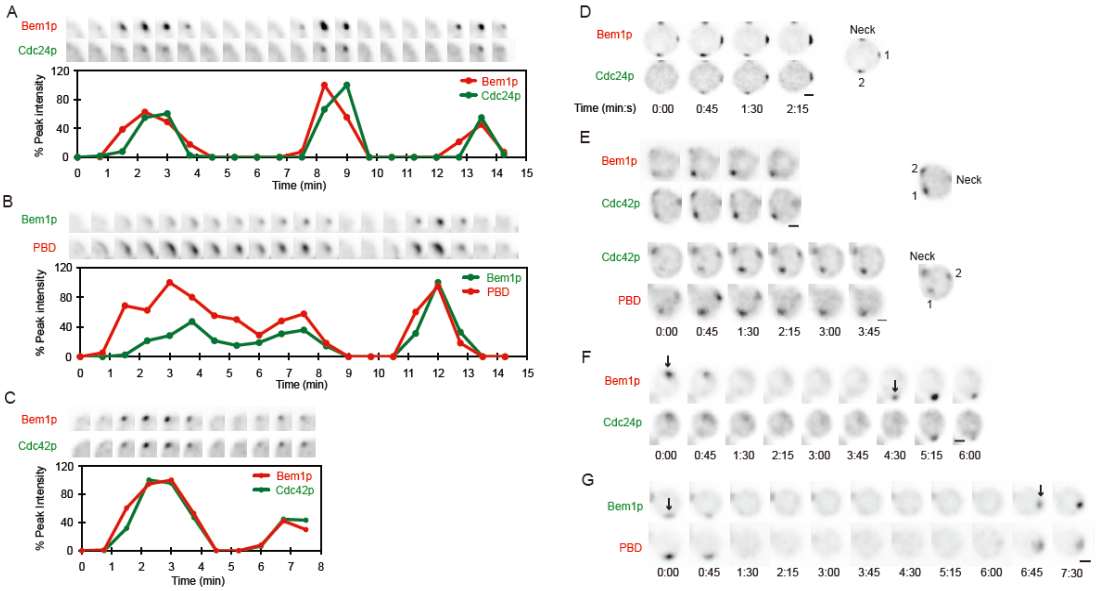

Figure 2.3 Cdc42p and Cdc24p cocluster and disperse with Bem1p

Two-color movies are process as described in Fig. 2.1. **(A)** Bem1p-tdTomato and Cdc24p-GFP (DLY13096) oscillate in parallel. Top panel is the cropped images of the polarized cluster at 45 sec intervals. Bottom panel is the quantification of the sum intensity changes at the polarized cluster. **(B)** Bem1p-GFP and GTP-Cdc42p (visualized by PBD probe, DLY13157) oscillate in parallel. **(C)** Bem1p-tdTomato and GFP-Cdc42p (DLY13158) oscillate in parallel. **(D)** Bem1p-tdTomato and Cdc24p-GFP (DLY13096) cocluster and compete (clusters are numbered in the key at right). **(E)** Bem1p-tdTomato and GFP-Cdc42p (top, DLY13158), and GFP-Cdc42p and PBD-tdTomato (bottom, DLY13164) cocluster and compete. **(F)** Bem1p-tdTomato and Cdc24p-GFP clusters relocate in parallel. **(G)** Bem1-GFP and PBD-tdTomato (DLY13157) clusters relocate in parallel. Arrows point at the clusters.

Cdc42p polarization was obtained using myc-GFP-Cdc42p (MG-CDC42) probe (Slaughter et al., 2009a; Wedlich-Soldner et al., 2004), but in those studies the probe was expressed along with endogenous Cdc42p. To test the functionality of MG-CDC42, we integrated a single copy (the expression level was comparable to that of endogenous Cdc42p) into the genome of a diploid strain deleted one copy of endogenous *CDC42* and sporulated and dissected the diploid strain. As shown in the left panel of Fig. 2.4A, all tetrads displayed 2:2 segregation for viability at 24℃ and the markers showed that all *cdc42Δ* spores were dead no matter they had MG-CDC42 or not. Therefore, at least in our strain background, MG-CDC42 was not able to rescue *cdc42Δ* at endogenous level of expression. We tested another GFP-Cdc42p probe which was reported to complement *cdc42Δ* in a temperature-sensitive manner (Bi et al., 2000). Consistent with that report, this probe was able to sustain the viability of *cdc42Δ* spore colonies in our strain background at 24℃ (circled in the right panel), but it failed to do so at 30℃ at which we usually filmed cells. Even if it was expressed on top of a copy of wild-type *CDC42*, this GFP-Cdc42p probe caused mild dominant toxicity and could lead to cell lysis of the heterozygous diploid strain (one copy of endogenous *CDC42* and one copy of *GFP-CDC42*) at 30℃ (Fig. 2.4C, third panel from the left). To avoid adverse effect by temperature sensitivity, all strains containing this GFP-Cdc42p probe were grown and filmed at 24℃.

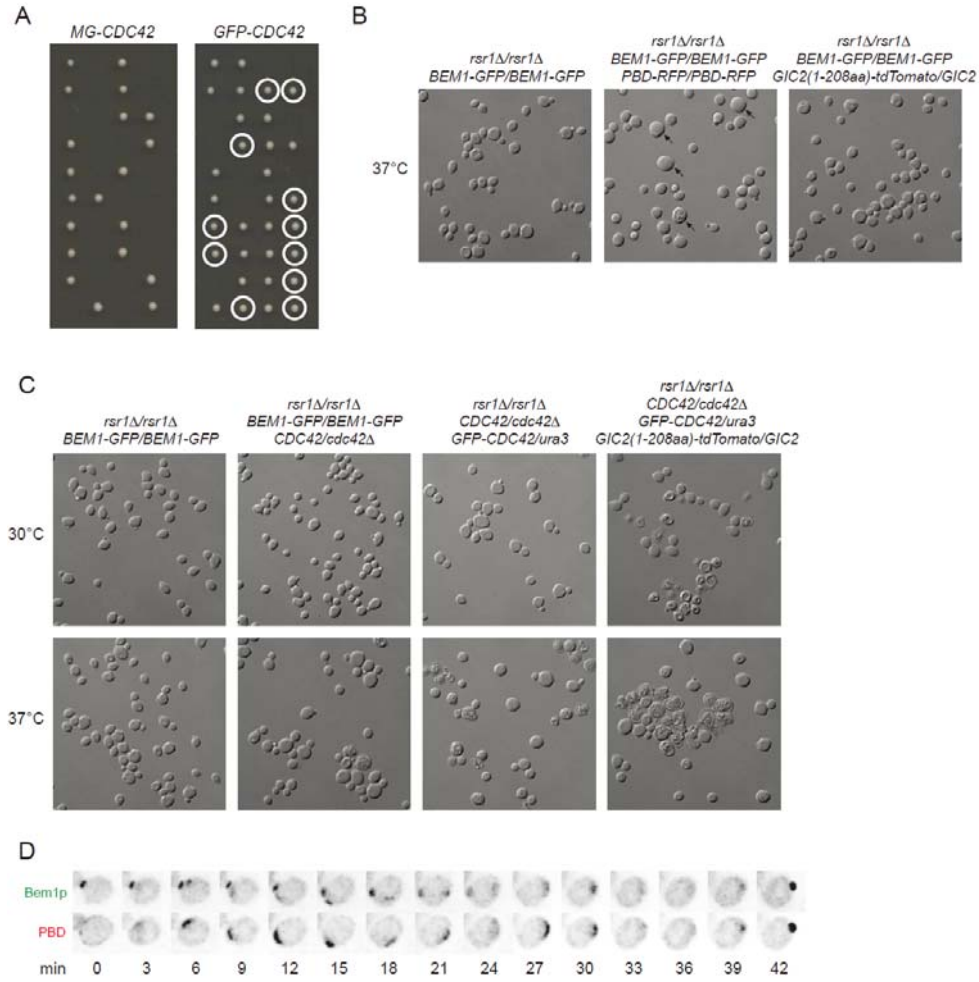

Figure 2.4 Functionality and toxicity of GFP-Cdc42p and PBD probes

(A) MG-Cdc42p and GFP-Cdc42p are not fully functional. Images show the result of tetrad dissection (4 spores in a row) of two diploid strains deleted with an endogenous copy of *CDC42* and integrated with a single copy of *MG-CDC42* (left, DLY12831) or *GFP-CDC42* (right, DLY12833) at the *URA3* locus. The 2:2 segregation of viability in the left panel indicates MG-Cdc42p is not functional in our strain background. White circles in the right panel mark the *cdc42Δ GFP-CDC42* spores growing at 24℃, meaning GFP-Cdc42p is functional at room temperature. **(B)** The PBD-RFP probe is somewhat toxic. Homozygous expression of the PBD-RFP probe integrated at the *URA3* locus leads to the appearance of large and lyzed cells (arrows), especially at 37℃. The newly-generated heterozygous

version of the same probe integrated at the *GIC2* locus reduced toxicity but did not eliminate the appearance of large and lyzed cells. **(C)** The GFP-Cdc42p probe causes mild toxicity at elevated temperatures, especially in combination with PBD-RFP probe. The panels from left to right show the controls (DLY9200), rare incidence of large and lyzed cells in hemizygous *cdc42Δ/CDC42* diploid strain (DLY13824), stronger defects in *cdc42Δ/CDC42* diploids expressing one copy of GFP-Cdc42p (DLY13859), and strongest defects in *cdc42Δ/CDC42* diploids expressing one copy of GFP-Cdc42p and one copy of PBD-RFP (DLY13164). **(D)** The PBD-RFP probe occasionally shows wave-like motion and leads to similar movement of Bem1p-GFP probe.

The PBD probe was developed based on the CRIB (Cdc42/Rac interactive binding) domain of a Cdc42p effector Gic2p that specifically binds to GTP-Cdc42p. The PBD probe used in previous studies was tagged with tdTomato and integrated at *URA3* locus. Homozygous expression of this probe led to the appearance of large cells, especially at elevated temperatures (Fig. 2.4B). To reduce toxicity, we generated the same probe at the endogenous *GIC2* locus and expressed this probe heterozygously. The new probe construction reduced but did not eliminate the incidence of large and lyzed cells. Combining this probe with GFP-Cdc42p in the same strain exacerbated cell lysis at higher temperatures (Fig. 2.4C). Besides toxicity, we noticed in some cells the PBD probe affected the behaviors of Bem1p-GFP: both probes formed broad patches that displayed wave-like motion around cell cortex, which is distinct from the nonmobile, oscillatory behavior observed in the strains with Bem1p-GFP probe alone (Fig. 2.4D). Such traveling waves were reported in a previous study on *rsr1Δ* mutants using several polarity factor probes (Ozbudak et al., 2005). A recent study from our lab also detected mobile Bem1p-GFP patch in *rsr1Δ* cells arrested in G1 phase by G1 cyclin-dependent kinase (CDK) inactivation (data not shown). Such rapid and random mobility of the polarity patch also happened in haploid *rsr1Δ* cells with normal G1 CDK function, but the patch was stabilized as soon as G1 CDK was activated (judged by the nuclear export of Whi5p-GFP probe). The patch mobility was less dramatic or even absent in diploid *rsr1Δ/ rsr1Δ* cells. In our filming condition, all cells budded within 15 min after polarization, but in the study by Ozbudak et al. cell took much longer (>50 min), raising the possibility that their cells were somehow delayed in G1 phase. We cannot rule out the

potential effect of strain background and differences between haploid and diploid cells, but we speculate the wave-like movement may be a non-physiological behavior caused by the toxicity of the PBD probe.

2.2.4 Oscillatory polarization is not due to downstream F-actin and septin action

The initial clustering of polarity factors are thought to occur via positive feedback (Goryachev and Pokhilko, 2008; Howell et al., 2009; Kozubowski et al., 2008), but positive feedback per se cannot result in the dispersal of the polarized clusters after they are formed. Instead, oscillatory behaviors in biology are generally involved negative feedback (Novak and Tyson, 2008). What could be the negative force that causes polarity factors to disperse? Cdc42p polarization leads to the reorganization of actin cytoskeleton which acts as tracks to transport materials for bud growth on secretory vesicles. Actin cable-mediated secretory vesicle trafficking could potentially perturb the polarity cluster by inserting new membrane (Layton et al., 2011) or by delivering Cdc42p-directed GAPs contained in the vesicles (Knaus et al., 2007; Ozbudak et al., 2005). Coincidently, the clustering of secretory vesicles (visualized by the vesicle marker Sec4p-GFP) was ~1.5 min after Bem1p (Chen et al., 2012), which was usually the dispersal period of Bem1p-GFP signal in the first oscillatory cycle. Cortical actin patches are thought to mark the sites of endocytosis (Kaksonen et al., 2003). It has been shown that actin-dependent endocytosis could disrupt polarity (Irazoqui et al., 2005; Yamamoto et al., 2010). Actin patches (labeled with Abp1p-mCherry) clustered around the polarization site ~1.5 min after Bem1p (Howell et al., 2009), correlating with Bem1p dispersal in both oscillation

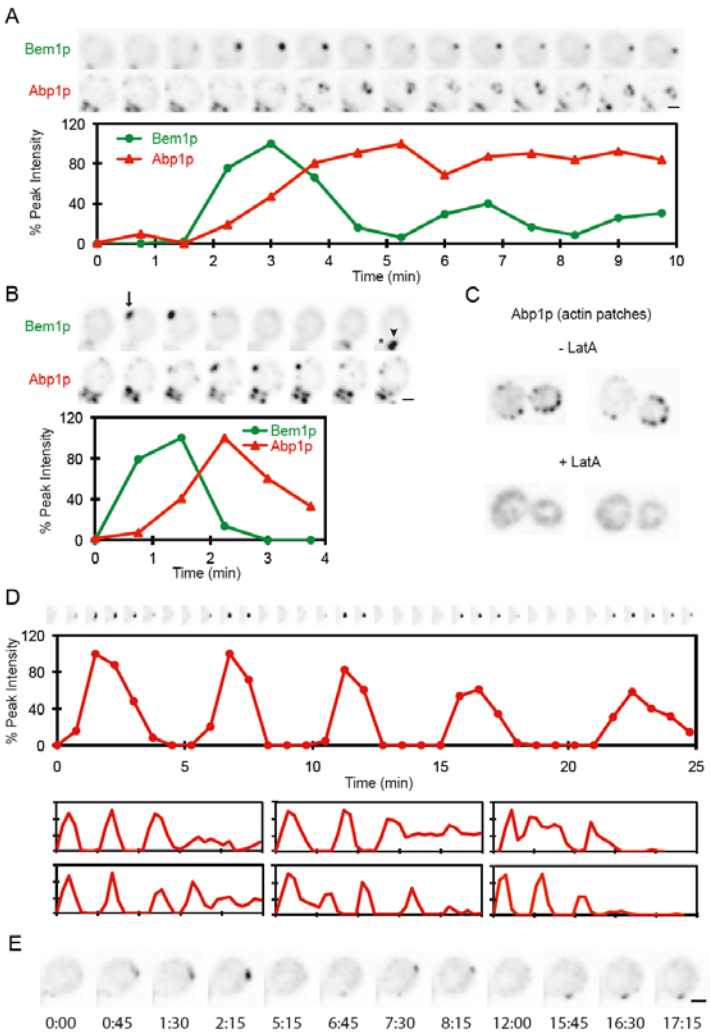

Figure 2.5 Actin polarization relative to Bem1p

Movies are processed as described in Fig. 2.1. **(A and B)** Actin patches (marked with Abp1-mCherry probe) cluster at the polarized site as Bem1p-GFP starts to disperse in oscillating (A) or relocating (B) clusters (DLY11320). Asterisk indicates the old mother-bud neck. Arrow and arrowhead indicate the initial and relocated clusters. **(C)** Latunculin A treatment disperses actin patches. **(D)** Lat A-treated diploid *rsr1Δ/rsr1Δ* cells (DLY9200) show prolonged, high-amplitude oscillations. Top panel is the cropped images of the Bem1p-GFP cluster. Middle panel is the quantification of the sum intensity changes. Lower panels are the quantifications of another six cells. **(E)** Relocation of Bem1p-GFP cluster in Lat A-treated cells (DLY9200). Scale bars, 2 μm.

and relocation (Fig. 2.5A-B). The above evidence strongly suggested that actin cytoskeleton is involved in the negative feedback. However, treatment with Latrunculin A (Lat A, an inhibitor of G-actin polymerzation) (Ayscough et al., 1997) to depolymerize actin did not stop oscillation and relocation of Bem1p-GFP clusters (Fig. 2.5C-E). Instead, Lat A-treated cells could keep oscillating at high amplitude for up to 5 cycles since bud emergence was abrogated in the absence of F-actin. These results indicated that F-actin is not required for Bem1p oscillation but may contribute to dampening such oscillation.

The septins are recruited by Cdc42p, assemble into a ring around the pre-bud site, and remain as a collar at the mother-bud neck for most of the cell cycle (McMurray and Thorner, 2009; Oh and Bi, 2011). The septins act as a scaffold that recruits a variety of proteins, whose correct localization to the neck is important for their functions. It is possible that the recruitment of the septins per se or the factors recruited by septins contribute to the dispersal of polarity factors. Two-color filming showed that the septin component Cdc3p accumulated at the pre-bud site ~5 min after the initial Bem1p clustering, when the oscillatory cycles were already completed in most cells (Fig. 2.6A). In cells either relocated the Bem1p cluster or had multiple clusters, septin recruitment only happened after relocation or competition had completed (Fig. 2.6B-C). The timing of septin recruitment indicates the septins do not contribute to the dispersal of polarity factors. However, septin accumulation happened around the period where high-amplitude Bem1p-GFP oscillation changed to lower steady state levels (Fig. 2.6A), suggesting septins are involved in damping oscillations. This potential role of septins may explain

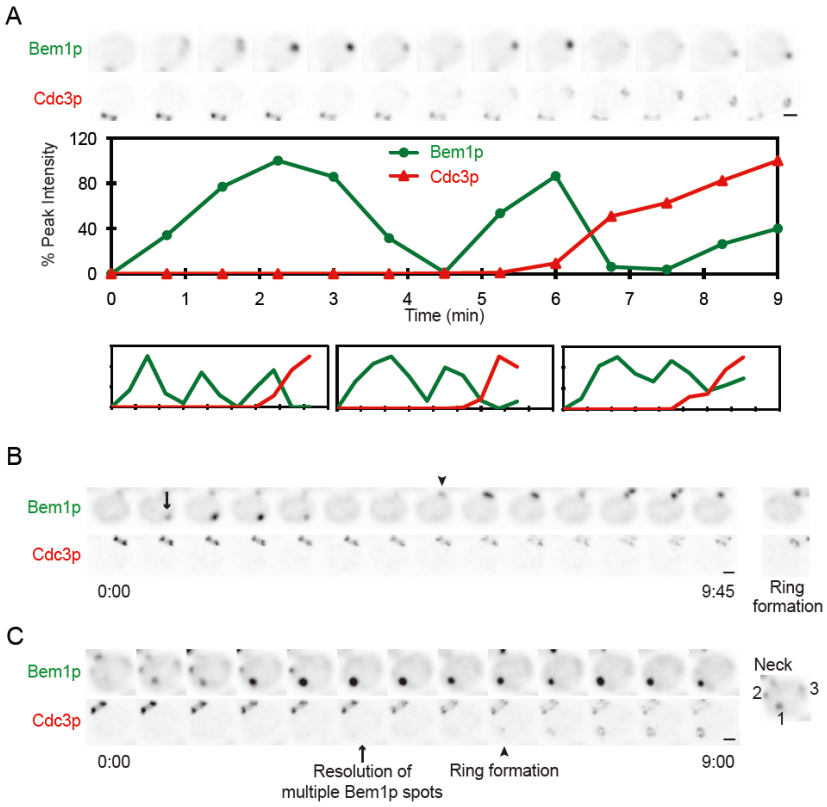

Figure 2.6 Septin polarization relative to Bem1p

(A) Septin accumulation (marked with Cdc3-mCherry) correlates with the dampening of Bem1p-GFP oscillation (DLY13098). Top panel is the cropped images of a cell showing Bem1p-GFP and Cdc3-mCherry signals. Middle panel is the quantification of the sum intensity changes. Lower panels are the quantifications of another three cells. **(B)** Septin accumulation happens after the relocation of Bem1p-GFP cluster. No septin signal is detected at the initial Bem1p-GFP cluster (arrow). Bem1p-GFP then relocates to a site near the old mother-bud neck where the remaining septins from cytokinesis obscure the new septin ring. **(C)** Septin accumulation (arrowhead) occurs after the competing clusters have resolved to a single cluster (arrow).

why we see more high-amplitude oscillations in Lat A-treated cells (Fig. 2.5D) because Latrunculin treatment is known to delay septin accumulation (Kozubowski et al., 2005).

2.2.5 Adding a negative feedback loop in a mathematical model of polarity establishment can lead to oscillatory polarization

Our findings indicate that the core polarity factors polarize in an oscillatory manner. The oscillations do not require the action of downstream F-actin and septins, thus the oscillations may be intrinsic to the core polarity factors. Current polarity establishment models with positive feedback that amplifies stochastic GTP-Cdc42p cluster can predict symmetry breaking polarization, but they are not able to explain oscillatory behavior. As mentioned above, oscillation phenomena in biology generally involve negative feedback (Novak and Tyson, 2008). We therefore tested if adding a negative feedback loop to the existing model of yeast polarity establishment could result in oscillatory polarization.

The starting positive feedback-only model (1), which was firstly developed by Goryachev and Pokhilko, incorporates Cdc42p, GDI, and a cytoplasmic Bem1p complex containing a Cdc42p effector PAK and Cdc42p-directed GEF (Goryachev and Pokhilko, 2008; Howell et al., 2009; Kozubowski et al., 2008). We simplified the model by eliminating GDI as a separate entity and subsuming its activity into the exchange of GDP-Cdc42p between membrane and cytoplasm (Fig. 2.7A). In this model, GTP-Cdc42p on the membrane binds to PAK and recruits Bem1p complexes, which in turn generates more GTP-Cdc42p by GEF in a positive feedback loop. Since the actual mechanism is not known, we tested two hypothetical negative feedback mechanisms that operate either

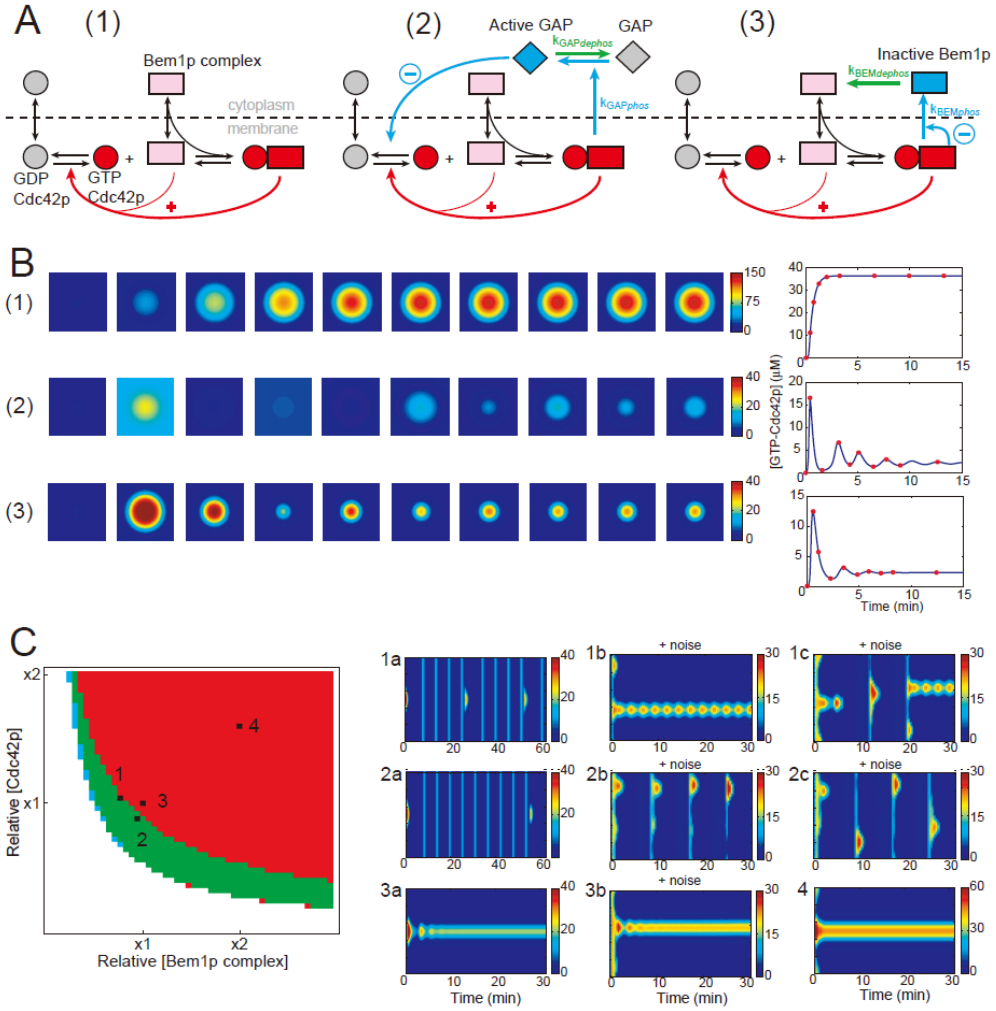

Figure 2.7 Incorporation of negative feedback to the current polarization model can generate several phenotypes observed in vivo

(A) Diagrams of the starting model (1) and two models incorporating either a GAP-mediated (2) or a Bem1p complex-mediated (3) negative feedback mechanism. Positive feedback and negative feedback are indicated as red and blue arrows, respectively. We assume GTP-Cdc42p/PAK activates the GAP (blue diamond in model 2) or inactivates Bem1p complex (blue rectangle in model 3). Dephosphorylation of the proteins resets their activity (green arrows). **(B)** Snapshots of simulations. The squares represent a two-dimensional plasma membrane flattened from a cell, and the color indicates the concentration of GTP-Cdc42p. Each red dot on the tracings to the right is from the snapshots, plotting GTP-Cdc42p concentration

versus time. **(C)** Behaviors of model 3. Left panel is the expanded view of the lower-left part of the [Cdc42]-[Bem1 complex] bifurcate diagram (Fig. 2.8D). The starting concentrations are designated as x1. (#1) Mixed Turing and Hopf Unstable: an initial perturbation leads to sustained oscillation, switching between uniform and localized patterns. (#2) Mixed Turing and Hopf Unstable: similar to (#1), but with less localized oscillation and more frequent uniform oscillations. (#3) Turing Unstable: a perturbation leads to dampened oscillation on the way to a steady polarized state. (#4) Turing Unstable (far away from the Turing-Hopf Unstable region): a small perturbation leads to a polarized steady state.

by activating an inhibitor (2) or inhibiting an activator (3). In model 2, we assume GTP-Cdc42p leads to the activation of Cdc42p-directed GAPs (perhaps by PAK-mediated phosphorylation), which then hydrolyze GTP-Cdc42p and disperse the cluster. Dephosphorylation of GAPs inactivates its activity, allowing another round of positive feedback to take place. In model 3, we assume that GTP-Cdc42p leads to the modification of the Bem1p complex (perhaps via PAK-mediated phosphorylation) and inactivates the Bem1p complex, thereby reducing the amount of complex available for the positive feedback. Dephosphorylation of the Bem1p complex restores its activity and allows another round of clustering.

Consistent with previous report, the simplified positive feedback-only model generated a stable GTP-Cdc42p cluster (Fig. 2.7B). In contrast, with appropriately tuned parameters, model 2 and 3 both displayed dampened oscillatory clustering of GTP-Cdc42p. In the oscillatory region of parameter space (green region in Fig. 2.7C), the dominant behavior predicted by the model was uniform and periodic accumulation of GTP-Cdc42p over the entire cortex (Fig. 2.7C, 1a and 2a). However, addition of noise in the models converted the spatially uniform oscillation into sustained oscillatory clustering (Fig. 2.7C, 1b and 1c). Moreover, simulations with noise in the negative feedback-containing models exhibited both competing and relocating clusters (Fig. 2.7C, 1b-c, 2b-c). Therefore, addition of negative feedback and noise to the positive feedback model predicts all the polarization dynamics observed in vivo.

2.2.6 Negative feedback improves robustness of polarity establishment

Why do yeast cells need a negative feedback in the polarity circuit? Intuitively, the negative feedback seems to be a self-destructive mechanism that can potentially destroy the polarized cluster. Although the positive feedback-only model 1 is good at forming a polarized cluster, we found that the ability of this model to polarize is very sensitive to the concentrations of GTP-Cdc42p and Bem1p complex. With 6.5-fold higher starting concentration of Cdc42p, model 1 initially could form a GTP-Cdc42p cluster but it eventually spread GTP-Cdc42p all over the plasma membrane, resulting in a uniform steady state (Fig. 2.8A). In contrast, incorporation of a negative feedback loop in model 2 and 3 allowed them to generate a stable, polarized GFP-Cdc42p cluster despite the elevated Cdc42p concentration. This prediction suggests that one advantage of negative feedback is to increase the robustness of polarity establishment in the face of fluctuating concentrations of polarity factors.

To determine how the behavior of our models responded to a broader range of polarity factor concentrations, we performed linear stability analysis. The models displayed four different types of steady-state behaviors as color-coded in Fig. 2.8B-D. The starting concentrations of Cdc42p and Bem1p complex used in the simulations for Fig. 2.7B are designated as x1. In the red region, the homogeneous state was not stable to small perturbations (Turing instability), and with any noise, the model evolved to a polarized state. In the white region, the homogeneous state was stable and even large perturbations could not induce the development of a polarized state. In the blue and grey regions, there was coexistence of uniform and polarized state. Only a sufficiently large perturbation was able to

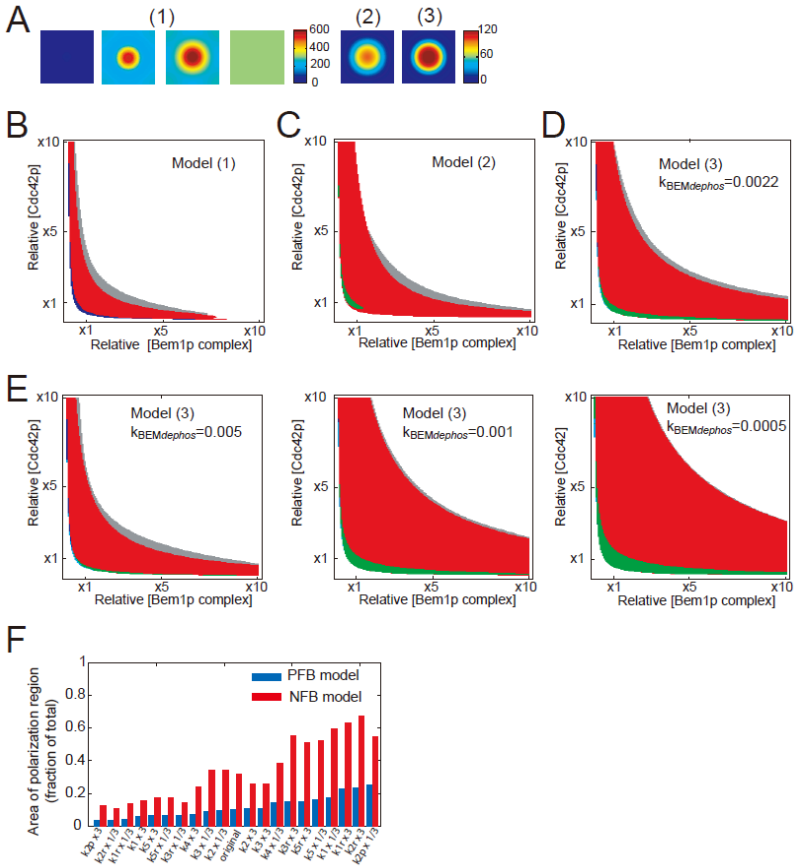

Figure 2.8 Negative feedback improves robustness of the polarity model

(A) Snapshots of simulations with 6.5-fold higher starting concentration of Cdc42p: model 1 spreads GTP-Cdc42p uniformly (left), whereas model 2 and 3 yield a polarized steady state (right). **(B)** Behavior of model 1 at varying polarity factor concentrations. (Red) Turning unstable region: polarization occurs in response to small perturbations. (Blue/grey) regions where both uniform and polarized states are stable: polarization occurs in response to large perturbation. (White) No polarized steady state. **(C)** Behavior of model 2. (Green) Sustained oscillations. **(D)** Behavior of model 3. **(E)** Robustness, indicated by the area of red regions, varies with changing negative feedback parameters. Model 3 was analyzed at the indicated values of $k_{BEMdephos}$. **(F)** Negative feedback increases the red polarization region in all cases. The area of the red region as a fraction of the total area in relative Cdc42p and Bem1p complex space is plotted as a measure of the model's robustness to varying concentrations of polarity factors. Blue and red bars report model 1 and 3 respectively. Paired bars use the same parameter sets, and pairs are ordered by increasing robustness of model 1.

make the transition from the uniform to the polarized state. In the green region, which only showed up in the negative feedback-containing models, small perturbations could induce sustained oscillation. The simulation in Fig. 2.7B was derived from the lower-left part of the red regions (also shown in Fig. 2.7C 3a-b). The parameters in the other part of the red region could not generate oscillation (Fig. 2.7C, 4).

For model 1, only a thin slice of parameter space developed a polarized state (Fig. 2.8B). Incorporation of either the GAP-mediated or Bem1p complex-mediated negative feedback both largely expanded the red region (Fig. 2.8C-D), indicating the negative feedback-containing models could effectively polarize GTP-Cdc42p with wider changes in polarity factor concentrations. The effect of negative feedback on increasing robustness was not sensitive to any rate constant value. Increasing or decreasing each parameter 3-fold from its original value did not prevent the expansion of the red region when a negative feedback loop was included (Fig. 2.8F). However, the increment of robustness was depended on the negative feedback parameters. For example, decreasing the dephosphorylation rate (green arrow in Fig. 2.7A) on Bem1p complex in model 3 progressively expanded the polarization-competent red region (Fig. 2.8E).

2.2.7 Polarity establishment is robust of overexpression of Cdc42p or GEF

To test whether the robustness of polarity establishment predicted by mathematical models indeed exist in yeast cells, we used the galactose-inducible promoter to overexpress Cdc42p or its GEF, Cdc24p. Because cells grow much more slowly and become more photosensitive when cultured in galactose, we employed a hybrid transcription factor (Gal4DBD-hER-VP16) that allows induction by β-estradiol in

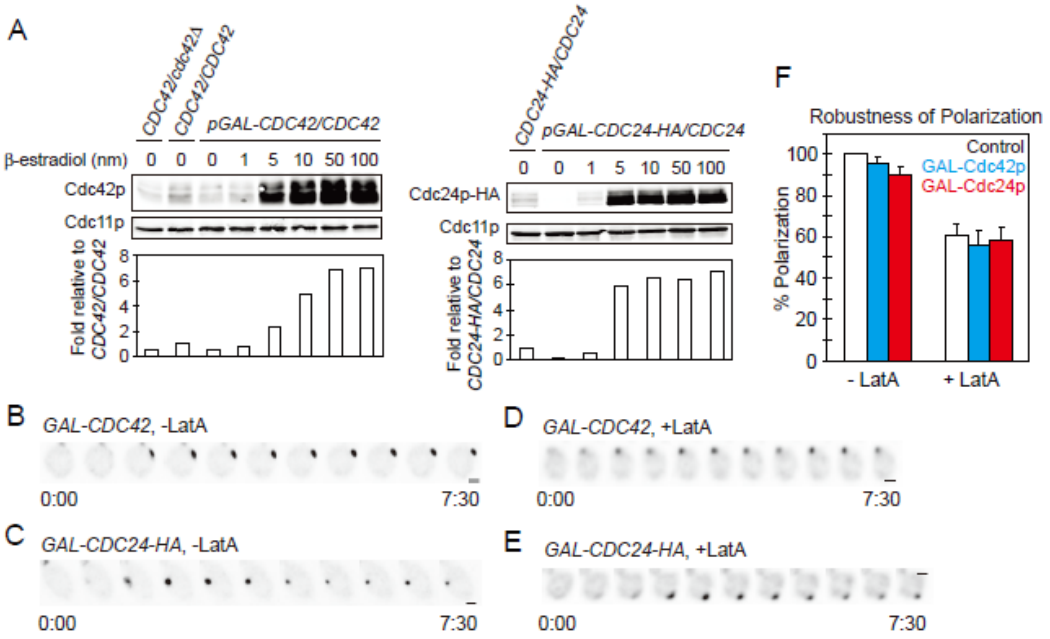

Figure 2.9 Polarity is robust to overexpression of Cdc42p and Cdc24p

(A) Western blot and quantification of Cdc42p (left, DLY12127) and Cdc24p (right, DLY13355) in response to β-estradiol (subsequent panels used 100 nM). **(B-E)** Bem1p-GFP polarization in representative cells overexpressing Cdc42p (B and D) or Cdc24p (C and E), in the absence (B and C) or presence (D and E) of Latrunculin A. **(F)** Quantification of the percentage of cells polarizing in control (white, DLY11971), Cdc42p-overexpressing (blue, DLY12127) or Cdc42p-overexpressing (red, DLY13355) strains in the absence or presence of Lat A (mean ± SEM).

glucose-containing media (Louvion et al., 1993; Takahashi and Pryciak, 2008). With ~7-fold overexpression of Cdc42p or Cdc24p (Fig. 2.9A), yeast cells still revealed robust polarization of Bem1p-GFP (Fig. 2.9B-C). A previous study reported that Cdc42p overexpression blocked polarization in cells lacking F-actin (Altschuler et al., 2008), but here we showed that Cdc42p or Cdc24p overexpressors exhibited comparable polarization efficiency to control cells, even in cells treated with Lat A (Fig. 2.9D-F). Thus, polarity establishment in yeast cells is indeed robust to elevated concentrations of Cdc42p or Cdc24p.

2.2.8 Polarity establishment with decreased amount of Cdc42p

The simulations that generated dampened oscillation were derived from the polarity factor concentrations in the lower-left part of the red region. Linear stability analysis predicted that small decreases in Cdc42p or Bem1p complex concentrations near this region could drive the parameter space into the green oscillatory region and develop several different behaviors, e.g. uniform oscillation, sustained oscillatory clustering (Fig. 2.7C) or excitable behavior (data not shown). Decreasing the concentrations even more could potentially drive the behavior into the homogeneous non-polarized steady state (white region). To test whether these behaviors could be observed experimentally, we decreased the expression of Cdc42p to sub-physiological levels. Initially, we used a hemizygous diploid strain (one copy of *CDC42* is deleted) which expressed 50% of the wild-type Cdc42p level (Fig. 2.10A). The cells were still able to polarize and Bem1p-GFP still displayed oscillatory clustering, even though the second peak and the eventual polarity level were much dimmer than the first peak (Fig. 2.10B). The cells also

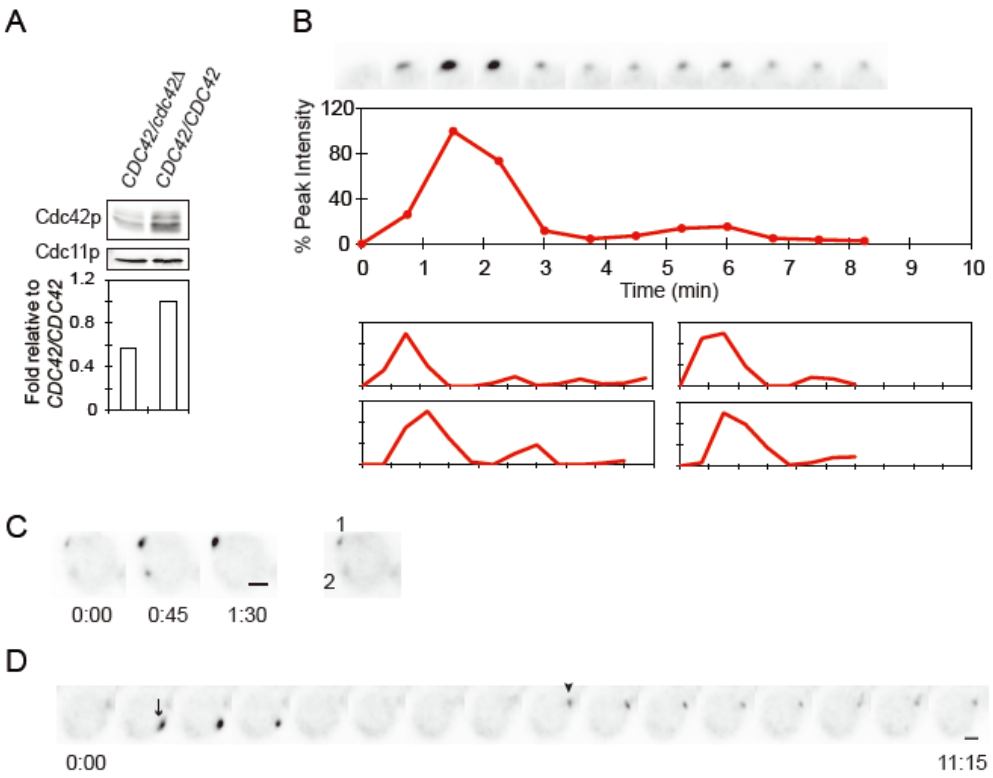

Figure 2.10 Polarity establishment in hemizygous *cdc42Δ/CDC42* strain

(A) Western blot and the quantification of Cdc42p in hemizygous *cdc42Δ/CDC42* (DLY13824) and homozygous *CDC42/CDC42* (DLY9200) diploid strains. **(B)** Oscillatory clustering of Bem1p-GFP in hemizygous *cdc42Δ/CDC42* diploid cells (DLY13824) pre-treated with HU. Top panel is the cropped images of the polarized cluster at 45 sec intervals. Middle panel represents the changes of Bem1p-GFP sum intensity at the polarized cluster. Bottom panels are the quantification of another four cells. **(C)** Growth and competition between multiple Bem1p-GFP clusters **(D)** Relocation of the Bem1p-GFP cluster. Scale bars, 2 μm.

displayed competition and relocation behaviors as predicted by the models (Fig. 2.10C-D). These results suggest that yeast polarity establishment is robust not only with increased component concentrations but also with decreased concentrations. We did not observe excitable behavior or uniform oscillation, but it is likely that with the detection limit of our microscope we are not able to detect these behaviors even if they did occur. We tried to further dial down the amount of Cdc42p by using β-estradiol-inducible system to express Cdc42p under the control of *GAL1* promoter (as the only copy of *CDC42*). Ideally, we could express very little Cdc42p by adding low concentrations of β-estradiol. However, we found that this promoter exhibited high cell-to-cell heterogeneity: some cells had normal shape, whereas others became large and round (i.e. failed to polarize) or even displayed irregular shapes. Due to the technical problems to systematically test the lower-expression regime, we did not continue studying the polarization behaviors under low polarity concentrations.

2.2.9 Effects of overexpressing a Cdc24p-Cla4p fusion protein

Although overexpressing Cdc24p did not affect the efficiency of polarization, it is unclear whether the amount of Bem1p complex increased with Cdc24p overexpression. The complex formation depends on the relative amount and the dynamic interactions between all three components, and potentially the components are subject to the regulation of negative feedback as posited in model 3. To circumvent the unknown regulation of complex assembly, we overexpressed a Cdc24p-Cla4p fusion protein that mimics the full complex (Kozubowski et al., 2008) (Fig. 2.11A). Time-lapse filming showed that most of the cells still polarized (upper panel of Fig. 2.11B), but some cells

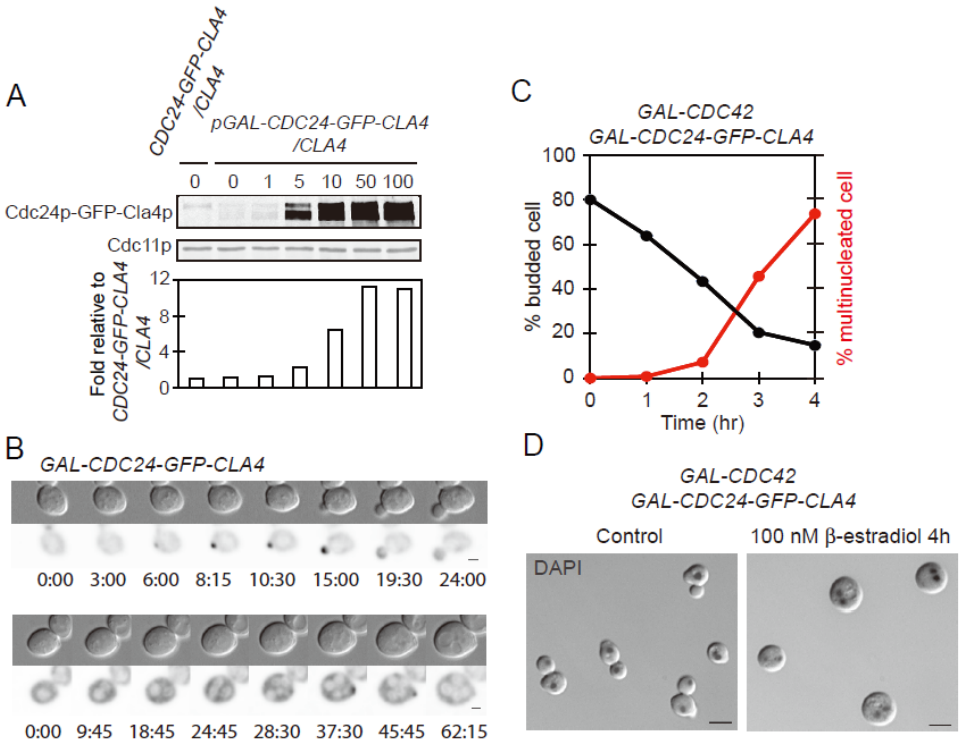

Figure 2.11 Effects of overexpressing a Cdc24p-Cla4p fusion protein

(A) Western blot and quantification of Cdc42p-GFP-Cla4p fusion protein. 1x indicates expression level from the *CDC24* promoter. **(B)** Cdc24p-GFP-Cla4p distribution in cells that do (top) or do not (bottom) polarize. Nuclei and vacuoles exclude the protein and appear light. **(C)** Plot of budding index and frequency of multinucleated cells following induction of bother Cdc42p and Cdc24p-GFP-Cla4p. **(D)** Representative cells from (C) after 0 hr (left) or 4 hr (right) of induction. Overlay of inverted DAPI staining and DIC images. Scale bars, 5 μm.

were delayed in polarization and a few cells underwent a full cell cycle without establishing polarity (lower panel of Fig. 2.11B). Overexpression of both Cdc42p and the Cdc24p-Cla4p fusion protein blocked the polarization in a majority of cells, leading to the accumulation of large, unbudded, multinucleated cells (Fig. 2.11C-D). The combined expression of Cdc42p and the fusion protein presumably drives the system into the upper-right white region of parameter space, where Cdc42p stays in a stable non-polarized steady state.

2.2.10 Cdc42p or Cdc24p overexpressors retained rapid competition between clusters and the ability to buffer GTP-Cdc42p level

Even though overexpressing Cdc42p or Cdc24p did not affect the efficiency of polarization, these overexpressors exhibited different polarization dynamics compared to control cells. Both Cdc42p and Cdc24p overexpression dampened oscillation and increased the frequency of forming multiple clusters (Fig. 2.12A, 2.9B-C). Cdc42p overexpressors also displayed a higher frequency of relocation. With elevated amount of Cdc42p or Cdc24p, we expected that multiple clusters would grow larger and thus take a longer time to compete (Howell et al., 2009). However, the majority of overexpressors with multiple clusters still resolve to a single cluster rapidly (Fig. 2.12B). We assessed the amount of GTP-Cdc42p polarized in the cluster using the PBD probe. Despite the cell-to-cell variation in the total amount of the probe in the cell, ~19% of the probe was polarized in late-G1 wild-type cells. Surprisingly, a similar percentage of PBD probe was polarized in Cdc42p overexpressors, suggesting yeast cells are able to buffer the level of

GTP-Cdc42p in the cluster against Cdc42p overexpression, explaining why competition remained fast.

To assess how models with and without negative feedback would affect competition time, we simulated the competition between two clusters starting with 55:45 Cdc42p content. Model 1 predicted that the increases in Cdc42p or Bem1p complex concentrations would elevate the steady-state level of GTP-Cdc42p (Fig. 2.12D), which correspondingly resulted in slower resolution of competition (Fig. 2.12E). In contrast, model 3 predicted that negative feedback could buffer the level of GTP-Cdc42p (Fig. 2.12F), which allowed competition to remain rapid (Fig. 2.12G), as observed experimentally. Therefore, another benefit of having negative feedback in the polarity circuit is that it ensures competition happens fast when multiple clusters form, even if the component concentrations are increased.

The buffering effect of negative feedback significantly speeded up competition in the majority of simulations, generating cluster coexistence times that are consistent with experimental results. However, there were exceptions in some of the parameter space. In model 3, competition failed at sufficiently high Cdc42p and Bem1p complex concentrations. With these parameters, the cluster equalized instead of competing, and simulations evolved to a steady state with two equal-sized clusters (Fig. 2.12H). In cells, this situation would lead to the growth of two buds. Interestingly, ~1% of cells overexpressing the Cdc24p-Cla4p fusion protein made two buds (Fig. 2.12I). Some two-budded cells stably polarized to two sites (Fig. 2.12J), whereas others abandoned one of the polarity clusters and formed two buds with unequal sizes.

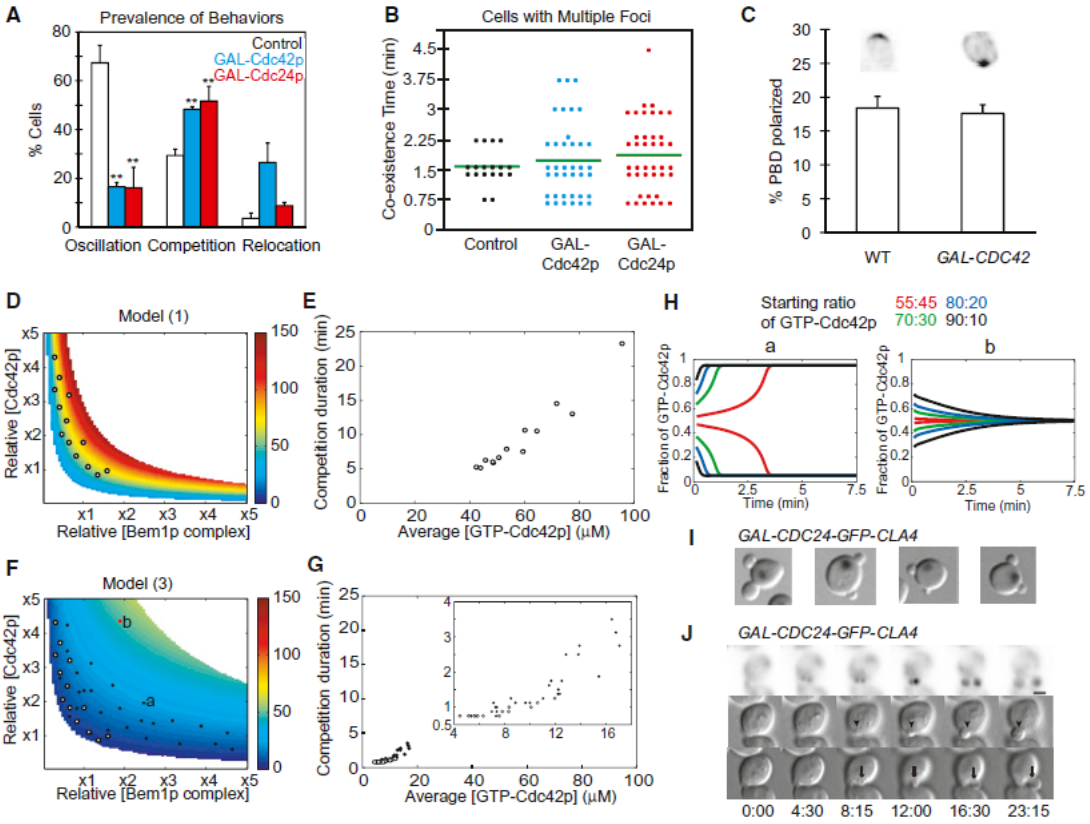

Figure 2.12 Negative feedback buffers the level of GTP-Cdc42p in the clusters and speed up competition

(A) Prevalence of high-amplitude oscillation (left), multicluster intermediates (middle), and relocating cluster (right) in control (white, DLY9200), Cdc42p-overexpressing (blue, DLY12127), or Cdc24p-overexpressing (red, DLY13355) strains (mean ± SEM). **p < 0.01 by two-tailed t test; significant difference between controls and overexpressors. **(B)** Quantification of the time taken to resolve multicluster intermediates. **(C)** The fraction of the PBD probe (mean ± SEM) that is polarized in late G1 cells is similar with (right) or without (left) Cdc42p overexpression. **(D)** Steady-state GTP-Cdc42p levels in model 1 change rapidly as component concentrations are increased. Color indicates steady-state GTP-Cdc42p concentration in the parameter space displaying Turing instability. Circles indicate points used for simulations in (E). **(E)** Correlation between GTP-Cdc42p concentration and the time taken to resolve competition. Each symbol represents a simulation, at parameter values from the circles in (D), of the competition between two unequal clusters (ratio 55:45), plotting the time taken to resolve competition (y

axis) and the average GTP-Cdc42p concentration of the two-cluster starting state (x axis). **(F)** Steady-state GTP-Cdc42p levels in model 3 are buffered against increases in component concentrations. Symbols indicate points used for simulations in (G). White circles are as in (D), whereas black symbols are in the expanded polarity region. Symbols labeled ‘‘a’’ and ‘‘b’’ indicate parameters used in (H). **(G)** Negative feedback maintains rapid competition in a broad range of parameter space. Kinetics of competition between clusters (as in E), at parameter values indicated in (F). (Inset) Expanded view of lower-left quadrant. **(H)** Negative feedback can lead to equalization of clusters instead of competition between clusters at high levels of polarity proteins. Simulations are as described in (E), with the indicated starting ratios between unequal clusters, using the parameter values from the symbols labeled ‘‘a’’ and ‘‘b’’ in (F). **(I)** Examples of two-budded cells from a culture induced to express Cdc24p-Cla4p fusion for 4 hr. Overlay of inverted DAPI staining and DIC images. **(J)** Simultaneous growth of two buds (arrow and arrowhead in different DIC Z planes) and polarization of Cdc24p-Cla4p fusion to both buds.

2.2.11 Testing candidate GAP-mediated negative feedback mechanisms in vivo

Inclusion of a GAP-mediated or Bem1p complex-mediated negative feedback mechanisms in the models both led to oscillatory clustering of polarity factors and buffering of GTP-Cdc42p level against variation in the polarity factor concentrations. To determine whether these mechanisms exist in vivo and play the role as predicted by the models, we first tested the candidate negative feedback mechanism including GAPs. We assume the disruption of negative feedback would lead to the reduction or elimination of oscillation. Deletion of a single GAP (*RGA1, RGA2* or *BEM3*) or the combination of *rga1Δ rga2Δ* did not stop Bem1p-GFP from oscillating (Fig. 2.13A-D), suggesting these GAP deletions did not abrogate negative feedback loop. However, we later found out that the oscillation behavior appears to be a rather fragile phenotype because slight stress or changes in filming conditions (e.g. exposure to higher intensity of light, or higher filming temperature, or overexpression of polarity factors) can easily reduce or eliminate oscillation. Thus, the reduction or elimination of oscillation does not provide strong evidence that the negative feedback has been altered. Alternatively, we postulate that the disruption of negative feedback would reduce or disable the buffering of GTP-Cdc42p level in the face of elevated amount of polarity factors, thereby leading to large, unbudded cells. Cells deleting a single GAP were still capable of polarizing Bem1p-GFP when Cdc42p was overexpressed (Fig. 2.13E-G), suggesting that Rga1p, Rga2p or Bem3p alone is not involved in the negative feedback. Due to the severe defects caused by *BEM2* deletion, we haven't assessed the potential involvement of Bem2p in the

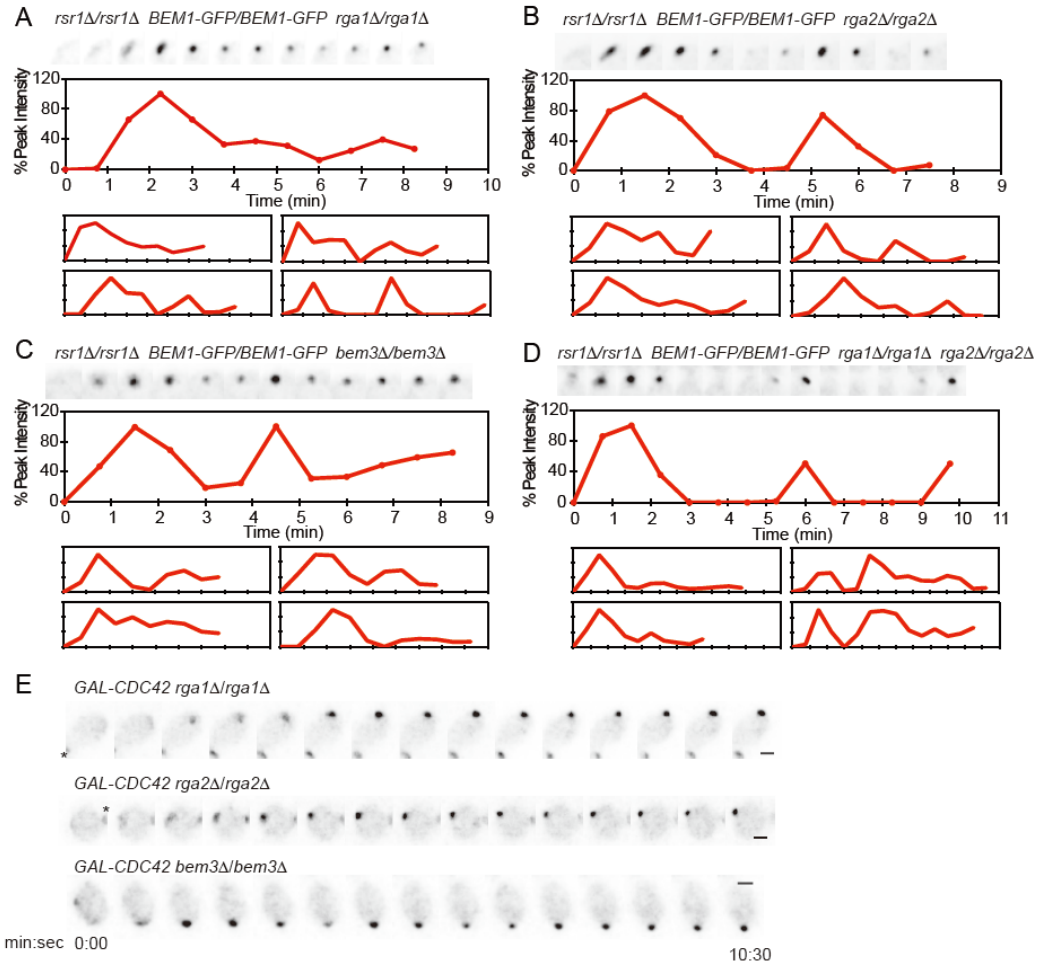

Figure 2.13 Testing GAP-mediated negative feedback mechanism in vivo

(A-D) Oscillatory clustering of Bem1p-GFP is still present in diploid strains with homozygous deletion of *RGA1* (A, DLY11223), *RGA2* (B, DLY11224), *BEM3* (C, DLY11225), or *RGA1* and *RGA2* (D, DLY11125). The cells are pre-treated with HU prior to filming. Top panels are the cropped images of the polarized cluster. Middle panels are the quantification of Bem1p-GFP sum intensity changes at the polarized cluster. Bottom panels are quantification of another four cells. **(E)** Single GAP deletion strains with overexpression of Cdc42p are able to polarize Bem1p-GFP. *rga1Δ* (DLY13961), *rga2Δ* (DLY14009), or *bem3Δ* (DLY14010) strains were incubated with 100 nM β-estradiol for 3 hr to induce Cdc42p overexpression and then mounted on the slab containing β-estradiol for filming. Asterisk indicates old mother-bud neck. Scale bars, 2 μm.

negative feedback. We also haven't systematically tested every combination of GAP deletions because some of them resulted in severe sickness or even lethality. Thus, we haven't completely ruled out the GAP-mediated negative feedback mechanism, but it may involved the action of several GAPs.

2.3 Discussion

2.3.1 Negative feedback during polarity establishment

Filming of symmetry-breaking polarization at high resolution under low-light imaging conditions revealed that clusters of polarity factors congregated rapidly (often within 45 s) and then unexpectedly dispersed, subsequently reforming and dispersing up to three more times before stabilizing (Figs. 2.2 and 2.3). The dispersal occurred even in cells that only displayed a single polarity cluster, indicating that dispersal is not due to competition between clusters. In some cases, the dispersal appeared to be complete, and cells went on to assemble a new polarity cluster elsewhere (''relocation''). Oscillatory clustering was not predicted by existing models of polarity establishment and suggests that positive feedback-mediated initial polarization is rapidly antagonized by a negative feedback loop. Mathematical modeling suggested that adding a negative feedback loop to a previous model for polarity establishment could lead to oscillatory clustering, and different negative feedback mechanisms (acting either through a Cdc42p-directed GAP or Bem1p complex) produced qualitatively similar results (Fig. 2.7B). The mechanism of negative feedback in cells remains to be determined.

The negative feedback models predicted that oscillation would be muted when the concentrations of polarity factors were increased (Fig. 2.7C), and this was confirmed experimentally (Fig. 2.12A). The sustained oscillations predicted by the models consisted mainly of spatially uniform accumulation of GTP-Cdc42p all over the cortex followed by GTP hydrolysis and return of Cdc42p to the cytoplasm. However, addition of noise eliminated such uniform oscillations and instead produced oscillatory clustering (Fig. 2.7C). Noise-containing simulations exhibited rapid multicluster competition followed by oscillation, as well as relocation of clusters. Thus, in appropriate parameter regimes, models that incorporate negative feedback and noise in addition to the previously modeled positive feedback can reproduce all of the polarity dynamics that we observed in cells.

Negative feedback-containing models produced either sustained or intrinsically damped oscillations, depending on the concentrations of polarity factors (Fig. 2.7C). However, in cells, the oscillatory clustering was always damped. Damping was correlated with the arrival of septins at the polarization site and was delayed in the absence of F-actin (a condition that delays septin assembly) (Figs. 2.5 and 2.6). Thus, it may be that the core polarity machinery has the capacity to produce sustained oscillatory clustering and that downstream cytoskeletal factors act to dampen the oscillation.

It is unclear what advantage could stem from high-amplitude oscillations in polarity factor concentration. When cells were exposed to more stressful imaging conditions, they exhibited lower-amplitude oscillation, as did cells that were filmed without the photoprotective hydroxyurea pretreatment (Howell et al., 2009). Given the

sensitivity of the behavior to filming conditions and component concentrations, it seems unlikely that such oscillation is important in and of itself. Instead, oscillation may have arisen as a byproduct of negative feedback. As discussed below, adding negative feedback to the polarity model improves its robustness. Interestingly, robustness could be further improved by lowering the rates at which a negative feedback-modified Bem1p complex or GAP returned to its baseline state. Lowering those rates introduces a delay (as the modified Bem1p complex or GAP accumulates rapidly but takes time to return to its basal state), which, in turn, favors oscillatory behavior. Thus, oscillations might arise as a byproduct of a negative feedback loop that is present to optimize robustness.

Oscillations in polarized growth (after polarity establishment) have been particularly well studied in plants (Hepler et al., 2001), in which the oscillatory growth of pollen tubes is thought to involve interlinked positive and negative feedback loops (Yan et al., 2009). It is unclear whether oscillation per se is advantageous, as pollen tubes switch from prolonged continuous growth to oscillatory growth without overt changes in overall elongation speed or morphology (Feijo et al., 2001). Thus, the use of negative feedback to promote homeostasis or robustness may lead in some cases to the appearance of unselected oscillations, which may or may not be beneficial in themselves (Cheong and Levchenko, 2010; Feijo et al., 2001).

2.3.2 Robustness of polarity establishment

Although capable of polarity establishment, a model with only positive feedback is fragile in that increasing concentrations of polarity factors quickly overwhelm the system, causing GTP-Cdc42p to spread all over the cortex. A benefit of negative

feedback is to improve robustness to such changes: the negative feedback prevents runaway accumulation of GTPCdc42p, so the model retains the ability to polarize over a much wider range of polarity factor concentrations. Similar robustness predictions were obtained regardless of the modeled feedback mechanism or specific parameters (Figs. 2.7 and 2.8). Thus, negative feedback confers improved robustness regardless of the precise feedback mechanism.

The modeling results prompted us to test whether yeast polarization is indeed robust to increased levels of polarity factors, and we found that cells polarized just as efficiently when Cdc42p or Cdc24p were overexpressed. The robustness that we observed is consistent with older reports that Cdc42p overexpression is tolerated by yeast (Ziman and Johnson, 1994) but is contrary to the conclusion from a recent study suggesting that Cdc42p overexpression blocked polarity establishment in cells lacking F-actin (Altschuler et al., 2008). The apparent difference between those results and ours may stem from the fact that we overproduced wild-type Cdc42p whereas they used a myc-GFP-Cdc42p construct that is somewhat toxic (Fig. 2.4). In addition, they used the same probe to score polarization, potentially making it difficult to detect a polarized signal above the high unpolarized background in overexpressing cells. We conclude that the yeast polarity establishment circuit is robust to increases in polarity factor concentration, even in cells lacking F-actin, and that robustness is likely to be conferred by negative feedback.

With the one-step negative feedback models that we considered, oscillations occur near the lower bound of the polarization competent parameter regime, perhaps suggesting

that cells sit near this boundary and would be very sensitive to any decrease in Cdc42p concentration. However, a 2-fold reduction in Cdc42p level (in hemizygous diploids, Fig. 2.10) does not prevent polarization. Adding extra steps to lengthen the negative feedback loop can dramatically expand the region of parameter space capable of sustaining oscillations (data not shown) so that cells displaying oscillations would be robust to both increases and decreases in polarity factor concentrations.

2.3.3 Competition between polarity clusters

A long-standing question in the polarity field concerns why cells develop one and only one ‘‘front.’’ We recently suggested that, in yeast, positive feedback could give rise to more than one polarity cluster, but then the clusters would compete with each other so that a single winner would emerge (Howell et al., 2009). Alternatively, the small absolute numbers of a limiting polarity factor might make it unlikely that more than one cluster could develop (Altschuler et al., 2008). With previous filming protocols, it was difficult to detect the multicluster intermediates predicted by the competition hypothesis, but with improved imaging, we now document such intermediates in ~25% of cells breaking symmetry (rising to ~50% upon overexpression of Cdc24p or Cdc42p). These numbers represent a lower bound for the real incidence of such intermediates, as technical issues may prevent us from detecting small and/or short-lived clusters. Thus, multicluster intermediates are very frequent, and competition between polarity clusters is critical to prevent the development of more than one front.

Multicluster intermediates were short-lived, generally resolving to a single cluster within 2 min. Surprisingly, competition was similarly rapid even in cells overexpressing

Cdc24p or Cdc42p, which were expected to build clusters containing more polarity proteins. As larger clusters take longer to dismantle during competition, it should take considerably longer to resolve the competition. Negative feedback can buffer the accumulation of polarity factors in clusters so that overexpression may not significantly increase the amount of Cdc42p or other factors in the cluster, explaining why competition did not take much longer in overexpressing cells than in controls. Thus, a second benefit of negative feedback in the polarity circuit is that, when more than one cluster forms, competition between clusters is more rapid.

The competition between clusters predicted by the modeling is biased such that larger clusters outcompete smaller ones (Howell et al., 2009). However, we detected rare instances in which a smaller cluster appeared to win (e.g., Fig. 2.1A, cell 3). Negative feedback could, in principle, explain this observation if such feedback includes a partly localized component. That is, growth of a cluster may induce a negative feedback that is slightly stronger in the vicinity of that cluster than it is in the rest of the cell. If that were the case, then an initially stronger cluster might self-destruct, whereas a later-emerging distant cluster succeeds.

An unexpected prediction from mathematical modeling of polarity circuits with negative feedback was that, at high Cdc42p and Bem1p complex concentration, competition should fail to resolve polarity clusters. Instead, two clusters would tend to equalize so that each contains the same amount of polarity proteins. Presumably, this would lead to the formation of two buds in yeast, perhaps explaining the observation of occasional two-budded cells in strains overexpressing Bem1p (Howell et al., 2009) or a

Cdc24p-Cla4p fusion (Fig. 2.11). However, such cells might also arise if competition were drastically slowed (Howell et al., 2009).

3. Interaction between Bud-Site Selection and Polarity-Establishment Machineries

Published as Wu et al. 2013 *Phil. Trans. R. Soc. B* 368(1629):20130006.
This chapter is a result of collaborative work. The author contributed to the experimental part of this work. Mathematical modeling was done by Natasha Savage.

3.1 Introduction

The direction of polarization can be determined by chemical or physical signals. In *Saccharomyces cerevisiae*, the site of Cdc42p activation is influenced by a 'bud-site-selection' system that depends on the Ras-family GTPase Rsr1p. However, yeast mutants lacking Rsr1p break symmetry and polarize to a single, apparently random, site (Bender and Pringle, 1989; Chant and Herskowitz, 1991). Theoretical analyses dating back to Turing (Turing, 1952) showed that spontaneous pattern formation from homogeneous starting conditions could occur if autocatalytic biochemical reactions amplified small clusters of 'morphogens' (in this context, polarity factors) arising from stochastic fluctuations. Symmetry breaking in yeast does not require polymerized actin or tubulin, but (at least in *rsr1Δ* cells) it does require a complex scaffolded by Bem1p (Irazoqui et al., 2003). Bem1p complex creates a positive feedback loop that amplifies small, stochastic cluster of GTP-Cdc42p and promotes the growth of a cortical cluster of GTP-Cdc42p (Goryachev and Pokhilko, 2008; Howell et al., 2009; Johnson et al., 2011; Kozubowski et al., 2008). The Bem1p complex diffuses rapidly in the cytoplasm, allowing the complexes to be rapidly recruited to a growing GTP-Cdc42p cluster. By contrast, GTP-Cdc42p diffuses slowly on the membrane, so the cluster does not dissipate too rapidly.

During symmetry breaking, some mechanism must ensure that only one among all of the potential sites develops into the cell's front. As shown in chapter 2, imaging of polarity establishment in *rsr1Δ* cells revealed that cells frequently 'grow' more than one cluster of Cdc42p, but the clusters then compete with each other and a single winner emerges (Fig. 2.1) (Howell et al., 2012). Computational simulations of the Cdc42p/Bem1p system indicated that nascent polarity clusters would compete with each other for cytoplasmic Bem1p complexes and that the largest cluster would eventually win (Goryachev and Pokhilko, 2008). Competition may be accelerated by the presence of negative feedback in the polarity pathway (Fig. 2.12G). Rapid competition could explain why cells only make one bud, and some experimental manipulations intended to slow competition resulted in the simultaneous formation of two buds (Howell et al., 2009) (Fig. 2.12I-J).

In wild-type yeast cells, polarization and bud emergence occur at sites influenced by positional markers or 'landmarks': transmembrane proteins deposited at specific places during bud formation, anchored to the rigid cell wall, and then inherited by daughter cells (Bi and Park, 2012; Chant, 1999; Harkins et al., 2001). During cytokinesis, the landmark protein Axl2p is deposited in a ring on either side of the cleavage furrow (Gao et al., 2007) (Fig. 3.1A). The distal (previously the bud tip) and proximal (previously the neck) poles of newborn cells are marked by the landmark proteins Bud8p and Bud9p, respectively (Harkins et al., 2001) (Fig. 3.1B). Haploid cells use Axl2p to select 'axial' sites, in which the new 'front' is established adjacent to the immediately preceding cytokinesis site, so that sequential buds emerge next to each other in a chain

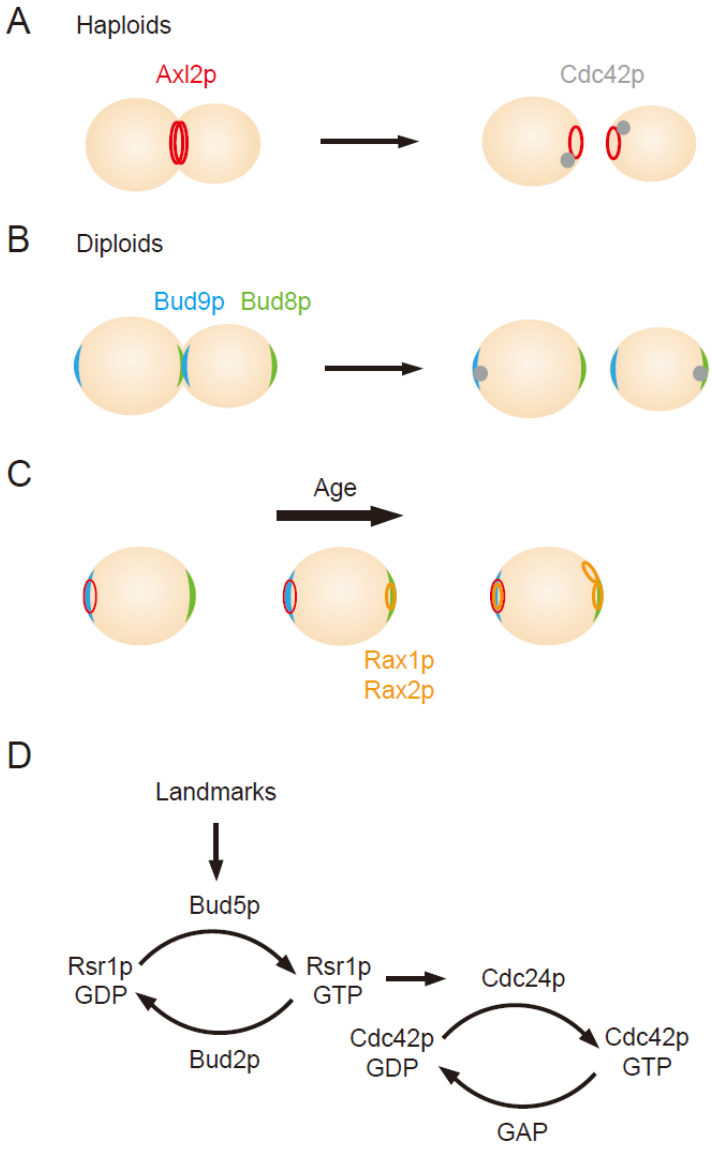

Figure 3.1 Bud-site selection in yeast

(A) Haploids. (B) Diploids. (C) Additional landmarks deposited as cells replicate. (D) Landmarks influence GTP-loading of Cdc42p via Rsr1p and its regulators.

(Chant and Pringle, 1995). Diploid cells use Bud8p and Bud9p to select new sites in a 'bipolar' pattern, in which the new 'front' is established at one of the two cell poles, and sequential buds may emerge at opposite ends (Chant and Pringle, 1995). Additional landmark proteins, Rax1p and Rax2p, are deposited in a ring marking each previous bud site, and also contribute to bud-site selection in diploids (Chen et al., 2000; Fujita et al., 2004; Kang et al., 2004).

Although haploids and diploids prefer to use different landmark proteins, all landmarks are deposited in both haploid and diploid cells. Moreover, genetic findings indicate that all landmarks are potentially active: if the preferred landmark-encoding gene is deleted, the other landmarks are used instead. Thus, a first-generation daughter cell is born with three landmarks, and mother cells acquire more marked sites as they age (Fig. 3.1C).

The landmark proteins interact with Bud5p, a GEF that promotes localized activation of Rsr1p (Bender, 1993; Kang et al., 2001; Marston et al., 2001; Park et al., 2002; Park et al., 1999; Zahner et al., 1996) (Fig. 3.1D). The GAP, Bud2p, promotes GTP hydrolysis by Rsr1p, thereby restricting Rsr1p-GTP accumulation to the vicinity of the landmarks (Bender, 1993; Park et al., 1993; Park et al., 1999). Rsr1p-GTP binds to the Cdc42p-directed GEF, Cdc24p, promoting localized GTP-loading of Cdc42p (Shimada et al., 2004; Zheng et al., 1995) (Fig. 3.1D). In this way, the pre-localized landmarks influence where Cdc42p GTP-loading takes place, and hence where a new front will form.

One could imagine that the symmetry breaking process is a backup pathway that is only used when the normal cues are absent. In this view, an intact bud-site-selection

system actually chooses the future polarity site prior to activating Cdc42p. If that is correct, then unlike in *rsr1Δ/rsr1Δ* cells, all *RSR1/RSR1* cells would form only one polarity cluster. Alternatively, the bud-site-selection system may simply activate a little Cdc42p at several landmark-designated 'permitted' sites for polarity. As has long been recognized (Chant and Pringle, 1995), the landmarks define many possible polarization sites: there is an entire ring of potential sites marked by Axl2p, and both poles are marked by Bud8p and Bud9p. In that scenario, we might see more than one initial polarity cluster in *RSR1/RSR1* cells, with the final polarity site determined by competition between clusters as seen in *rsr1Δ/rsr1Δ* cells.

3.2 Results

3.2.1 Multicluster intermediates resolved to a single site in *RSR1* cells

To image polarity establishment in *RSR1* cells, we used the same hydroxyurea arrest-release synchronization protocol to enrich the population of cells about to polarize and monitored Bem1p-GFP probe. HU treatment added benefit of reducing phototoxicity, allowing imaging at higher spatiotemporal resolution. In both haploid (*RSR1*) and diploid (*RSR1/RSR1*) cells, polarity sites were established in the expected locations (adjacent to the division site in haploids, at one or the other pole in diploids).Many cells (40 of 65 diploids imaged) initially developed more than one polarity cluster, and the multicluster intermediates resolved to a single site in a manner suggestive of competition (Fig. 3.2A-B). This observation suggests that polarity establishment in *RSR1* cells proceeds via the

same basic positive feedback and competition process as in cells breaking symmetry, with the exception that Rsr1p biases the location of initial polarity cluster growth.

Quantification of the time taken to resolve multicluster intermediates indicated that competition was slower in *RSR1/RSR1* cells than in *rsr1Δ/rsr1Δ* cells (Fig. 3.2C). Potential reasons for this difference are considered in the Discussion.

It was conceivable that the synchrony protocol we used might alter the polarization process. However, we detected competition between polarity clusterseven in unsynchronized proliferating cells (15 of 40 diploids imaged; Fig. 3.2D).

To assess how polarization dynamics might be affected by actin-mediated processes like vesicle trafficking, we imaged unsynchronized cells treated with Latrunculin A to depolymerize F-actin. As before, several cells (eight of 32 diploids imaged) displayed competition between polarity clusters (Fig. 3.2E). However, whereas in untreated cells the polarity site remained stably located until bud emergence, a subset of Latrunculin-treated cells (nine of 32 diploids imaged) displayed polarity-site 'relocation' (Fig. 3.2F). In these cases, the Bem1p cluster disappeared from one pole and appeared at the other, sometimes repeatedly (a 'ping-pong' pattern: Fig. 3.2G). This phenotype suggests that in the absence of F-actin, landmarks at both poles (in diploids) continue to compete for polarity proteins even after a large polarity cluster has formed. Thus, F-actin may be needed to 'lock in' the initially chosen polarity cluster.

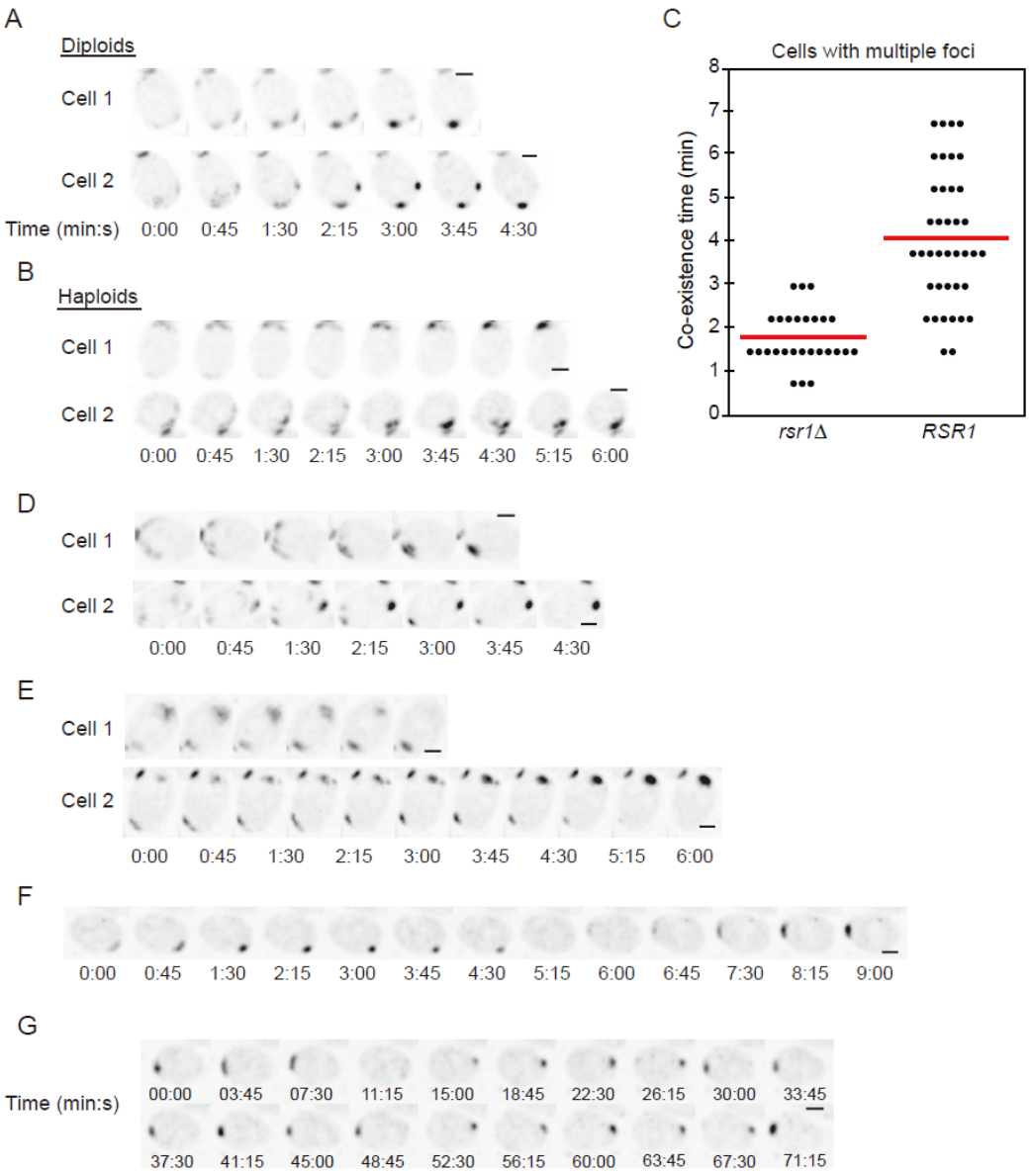

Figure 3.2 Competition among polarity clusters in wild-type cells

(A-B) Growth of multiple Bem1p-GFP clusters and resolution to a single cluster in wild-type diploid (A, DLY9201) and haploid (B, DLY9069) cells. Cells were pre-treated with HU prior to filming. The old mother-bud neck signal left from the previous cytokinetic site is visible at the top (A) and bottom (B) of the cropped images. t = 0 indicates the first detection of multiple clusters. **(C)** Coexistence time

of multiple clusters: time between the detection of multiple clusters and the first time frame with only one cluster in *rsr1Δ/rsr1Δ* (n = 27) and *RSR1/RSR1* cells (n = 39). Each dot represents one cell, and the red line is the average coexistence time. **(D)** Competition between Bem1p-GFP clusters is also observed in unsynchronized *RSR1/RSR1* cells. **(E)** Competition between Bem1p-GFP clusters is also observed in Latrunculin A-treated *RSR1/RSR1* cells lacking F-actin. **(F)** Latrunculin A-treated *RSR1/RSR1* cells sometimes displayed relocation of the Bem1p-GFP cluster from one pole to another. **(G)** In extreme cases, Bem1p-GFP in Latrunculin A-treated cells relocates back and forth between the two poles. Scale bars, 2 μm.

3.2.2 Dynamics of polarization in *RSR1* cells

In *rsr1Δ/rsr1Δ* cells, initial clustering of polarity factors is followed by dispersal and re-clustering in an oscillatory manner, presumably as a result of negative feedback in the polarity circuit (Figs. 2.1 and 3.3A). Comparison of *RSR1/RSR1* and *rsr1Δ/rsr1Δ* cells revealed significant differences in the dynamics of polarity clusters: the initial clustering was slower in *RSR1/RSR1* cells, and subsequent dispersal was also slower (Fig. 3.3B). As a result, Bem1p levels did not oscillate with high amplitude in *RSR1/RSR1* cells (because haploid cells polarize near the previous cytokinesis site and

Bem1p is localized to both the cytokinesis site and the polarity site, the dynamics of polarization are harder to distinguish in haploids so this analysis focused on diploid cells). Peak levels of Bem1p at the polarity site were lower in *RSR1/RSR1* cells than they were in *rsr1Δ/rsr1Δ* cells (Fig. 3.3C). In addition to the differences discussed above, a subset of *RSR1* and *RSR1/RSR1* cells (17 of 51 haploids and 12 of 65 diploids) exhibited a behavior not seen in *rsr1Δ/rsr1Δ* mutants: Bem1p accumulated to intermediate levels at one pole but then appeared to fluctuate rapidly at that pole for 10-20 min before strengthening and coalescing to a tighter spot prior to bud emergence (Fig. 3.4). This subset of cells appears to polarize by a two-step process in which an initial stage (not obvious in the majority of cells imaged) involves low-level noisy recruitment of Bem1p to Rsr1p-demarcated sites. Possible interpretations of this result are considered in the Discussion.

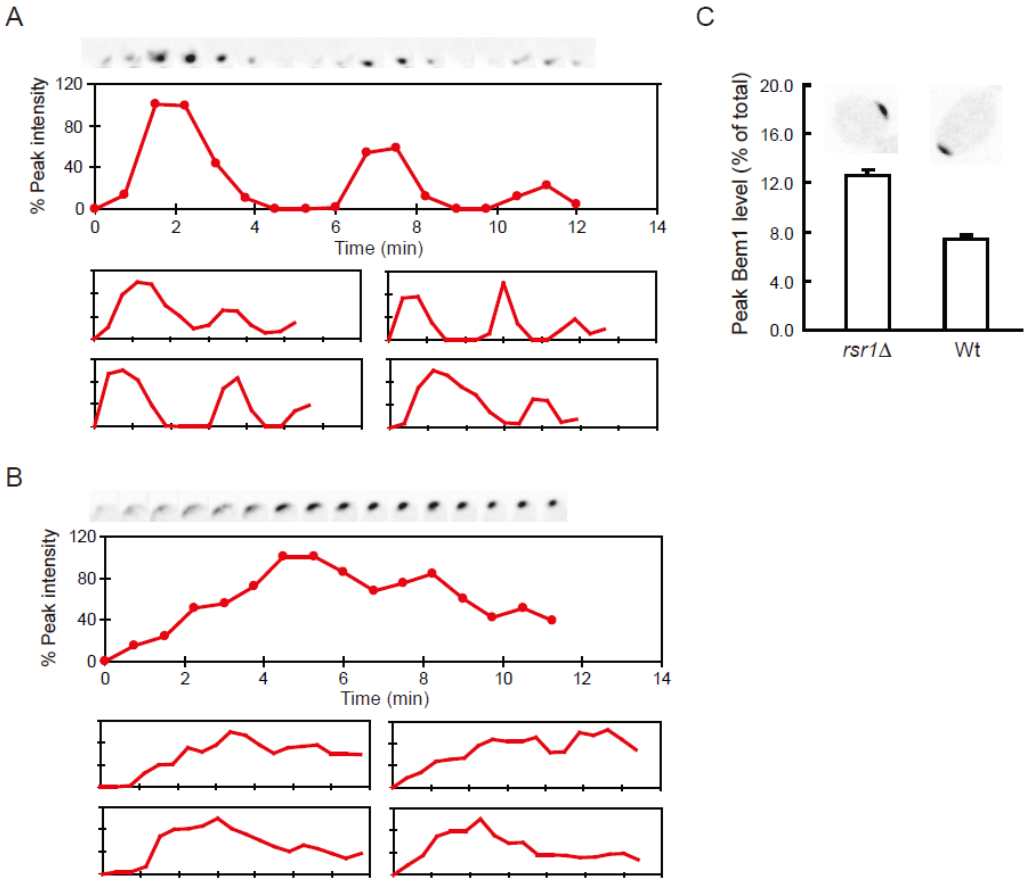

Figure 3.3 Dynamics of Bem1p-GFP polarization in diploids

(A-B) Clustering of Bem1p-GFP in *rsr1Δ/rsr1Δ* (A, DLY9200) and *RSR1/RSR1* (B, DLY9201) cells. Top panels are cropped images of polarization sites at 45 sec intervals. t = 0 is 45 sec before the first detection of polarized signal. Middle panels show the intensity changes of Bem1p-GFP in the cluster. The trace ends at bud emergence. Bottom panels are traces of four other cells. **(C)** The fraction of Bem1p-GFP that is polarized at the peak frame (mean ± SEM) in *rsr1Δ/rsr1Δ* (DLY11780) and *RSR1/RSR1* (Wt; DLY9201) cells (n = 10). Representative images are shown at top.

3.2.3 Modeling of bud-site selection

As mentioned in the introduction, bud-site-selection landmark proteins are thought to promote local accumulation of Rsr1p-GTP, which recruits Cdc24p to sites specified by the landmarks. This would generate a ring of GEF in haploids, and two patches of GEF at opposite poles in diploids. To ask whether such GEF patterns would, in combination with the known symmetry-breaking mechanism, lead to the polarity protein localization observed in *RSR1* cells, we turned to computational modeling.

We adapted a model that was originally developed to describe symmetry-breaking polarization in yeast (Goryachev and Pokhilko, 2008; Howell et al., 2012; Howell et al., 2009) (which was also employed in chapter 2). The model contains positive feedback owing to the Bem1p complex as well as negative feedback via modification of the Bem1p complex to an inert cytoplasmic state (model 3 in Fig. 2.7A). Stochastic noise was added to the least abundant species (Bem1p complex) as described in chapter 2. However, the model does not incorporate downstream cytoskeletal polarization, and therefore lacks F-actin, which has been suggested to either reinforce (Ozbudak et al., 2005; Slaughter et al., 2009; Wedlich-Soldner et al., 2003; Wedlich-Soldner et al., 2004) or perturb (Dyer et al., 2013; Layton et al., 2011; Ozbudak et al., 2005; Savage et al., 2012) polarity. The model exhibits the formation of multiple Cdc42p clusters that compete, resulting in a single final polarity cluster (Fig. 3.5A). With our model parameters (Table 2), the simulations evolve to a single polarity peak in 3-7 min, which is a bit slower than the approximately 2 min it takes, on average, in vivo (Fig. 3.2C).

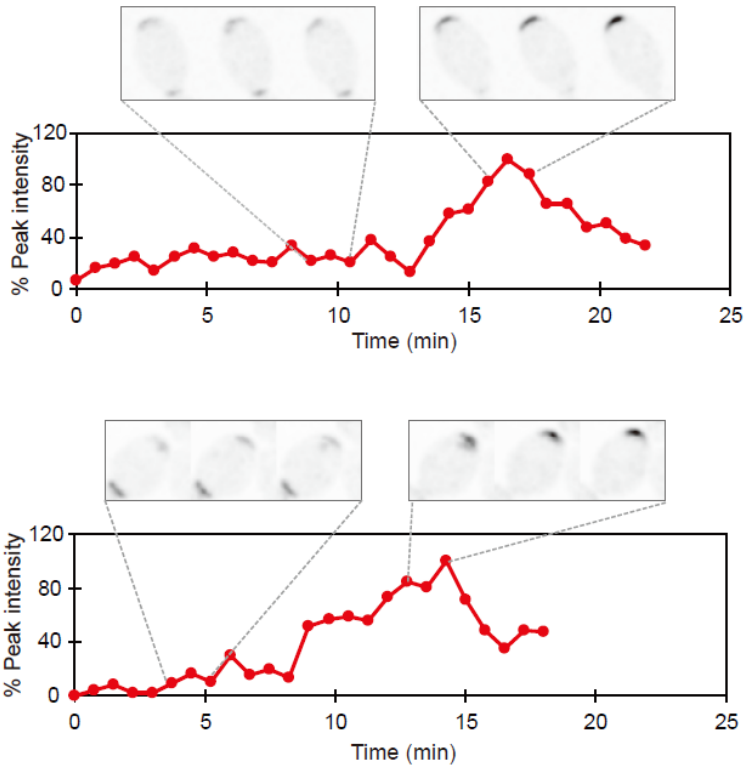

Figure 3.4 Fluctuating Bem1-GFP clusters

A subset of *RSR1/RSR1* cells (DLY9201) initially display a low-level recruitment of Bem1p-GFP, which then coalesces to a tighter cluster before bud emergence. Bottom panels: quantification of localized Bem1-GFP signal. Representative frames of cropped images show the fluctuating (top left) and coalescing stages (top right) in two individual cells. Residual Bem1p-GFP signal at the previous cytokinesis site is also visible at the bottom of the cropped frames.

To this symmetry-breaking model, we added spatially patterned GEF activity to represent the Cdc24p recruited by Rsr1p (hereafter 'Rsr1p–GEF'). Haploid *RSR1* cells were modeled with a ring of Rsr1p-GEF activity surrounding the cytokinesis site. The total Rsr1p-GEF activity was initially set equal to 2.5% of the Bem1p-associated GEF in the model. Under these conditions, Cdc42p accumulated in a ring and remained there for more than 1000 s without evolving to a single peak at the periphery of the ring (Fig. 3.5B). As we never observed a ring of Cdc42p in cells, this model fails to recapitulate the effect of Rsr1p on polarity establishment.

Our simulations indicate that even a modest amount of spatially patterned GEF can have a powerful influence on the symmetry-breaking system, overriding its ability to generate a single peak. We considered two possible adjustments that might limit this effect. First, we eliminated the Rsr1p-GEF after initiating the simulation. As shown in Fig. 3.5C, shutting Rsr1p-GEF off did allow the system to evolve to a single peak, but the peak was always centered in the middle of the ring. Second, we tested whether a weaker Rsr1p-associated GEF might bias (rather than override) the Bem1p system. With a persistent Rsr1p-GEF at 0.025% of the Bem1p-GEF, the initial ring also evolved to a single Cdc42 peak centered in the middle of the ring (Fig. 3.5D).

In cells, polarization in the center of the ring would lead to formation of a bud within the previous division site. Although this does not occur in wild-type cells, it does occur at high frequency in *rga1Δ* mutants (Tong et al., 2007). Rga1p is a Cdc42p-directed GAP that accumulates at the division site in cells undergoing cytokinesis. It is

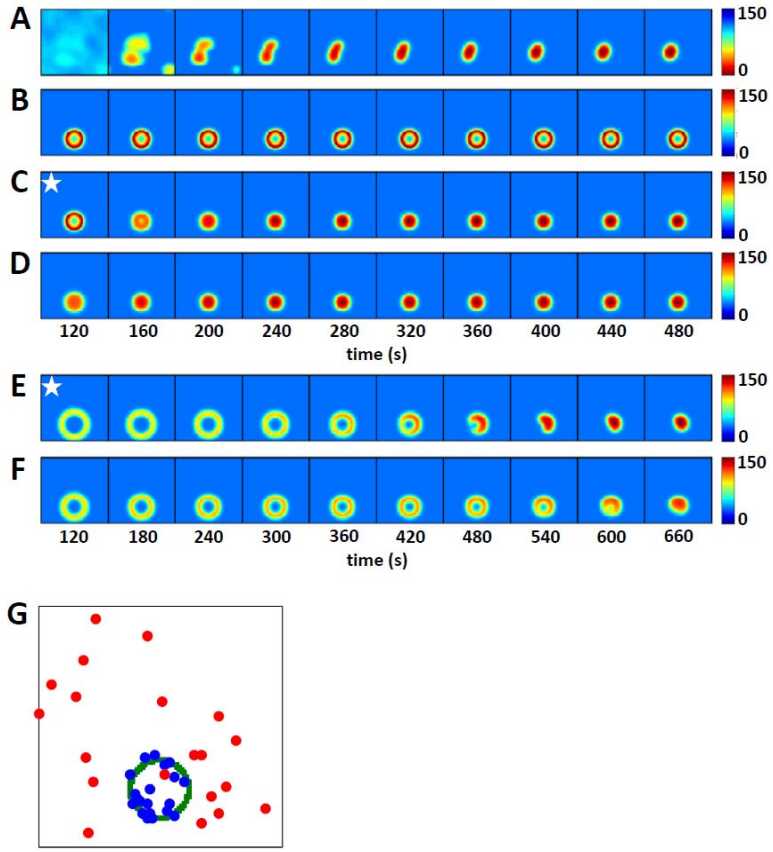

Figure 3.5 Modeling polarity establishment in haploid cells

Each panel represents the concentration of Cdc42p (color) at the plasma membrane (square) at a particular time (indicated below) after initiating a simulation. **(A)** Positive and negative feedback loops with noise in the Bem1p complex, no Rsr1p-GEF or Rga1p-GAP. Because polarity is initiated by noise in this case, each simulation evolves differently. **(B)** Rsr1p-GEF ring added. Rsr1p-GEF at 2.5% of total Bem1p-GEF. **(C)** Rsr1p-GEF turned off at 120 s (indicated by star). **(D)** Persistent Rsr1p-GEF at 0.025% of total Bem1p-GEF. **(E)** Rga1p-GAP plug in the center of a transient Rsr1p-GEF ring. Rsr1p-GEF at 2.5% of total Bem1p-GEF, turned off after 15 s. Rga1p-GAP turned off after 120 s (star). **(F)** Rga1p-GAP plug in the center of a weak Rsr1p-GEF ring. Persistent Rsr1p-GEF at 0.025% of total Bem1p-GEF. Note longer timescales for (E and F): whereas simulations in (A-D) change little after the last panel, (E) and (F) continue to evolve towards a single peak. **(G)** Locations of the Cdc42p peak for 20 simulations of the type shown in (A) (red dots: no Rsr1p-GEF) or (F) (blue dots: Rsr1p-GEF ring depicted in green). The dots indicate positions with maximum Cdc42p concentration after 1000 s.

thought to remain after cytokinesis, creating a 'plug' within the Rsr1p-GEF ring that discourages polarization within the ring (Tong et al., 2007).

To take into account the localized GAP activity provided by Rga1p, we raised the model GAP activity within the ring. We then simulated the two scenarios above: transient Rsr1p-GEF or weak Rsr1p-GEF. In the transient Rsr1p-GEF simulation, we also made the Rga1p-GAP plug transient, as Rga1p relocalizes to the polarity site following polarization (Caviston et al., 2003). If both Rsr1p-GEF and Rga1p-GAP were turned off simultaneously, simulations again evolved to a peak in the center of the ring (not shown). But if the Rga1p-GAP was switched off more than 45 s after the Rsr1p-GEF, then the initial ring gradually evolved to a Cdc42 peak at the ring periphery (Fig. 3.5E). With a weak persistent Rsr1p-GEF, the system also evolved to a single Cdc42p peak at the periphery of the ring (Fig. 3.5F). The final position of the peak varied from simulation to simulation as a result of noise, but in contrast to the random placement observed without Rsr1p-GEF, most peaks were near the ring (Fig. 3.5G). Thus, an immobile ring of Rsr1p-GEF with an internal plug of Rga1p-GAP can recapitulate the final Cdc42p distribution attained in *RSR1* haploids, but only if the Rsr1p-GEF is either weak or transient.

Diploid *RSR1/RSR1* cells were modeled by assuming that they have two patches of Rsr1p-GEF at the proximal and distal poles. An Rga1p-GAP plug was added at the proximal pole, as described above. In this scenario, simulations rapidly developed a single peak of Cdc42p at the distal pole (Fig. 3.6A). Similar behavior was observed for weak Rsr1p-GEF (0.025% of Bem1p-GEF: Fig. 3.6B). Polarization was more rapid than it was in simulations lacking the Rsr1p-GEF (Fig. 3.5A), and the *RSR1/RSR1* diploid

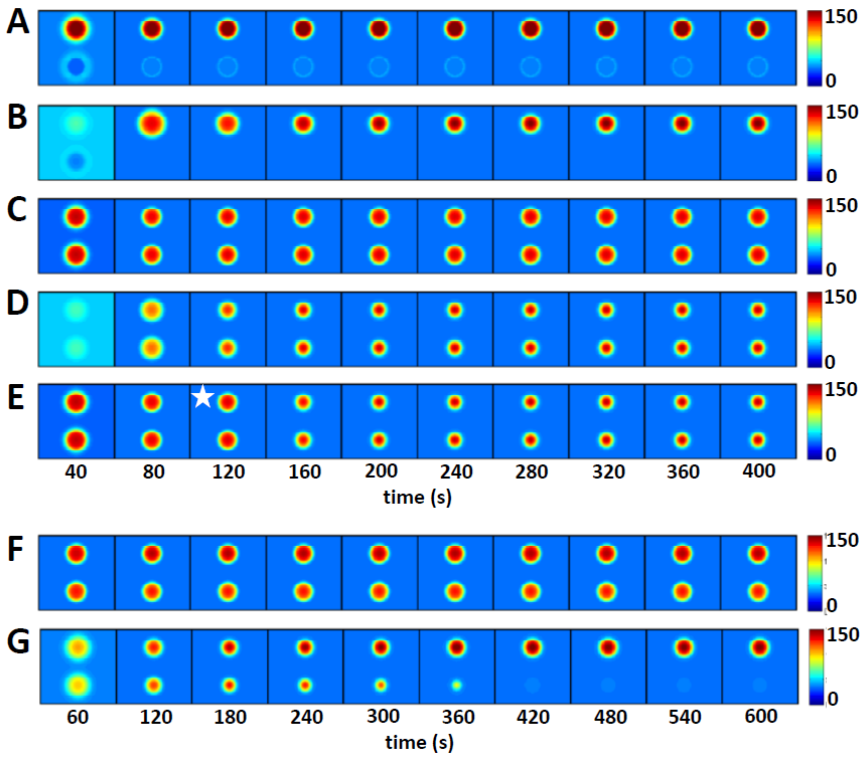

Figure 3.6 Modeling polarity establishment in diploid cells

(A) An Rsr1p-GEF patch was placed at either end of the cell, with an Rga1p-GAP plug in the lower patch. Rsr1p-GEF at 2.5% of Bem1–GEF. **(B)** Rsr1p-GEF patches with an Rga1p-GAP plug in the lower patch. Rsr1p-GEF at only 0.025% of Bem1p-GEF. **(C)** Rsr1p-GEF patches with no Rga1p-GAP plug. Rsr1p-GEF at 2.5% of Bem1p-GEF. **(D)** Rsr1p-GEF patches with no Rga1p-GAP plug. Rsr1p-GEF at only 0.025% of Bem1p-GEF. **(E)** Rsr1p-GEF patches with no Rga1p-GAP plug. Rsr1p-GEF at 2.5% of Bem1p-GEF but Rsr1p-GEF was turned off at 120 s (indicated by star). **(F)** Uneven Rsr1p-GEF patches (55:45 ratio), with no Rga1p-GAP. Rsr1p-GEF at 2.5% of Bem1p-GEF. **(G)** Uneven Rsr1p-GEF patches (55:45 ratio), with no Rga1p-GAP. Rsr1p-GEF at only 0.025% of Bem1p-GEF.

simulations never developed more than one polarity cluster. Thus, a little Rsr1p-localized GEF is sufficient to bias the location of polarization.

We also simulated a diploid lacking the Rga1p-GAP, and in this case, the simulations developed two peaks of Cdc42p, one at each pole (Fig. 3.6C). Even with weak Rsr1p-GEF (0.025% of Bem1p-GEF: Fig. 3.6D), or transient Rsr1p-GEF (Fig. 3.6E), we did not observe competition between the peaks.

The ineffective competition in these simulations could result from the development of comparably-sized Cdc42p peaks. During competition, the relative advantage of the winning peak depends on the magnitude of the difference between the peaks (Howell et al., 2009). Thus, close-to-equal peaks take a long time to develop asymmetry. Consistent with this hypothesis, simulations lacking the Rga1p-GAP in which the Rsr1p-GEF was uneven (so that more Cdc42p was recruited to one pole than the other) led to more effective competition between the two peaks (Fig. 3.6F-G).

Competition was considerably slower with high Rsr1p-GEF (2.5% of Bem1p-GEF: Fig. 3.6F) than with low Rsr1p-GEF (0.025% of Bemp-GEF, Fig. 3.6G), indicating that the continuing presence of the Rsr1–GEF antagonizes competition.

3.2.4 Imaging Bem1p-GFP in *rga1Δ/rga1Δ* diploid cells

To ask whether diploids lacking Rga1p would develop two polarity peaks at opposite poles, we imaged polarity establishment in *rga1Δ/rga1Δ* homozygous mutants. Most cells developed a single peak (Fig. 3.7A). Some cells (four of 21 diploids imaged) did develop two polarity clusters, but these intermediates were rapidly resolved to a single peak (Fig. 3.7B). Under our imaging conditions, *RSR1/RSR1* diploids had a

marked preference to polarize at the pole opposite the neck (62 of 65 cells). This preference was less strong in the *rga1Δ/rga1Δ* mutants (16 of 21 cells), suggesting that the Rga1p GAP accounts for part, but not all, of the bias.

3.3 Discussion

3.3.1 Wild-type cells exhibit competition between polarity clusters

The bud-site-selection system in yeast is often said to dictate the position at which the next bud will emerge. However, it has long been recognized that bud-site-selection landmarks actually specify a restricted subset of preferred positions, rather than dictating a single site (Chant and Pringle, 1995); the basis for selecting the final bud-site position (and the reason why there is only one) has been mysterious. One possibility is that Rsr1p, which has the capacity to oligomerize (Kang et al., 2010), picks one among the permitted positions and then recruits Cdc42p and other polarity factors to the chosen site. In this view, the yeast cell's symmetry-breaking capability might be considered a backup or failsafe system, not normally called upon to participate in wild-type cells.

Arguing against the idea that Rsr1 picks a unique site, we found that *RSR1/RSR1* cells often developed more than one cluster of polarity factors before evolving to a single polarity peak. This behavior suggests that competition between the clusters is important in selecting the single winning polarity site in wild-type cells. It could be that Rsr1p simply biases the symmetry-breaking process to initiate polarity clusters at any of the permitted sites. In this view, polarity establishment occurs in much the same way with or

Figure 3.7 Polarization of *rga1Δ/rga1Δ* cells

Diploid *rga1Δ/rga1Δ* cells (DLY15125) polarizing with (A) single or (B) multiple clusters. Scale bar, 2 μm.

without bud-site selection, and the uniqueness of the final polarity site is attained by competition (between distant clusters) and/or merging (of nearby clusters).

3.3.2 Effect of bud-site-selection system on the dynamics of polarization

The dynamics of polarity establishment, as revealed by imaging Bem1p-GFP, displayed surprising differences between *RSR1/RSR1* and *rsr1Δ/rsr1Δ* cells. As reported in chapter 2, in *rsr1Δ/rsr1Δ* cells Bem1p clusters formed rapidly, and then dispersed and reformed in an oscillatory manner (Howell et al., 2012). By comparison, in *RSR1/RSR1* cells the Bem1p clusters grew more slowly, peaked at a lower intensity and then approached an intermediate intensity without marked oscillation (Fig. 3.3). These features may all be linked: given a system with both positive feedback and delayed negative feedback, the dynamics of the system will depend on the relative timeframe with which the feedback loops take effect. If positive feedback is fast, then the system will tend to polarize a lot of Bem1p before the negative feedback kicks in, after which the strongly activated negative feedback would disperse much of the polarized protein. But if the initial positive feedback is slow, then the negative feedback will 'catch up' as the system polarizes, reducing the peak polarity and dampening oscillations. Given these considerations, we interpret the observed differences in polarity dynamics to stem from a primary difference in the rate at which positive feedback builds the polarity cluster. The unexpected conclusion is that the presence of Rsr1p somehow slows the initial growth of the polarity cluster.

How might Rsr1p slow initial polarization? It seems possible that at early stages during polarity establishment, the Rsr1p-GEF distributed over a relatively large area

leads to prolonged competition between the allowed sites. This scenario might explain another behavior we observed in a subset of both haploid *RSR1* and diploid *RSR1/RSR1* cells (Fig. 3.4): a faint and fluctuating Bem1-GFP signal was observed for several minutes in the areas expected to harbor active Rsr1p (the division site in haploids and the distal tip in diploids) prior to development of a single strong polarity site. Perhaps this reflects prolonged and ineffective competition, as seen in our simulations containing an Rsr1p-GEF ring. However, our simulations of wild-type diploids did not capture this effect: with a circular patch (rather than a ring) of Rsr1p-GEF, the simulations rapidly polarized towards the center of the patch (Fig. 3.6A). Thus, it remains unclear why *RSR1/RSR1* cells would polarize more slowly than mutants lacking Rsr1p.

3.3.3 Modeling bud-site selection

Previous studies showed that GTP-Rsr1p binds to Cdc24p and that this interaction is required for bud-site selection (Shimada et al., 2004; Zheng et al., 1995). Thus, the simplest hypothesis to explain how Rsr1p biases polarization is that it recruits Cdc24p from the cytoplasm to all cortical sites containing landmark proteins. Using a computational model previously developed to simulate symmetry-breaking polarization, we explored whether such a localized Rsr1p-GEF would suffice to yield the polarity protein behavior observed in cells. With no Rsr1p-GEF, this model initiates Cdc42p clusters owing to molecular noise, and as the clusters grow, they compete or merge with each other to yield a final strong polarity peak (Fig. 3.5A).

We added a localized Rsr1p-GEF either as a ring, representing Axl2p/Rsr1p-mediated Cdc24p recruitment in haploids, or as two patches, representing Bud8p/Rsr1p-

and Bud9p/Rsr1p-mediated Cdc24p recruitment in diploids. We also added a central 'plug' with higher GAP activity in the middle of the ring (or one of the patches) to simulate the reported exclusion zone enforced by the centrally located GAP, Rga1p (Tong et al., 2007). Our simulations indicated that this system could yield a single polarity site at an appropriate location. However, to obtain that result it was necessary to make the Rsr1p-GEF either very weak or transient.

3.3.4 Localized Rsr1p-GEF could interfere with competition

Models containing an Rsr1p-GEF ring totaling 2.5% of the Bem1p-GEF available for positive feedback recruited polarity factors to a stable ring, which did not resolve to a single peak of Cdc42p (Fig. 3.5B: this was not affected by the presence or absence of a GAP plug in the center of the ring). Thus, the presence of even a relatively weak Rsr1p-GEF was sufficient to suppress the competition process that yields a single peak. This effect could be overcome either by greatly reducing the amount of Rsr1p-GEF or by making the Rsr1p-GEF transient. The ability of Rsr1p-GEF to interfere with competition may explain the unexpected finding that *RSR1/RSR1* cells took longer than *rsr1Δ/rsr1Δ* cells to transition from a two-polarity- cluster intermediate to the final single-polarity-site state (Fig. 3.2C).

Models containing two patches of Rsr1p-GEF but lacking a GAP plug (simulating *rga1Δ/rga1Δ* mutant diploids) developed two polarity peaks that did not resolve to a single peak in a relevant (approx. 10 min) timeframe, even with a very weak or transient Rsr1p-GEF (figure 7). By contrast, *rga1Δ/rga1Δ* mutant cells displayed rapid

competition and no defect in developing a single polarity site (Fig. 3.7). Why is competition so much more powerful in cells than it is in our model simulations? In the model, competition builds on initial differences between peaks that develop owing to molecular noise. In cells, it may be that noise stemming from vesicle traffic (not present in our model) is more powerful in generating these differences, promoting competition.

It is also possible that competition is enabled by some other factor that discourages polarization at the previous division site. Although haploid *rga1Δ* cells polarize preferentially at the division site (Tong et al., 2007), we found that diploid *rga1Δ/rga1Δ* mutants retained a bias to polarize away from the division site. A very recent study identified a new Cdc42p antagonist present at the division site that collaborates with Rga1p to prevent budding at that site (Meitinger et al., 2013). Modeling a situation with two uneven patches, competition was more effective and our simulations did evolve towards a single polarity site. However, even in this case, a persistent Rsr1p-GEF impaired competition (Fig. 3.6). Thus, as for the haploid ring simulations, effective polarization would occur only if the Rsr1p-recruited GEF were very weak or transient.

3.3.5 The role of actin

We found that in diploids treated with Latrunculin to depolymerize F-actin, the winning polarity site sometimes relocated from one landmark-designated position to another. This observation suggests that F-actin may be required to stop the 'losing' landmarks from continuing to attract polarity factors once a large polarity cluster is formed. A role for actin-mediated vesicle traffic in providing positive feedback for the polarity site has been vigorously advocated by previous studies (Slaughter et al., 2009;

Wedlich-Soldner et al., 2003; Wedlich-Soldner et al., 2004). In those studies, it was assumed that actin reinforced polarization by delivering Cdc42p itself to the polarity site, whereas here we suggest that it may deliver a landmark that serves to activate Rsr1p at that site. Consistent with a role for actin and Rsr1p in the same pathway, both deletion of Rsr1p (Irazoqui et al., 2003) and depolymerization of F-actin (Wedlich-Soldner et al., 2004) can block polarization when cells lack Bem1p. Testing the hypothesis will require identification of the proposed landmark(s).

In a few of the Latrunculin-treated cells, the polarity site repeatedly switched from one end of the cell to the other in a 'ping-pong' manner. This behavior is strikingly reminiscent of the oscillatory relocation of Cdc42p between the two cell ends that was recently reported to occur during bipolar growth of the cylindrical fission yeast, *Schizosaccharomyces pombe* (Das et al., 2012). However, whereas in *S. cerevisiae* the behavior is only seen in cells with depolymerized actin, in *S. pombe* it requires F-actin, so the role of actin must be different in the two systems. Three factors are likely to underlie oscillatory relocation in both systems: (i) the two cell ends contain tip proteins that can attract polarity factors to those sites; (ii) competition for limiting factors may explain why only one site at a time can accumulate large amounts of Cdc42p; and (iii) negative feedback loops may explain why the winning site then disperses Cdc42p, allowing the other tip to gain the upper hand (as reported in chapter 2) (Das et al., 2012; Howell et al., 2012; Wu and Lew, 2013).

4. The role of Guanine Nucleotide Dissociation Inhibitor (GDI) in polarization dynamics

4.1 Introduction

A polarized cell usually has a single directional axis: a "front" and a "back", (here refers to as singularity). The determination of the front depends on the highly conserved Rho-type GTPase Cdc42p (Etienne-Manneville, 2004). As with other GTPases, the activity of Cdc42p is regulated by guanine nucleotide exchange factors (GEFs) and GTPase activating proteins (GAPs). The C-terminal geranylgeranyl modification of Cdc42p and the lysine-rich polybasic motif preceding it are required for the membrane anchorage of Cdc42p, which is important for its function (Ziman et al., 1991). Another regulator of Cdc42p, GDI (Rdi1p in yeast), can bind to the prenyl group of Cdc42p and extract Cdc42p from the membrane into the cytoplasm.

In *S. cerevisiae*, the accumulation of the active GTP-Cdc42p at the front (where the bud emerges) relies on an amplification mechanism involving a scaffold protein Bem1p. Bem1p brings Cdc24p, the sole Cdc42p-directed GEF, and a Cdc42p effector, p21-activating kinase (PAK), together to form a cytoplasmic three-way complex (Bose et al., 2001; Gulli et al., 2000; Kozubowski et al., 2008). PAK binds to GTP-Cdc42p on the plasma membrane and allows the GEF in the same complex to active nearby Cdc42p, which in turn brings more Bem1p complexes in a positive feedback to amplify the GFP-Cdc42p cluster (Goryachev and Pokhilko, 2008; Kozubowski et al., 2008).

In wild-type yeast cells, polarization and bud emergence occurs at sites dictated by transmembrane landmark proteins (Bi and Park, 2012; Chant, 1999). Even though landmarks bias the location for polarization, they actually define many possible sites: an entire ring of potential sites marked by Axl2p in haploids and both poles marked by Bud8p and Bud9p in diploids (Chant and Pringle, 1995). In the context of symmetry breaking, where the positional cues are absent (e.g. *rsr1Δ*), yeast cells can still polarize to a random, single front with no defect in budding efficiency and timing (Bender and Pringle, 1989; Chant and Herskowitz, 1991). Positive feedback mechanism allows stochastic fluctuations to develop a polarized GTP-Cdc42 cluster, but how do cells choose a single polarity front from many potential sites?

Time-lapse imaging of Bem1p-GFP probe revealed that multiple polarization clusters can form in *rsr1Δ* cells (Fig. 2.1) (Howell et al., 2012). Similarly, multicluster intermediates are observed in the regions marked by landmarks in wild-type cells (Fig. 3.2) (Wu et al., 2013), indicating that positive feedback mechanism can potentially amplify GTP-Cdc42p clusters at multiple sites. However, in these cells, usually one of the coexisting clusters grows while the other(s) shrinks, suggesting the polarity clusters compete with each other (merging of nearby clusters occurs in some cells). Competition and merging usually happen rapidly (~1.5 min) and leave only one winning cluster, ensuring that only one bud will form.

If competition between clusters is responsible for assuring that only one front will form, then it is important to understand the molecular basis for such competition. Mathematical modeling suggested that, although more than one cluster

could be amplified by Bem1p complex-mediated positive feedback, the abundance of Bem1p complex is limited and would soon be depleted from the cytoplasm, after which the clusters compete with each other and the largest one would win (Goryachev and Pokhilko, 2008; Howell et al., 2009). In most instances where two foci appeared, one focus subsequently grew while the other disappeared, and a single bud emerged from the site of the winning focus. This finding provides strong evidence that foci interact with each other in a competitive manner that leads to the growth of one focus at the expense of the other (Howell et al., 2009). It is conceivable that increasing the amount of the Bem1p complex would not only take cells longer time to deplete the Bem1p complexes from the cytoplasm before competition starts, but also would take the large cluster longer time to suck up the Bem1p complexes from other smaller clusters since there are more materials in every cluster. If competing for the limiting Bem1p complexes is the key to guarantee singularity, then competition would be slower with increased amount of the Bem1p complexes. Indeed, overexpression of Bem1p in yeast cells led to slower competition and occasional formation of two buds (Howell et al., 2009). Thus, Bem1p complex-mediated positive feedback combined with competition for a limiting pool of the Bem1p complexes could explain why yeast cells polarize to one and only one front.

Mathematical modeling suggested that Bem1p complex-mediated positive feedback can generate and sustain a cluster of GTP-Cdc42p, but it does not raise the local concentration of GTP-Cdc42p above the surrounding GDP-Cdc42p (Johnson et al., 2011). The inward membrane diffusion of GDP-Cdc42p to the clusters (and the conversion to GTP-bound form) is counterbalanced by the outward diffusion of GTP-Cdc42p (and the

hydrolysis of GTP), so the total Cdc42p concentration (GDP + GTP) stays uniform on the cortex. However, previous immunofluorescence experiments and imaging of GFP-Cdc42p probe showed that total Cdc42p is concentrated at the polarization site (Richman et al., 2002; Ziman et al., 1993). The ability of GDI to shuttle Cdc42p in a complex between membrane and cytoplasm makes it a candidate for Cdc42p concentration. Given the much faster diffusion rate in the cytoplasm, it has been proposed in a mathematical model that GDI-mediated cytoplasmic flux of Cdc42p can counteract the diffusive spread of the polarized cluster (Goryachev and Pokhilko, 2008). GDI prefers to extract GDP-bound Cdc42p from the membrane (Freisinger et al., 2013; Johnson et al., 2009), so the net result of GDI-mediated Cdc42p transport is to pluck GDP-Cdc42p from the membrane further away from the polarized cluster and deliver it to the cluster center, where GDP-Cdc42p is depleted by quick conversion to the GTP-bound form. In vivo, the importance of GDI in Cdc42p transport has been supported by measurements from fluorescence recovery after photobleaching (FRAP) showing that the dynamics of GFP-Cdc42p are much slower in yeast cells lacking the sole GDI, Rdi1p (Slaughter et al., 2009).

Although it is plausible that GDI is important of Cdc42p concentration and recycling, deletion of *RDI1* did not cause obvious defects in polarity establishment or budding (Masuda et al., 1994). How do yeast cells concentrate Cdc42p in the absence of GDI? It has been proposed that an actin-mediated mechanism works in parallel with GDI to concentrate Cdc42p. In this mechanism, directed transport of Cdc42p-containing exocytic vesicles on actin cables and Cdc42p recycling by endocytosis can maintain

Cdc42p polarization (Marco et al., 2007; Slaughter et al., 2009). Depolymerization of actin with Latrunculin B (Lat B) in *rdi1Δ* cells blocked polarization of Cdc42p, supporting the idea that GDI and actin act in distinct and parallel mechanisms for Cdc42p cycling (Freisinger et al., 2013; Smith et al., 2013).

Even though the lack of Rdi1p did not cause severe problems in polarization and budding, in this study we show that *rdi1Δ* cells actually have different polarization kinetics from wild-type cells. In the absence of Rdi1p the initial clustering of polarity factors is slowed, and competition is also much slower: in some cases cells still have two clusters at the time of bud emergence and they form two buds. We suggest that in the absence of Rdi1p, the clusters compete for a limiting pool of Cdc42p (instead of Bem1p complex), and that slow exchange of Cdc42p on and off the membrane in *rdi1Δ* cells leads to slow competition. As we were characterizing *rdi1Δ* cells, we surprisingly found out that *rdi1Δ* cells treated with Lat A were able to polarize, which is contradictory to previous reports (Freisinger et al., 2013; Slaughter et al., 2009). The second focus of this chapter will be the characterization of cell polarization in the absence of Rdi1p and polymerized actin, and the testing of other possible mechanisms that may contribute to Cdc42p concentration.

4.2 Results

4.2.1 Polarization dynamics of Bem1p-GFP is altered in *rdi1Δ* cells

Early studies on yeast cells lacking Rdi1p showed that *rdi1Δ* cells are indistinguishable from wild-type cells in terms of cell morphology and growth, indicating the loss of Rdi1p function does not cause obvious defects in polarization (Masuda et al., 1994; Tiedje et al., 2008). *rdi1Δ* cells are able to maintain a concentrated Cdc42 patch at the front of the cell, but the replenishment of the patch after photobleaching is slower (Slaughter et al., 2009), suggesting the absence of Rdi1p influences Cdc42p transport. In order to get a closer look at the polarization dynamics in *rdi1Δ* cells, we employed time-lapse live-cell imaging to monitor the clustering of Bem1p-GFP at the polarization site. The strains used in this study were all diploids synchronized by hydroxyurea (HU) arrest/release method (as described in chapter 2) (Howell et al., 2012). With the bipolar budding pattern, some diploids tend to polarize toward the neck. To have a clear separation between newly polarized signal and residual neck signal left from the previous cytokinesis, the landmark gene *RSR1* was deleted from all strains to randomize the bud site.

As shown in chapter 2, in diploid *rsr1Δ/rsr1Δ* cells, the concentration of Bem1p-GFP and other polarity probes oscillated at the polarization site. Bem1p-GFP rapidly clustered and dispersed, followed by one or two more cycles of clustering and dispersal before bud emergence (Fig. 2.2, 3.3A, 4.1A) (Howell et al., 2012). The deletion of *RDI1* in *rsr1Δ/rsr1Δ* cells did not impede the formation of a Bem1p-GFP patch; however, both the rapid initial clustering and oscillation behavior were lost. Bem1p-GFP intensity

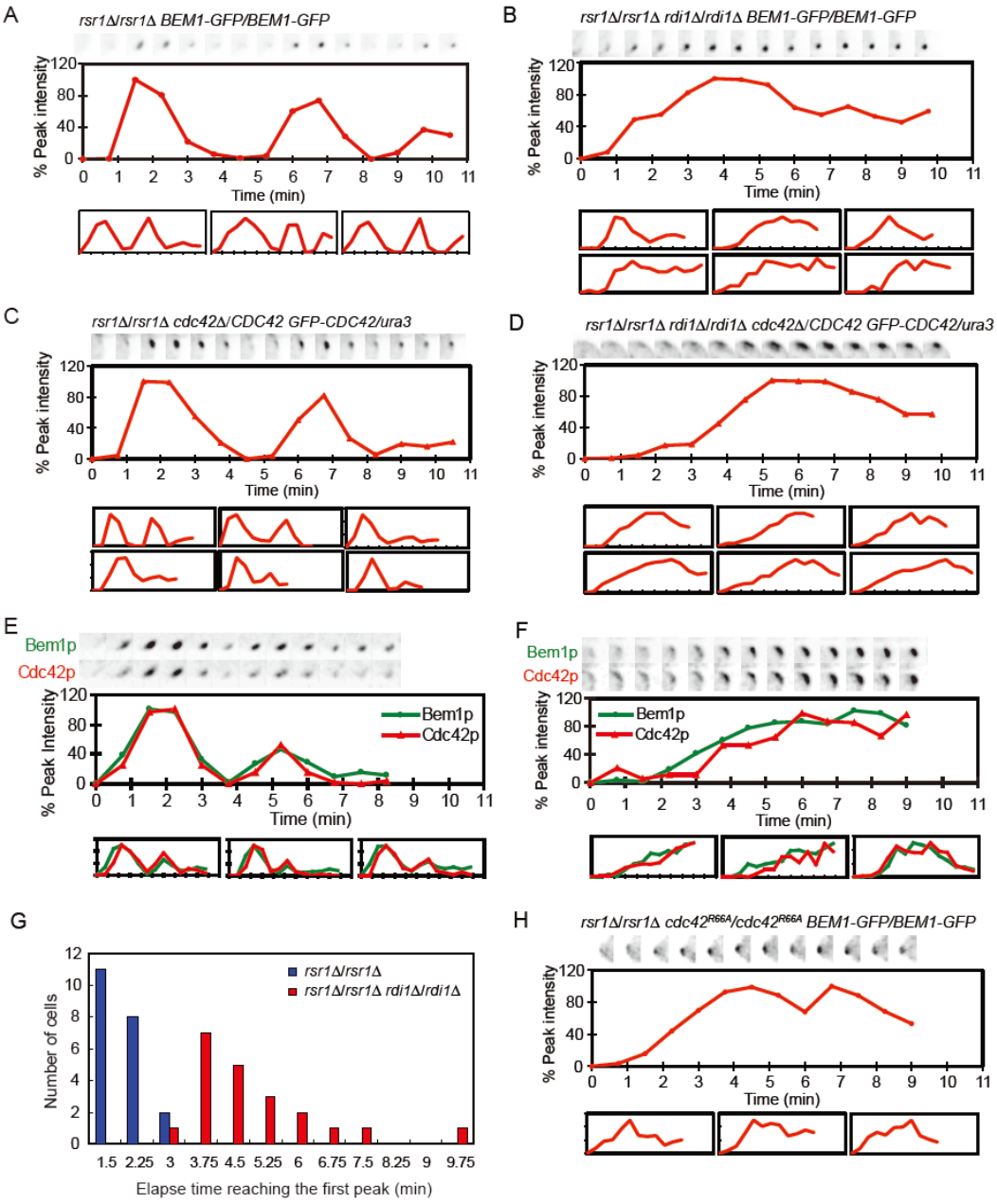

Figure 4.1 *rdi1Δ* cells polarize slowly and lack oscillation

(A and C) Oscillatory clustering of Bem1p-GFP (A, DLY9200) or GFP-Cdc42p (C, DLY13984) in *rsr1Δ/rsr1Δ* diploid cells pre-treated with HU. Top panels are the cropped images of the polarized cluster at 45 sec intervals. Middle panels represent

represent the changes of Bem1p-GFP sum intensity at the polarized cluster. t = 0 is 45 sec before the first detection of polarized signal. The trace ends at bud emergence. Bottom panels are quantifications for six more cells. **(B and D)** Slow clustering and lack of oscillation of Bem1p-GFP (B, DLY12577) or GFP-Cdc42p (DLY14469) in *rsr1Δ/rsr1Δ rdi1Δ/rdi1Δ* diploid cells pre-treated with HU. Both probes show no oscillation in the absence of Rdi1p. **(E and F)** Two-color filming using Bem1p-GFP and Cdc42p-mCherry^{SW} probes showed that the polarization of these two polarity factors is concerted in both *rsr1Δ/rsr1Δ* (E, DLY17110) and *rsr1Δ/rsr1Δ rdi1Δ/rdi1Δ* (F, DLY17109) diploid cells. **(G)** The initial clustering is quantitatively faster in *rsr1Δ/rsr1Δ* cells. The time from t = 0 to the timeframe when Bem1p-GFP sum intensity reaches the first peak was quantified. Bar graph showed the number of cells reaching the first peak at indicated time. **(H)** Slow clustering and lack of oscillation of Bem1p-GFP signal in *cdc42*^{R66A}*/cdc42*^{R66A} diploid cells (DLY15572).

slowly increased and reached the peak at least 3-4 minutes after polarization started (compared to ≤ 2.25 minutes in *rsr1Δ/rsr1Δ* cells, Fig. 4.1B and G). In some cells the intensity stayed high before bud emergence, while in other cells the intensity went down from the peak without subsequent oscillatory cycles.

4.2.2 Polarization behaviors of Cdc42p paralleled those of Bem1p in *rdi1Δ* cells

We next asked whether the phenotype changes of Bem1p-GFP in the absence of Rdi1p were shared by Cdc42p. Given the fact that fluorescent Cdc42p probes used in previous studies were either nonfunctional or temperature sensitive in our strain background, we tried to lower the toxicity of the tagging by adding a linker (APPRRLVHP) between N-terminal GFP and Cdc42p (Fig. 4.2A) (Kohli et al., 2008). As previous probes, this new GFP-Cdc42p was integrated at the *URA3* locus of a diploid strain with one copy of endogenous *CDC42* deleted. Western blot analysis revealed that these probes (including the old GFP-Cdc42p used in chapter 2) are usually overexpressed compared to the endogenous Cdc42p (Fig. 4.2B), potentially due to multiple integration of the constructs or elevated expression due to the different chromatin structure at *URA3* locus. In order to generate a strain with comparable expression levels between GFP-Cdc42p and endogenous Cdc42p, we integrated a single copy of the probe at *CDC42* locus. We were able to obtain viable spores with single copy of the new probe as the only source of Cdc42p (Fig. 4.2C); however, with endogenous expression level, it could only sustain viability at 24℃ (Fig. 4.2D) and led to large, misshapen cell morphology, suggesting the new GFP-Cdc42p was still not fully functional. Multiple integrants with

overexpression of the new probe had increased viability in a dose-dependent manner. The one with 8-fold expression showed comparable viability to the wild-type at 30℃ (Fig. 4.2C), the temperature at which we image cells. We thus used this new probe (with 8-fold overexpression) to detect total Cdc42p. To avoid potential effect of reduced function, cells also contained a copy of endogenous *CDC42*.

We first tested the behavior of this GFP-Cdc42p probe in *rsr1Δ/rsr1Δ* cells. We previous reported that oscillation is a fragile phenotype which can be eliminated or reduced with overexpression of polarity factors (Fig. 2.12A). Interestingly, with 8-fold overexpression, this probe still exhibited fast initial clustering and oscillation similar to Bem1p-GFP (Fig. 4.1C). It is possible that the partial functionality of this probe makes it less potent to disrupt oscillation when it is overexpressed. In *rsr1Δ/rsr1Δ rdi1Δ/ rdi1Δ* cells, GFP-Cdc42p also accumulated at the polarization site slowly and lacked oscillation (Fig. 4.1D), indicating the altered polarization dynamics are shared by Bem1p and Cdc42p.

Even though Bem1p-GFP and GFP-Cdc42p behaved similarly in *rsr1Δ/rsr1Δ rdi1Δ/rdi1Δ* cells, it was not clear whether the two proteins concentrated in parallel in the individual cells. To answer this question, we generated another red fluorescent Cdc42p probe to compare its behavior with Bem1p-GFP in the same strain. We failed in the attempts to N-terminally tagged mCherry or tdTomato to Cdc42p. Alternatively, we inserted a mCherry tag into a less conserved C-terminal region (after Leu134) of Cdc42p (Fig. 4.2A, personal communication with Sophie Martin's lab). Strains with this probe as the only source of Cdc42p (integrated at the *URA3* locus) had viability comparable to

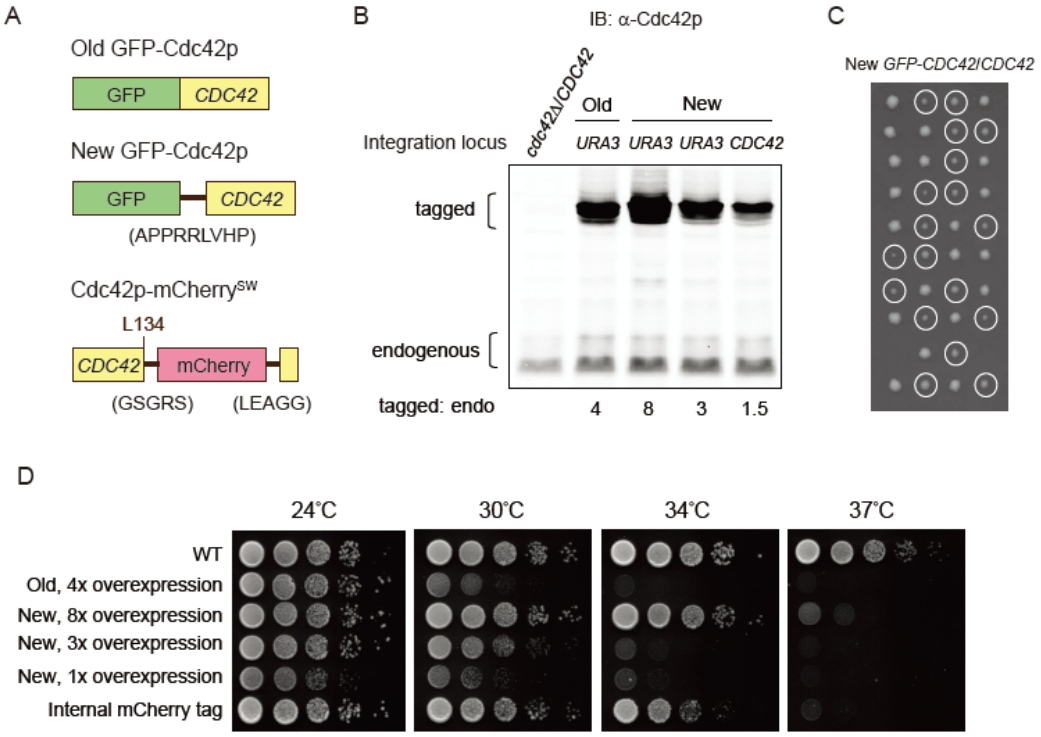

Figure 4.2 New GFP-Cdc42p and Cdc42p-mCherry^{SW} probes

(A) Diagrams of different Cdc42p probes. **(B)** Expression levels of different Cdc42p probes. Transformants with different expression level of the new GFP-Cdc42p probe were compared in this blot. The ratio of expression level between tagged and endogenous Cdc42p are indicated at the bottom. From left to right: DLY12658, DLY12833, DLY13878, DLY16487, and DLY15015. **(C)** The diploid strain is integrated with a single copy of the new GFP-Cdc42p at endogenous *CDC42* locus, sporulated and dissected. The circled spores are those with GFP-Cdc42p, which generally formed smaller colonies, suggesting the new probe is not fully functional. **(D)** The viability of different Cdc42p probes at different temperatures. None of the probe is fully functional at higher temperatures. The strains used here are all haploids with the tagged Cdc42p as the only source of Cdc42p (except wild-type). From top to bottom: DLY8155, DLY12844, DLY13891, DLY16730, DLY15016, and DLY16855.

wild-type up to 34℃ (Fig. 4.2D). Unfortunately, we were not able to determine the expression level of this probe because the internal tagging interfere the C-terminal antigenic region for Cdc42p antibody recognition.

In *rsr1Δ/rsr1Δ* cells, two-color imaging showed that the behavior of Bem1p-GFP paralleled that of the red probe detecting total Cdc42p (Fig. 4.1E), as reported before using Bem1p-tdTomato and old GFP-Cdc42p (Fig. 2.3C). In *rsr1Δ/rsr1Δ rdi1Δ/ rdi1Δ* cells, total Cdc42p also paralleled Bem1p behavior, confirming the polarization of these two factors remained coupled (Fig. 4.1F).

In addition to Cdc42p, Rho1p and Rho4p are other binding partners of Rdi1p (Tiedje et al., 2008). The dynamics alterations we observed in *rsr1Δ/rsr1Δ rdi1Δ/rdi1Δ* cells could indirectly result from the loss of Rdi1p-Rho1p or Rdi1p-Rho4p interaction. To test this possibility, we employed $cdc42^{R66A}$ mutant which cannot bind to Rdi1p. Diploid strains with $cdc42^{R66A}$ as the only source of Cdc42p revealed the same phenotypes as *rdi1Δ* strains, indicating the slower polarization dynamics were caused by the disruption of direct Cdc42p-Rdi1p interaction (Fig. 4.1H).

4.2.3 *rdi1Δ* cells have slower competition between polarity clusters and occasionally violate singularity

As reported in chapter 2 and 3, fast time-lapse imaging of Bem1p-GFP in wild-type and *rsr1Δ/rsr1Δ* cells revealed that multiple polarity clusters could form in the beginning of polarity establishment (Howell et al., 2012; Wu et al., 2013). In all cases, either competition or merging between clusters happened rapidly to resolve only one cluster, thereby guaranteeing singularity. Multicluster intermediates were also observed

in 59% (n = 77) of *rsr1Δ/rsr1Δ rdi1Δ/rdi1Δ* cells, but the behaviors of these clusters were clearly different from those in *rsr1Δ/rsr1Δ* cells. In the majority of *rsr1Δ/rsr1Δ* cells forming multiple clusters, one cluster started with dominant advantages in brightness/size and became the winning cluster after competition. In the absence of Rdi1p, there were a higher percentage of cells forming more than two clusters (36% opposed to 9% in *rsr1Δ/rsr1Δ*) that tended to start with similar brightness and sizes. The resolution to a single cluster sometimes involved both competition and merging between clusters. Interesting, we did not observe any relocation cluster in *rsr1Δ/rsr1Δ rdi1Δ/rdi1Δ* cells.

In *rsr1Δ/rsr1Δ* cells, competition or merging between Bem1p clusters happened fast and was usually completed within 2 min. Strikingly, Bem1p clusters in *rsr1Δ/rsr1Δ rdi1Δ/rdi1Δ* cells had the tendency to coexist for a longer time before a winning cluster was resolved (Fig. 4.3A). The long competition was also observed with Cdc42p and PBD probes (Fig. 4.3B), indicating that the core polarity factors still concentrate and disperse in concert in *rsr1Δ/rsr1Δ rdi1Δ/rdi1Δ* cells. The average coexistence time between Bem1p clusters increased ~3-fold in the absence to Rdi1p (6.4 min, Fig. 4.3C). Although a small population of *rsr1Δ/rsr1Δ rdi1Δ/rdi1Δ* cells had fast-competing/merging clusters comparable to those in *rsr1Δ/rsr1Δ* cells, the majority of cells had a coexistence time falling within 3-8 min range. These cells could finish competition before bud emergence, thereby generating only one bud. However, there were few extreme cases in which the cells failed to resolve multiple clusters before bud emergence, leading to simultaneous formation of two buds (Fig. 4.3F). We noticed that there were about 4% of two-budded

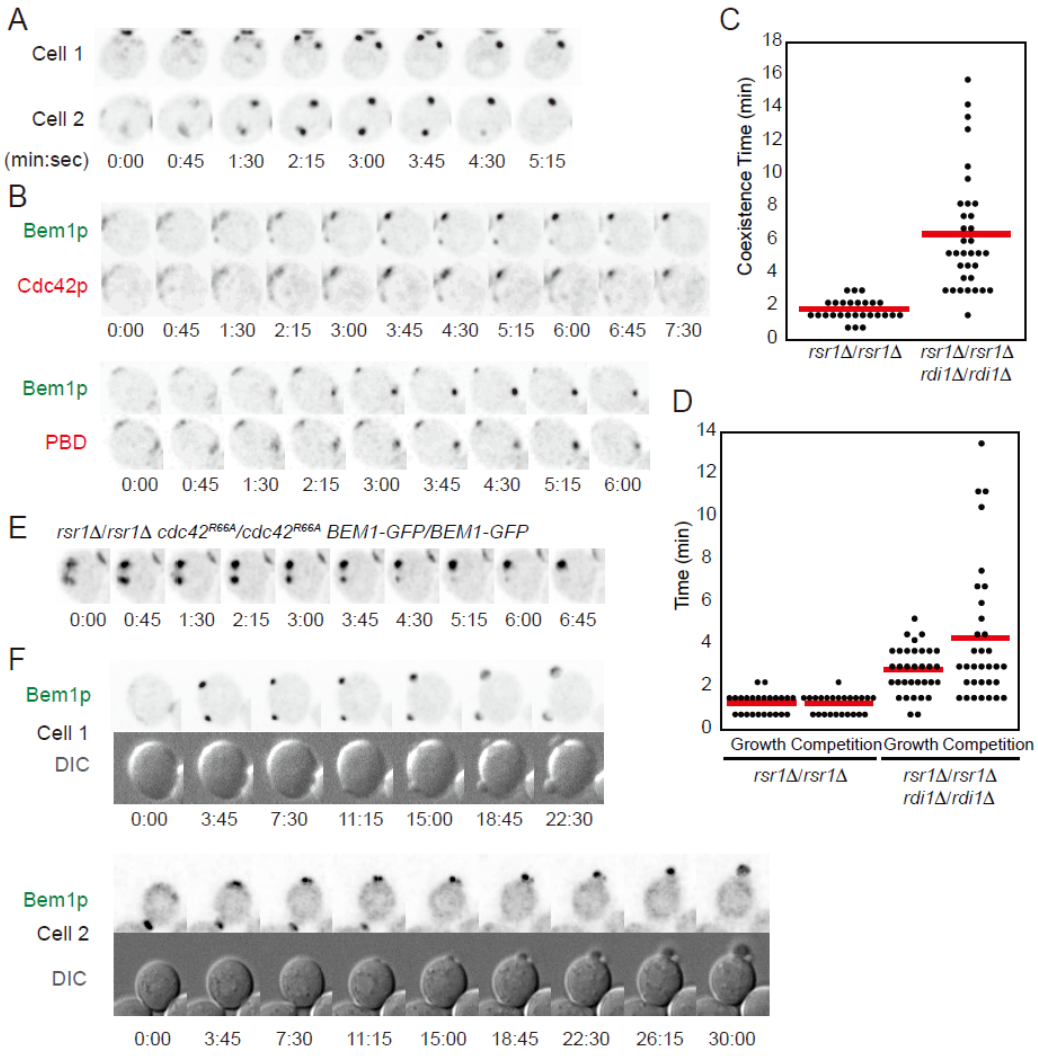

Figure 4.3 *rdi1Δ* cells displayed slow competition and violate singularity

(A) Growth and competition between Bem1p-GFP clusters in *rsr1Δ/rsr1Δ rdi1Δ/rdi1Δ* cells (DLY14535). A residual neck signal left from the previous cytokinesis is present at the top of cell 1. Images are deconvolved, cropped and inverted from maximum projections of 30 Z stacks (0.24 µm per Z step). t = 0 indicates the first detection of multiple clusters. The strip ends at the first timeframe when a winning cluster is resolved. **(B)** Parallel clustering and dispersal of Bem1p-GFP and Cdc42p-mCherry^{SW} clusters (DLY17109) or Bem1p-GFP and PBD clusters (DLY15782). Images are from maximum projection of 15 Z stacks

(0.5 μm per Z step). **(C)** Coexistence time between the first detection of multiple clusters and the first frame showing the resolution to a single cluster is 3-fold longer in *rsr1Δ/rsr1Δ rdi1Δ/rdi1Δ* (DLY14535, n = 35) cells than in *rsr1Δ/rsr1Δ* (DLY13098, n = 27). Each dot indicates an individual cell. The red line is the average coexistence time. **(D)** Separation of the cluster growth time from competition time from (C). Both time periods are longer in *rsr1Δ/rsr1Δ rdi1Δ/rdi1Δ* cells. **(E)** Growth and competition between Bem1p-GFP clusters in $cdc42^{R66A}/cdc42^{R66A}$ cells (DLY15572). **(F)** Failure to resolve multiple Bem1p-GFP clusters and the consequent simultaneous growth of two buds in *rsr1Δ/rsr1Δ rdi1Δ/rdi1Δ* cells. GFP images are maximum projections of 30 Z stacks (0.24 μm per Z step). DIC images are single, middle planes selected from the Z stacks.

rsr1Δ/rsr1Δ rdi1Δ/rdi1Δ cells in the population. The observation of two-budded cells in *rdi1Δ* cells was also recently reported by another group (Freisinger et al., 2013).

Interestingly, we found the clusters in *rsr1Δ/rsr1Δ rdi1Δ/rdi1Δ* cells had a period of growth time which was rarely observed in *rsr1Δ/rsr1Δ* cells (Fig. 4.3A, time frames 1-5 of both cells). The clusters in *rsr1Δ/rsr1* cells were usually fully grown when first detected, and then competition ensued in the next time frame (45 sec interval) and happened rapidly. In *rsr1Δ/rsr1Δ rdi1Δ/rdi1Δ* cells, however, we could catch several time frames (2.8 min on average) during which the clusters either kept growing or stayed the same brightness/size before competition initiated (judged by the shrinkage of one or more clusters) (Fig. 4.3D). The competition time between clusters was also longer in *rsr1Δ/rsr1Δ rdi1Δ/rdi1Δ* cells, lasting 4.3 min on average as opposed to 1.2 min in *rsr1Δ/rsr1Δ* cells (Fig. 4.3D). Therefore, the longer coexistence time in *rsr1Δ/rsr1Δ rdi1Δ/rdi1Δ* cells was contributed by both longer cluster growth and competition time.

Among all the two-budded cells we caught in time-lapse imaging, some of them maintained two equal-sized clusters which sustained simultaneous growth of two buds (cell 1, Fig. 4.3F). In other cells the competition weakened one of the clusters but did not eliminate it, leading to unequal-sized clusters that formed buds with different growth rate (cell 2, Fig. 4.3F). Most, if not all, of these cells continued competition even after the clusters were already in separate buds and it lasted until the weaker cluster disappeared from the bud tip, resulting in the abandonment of the smaller bud. Interestingly, in some cases the adjacent clusters failed to merge and grew into two neighboring buds (cell 2, Fig. 4.3F), further supporting the fact that the dynamics of polarity factors were much

slower in the absence of Rdi1p. Slow competition between Bem1p-GFP clusters and occasional formation of two buds were also observed in *rsr1Δ/rsr1Δ cdc42*^{R66A}*/cdc42*^{R66A} cells, reassuring that the polarity defects were due to the loss of Cdc42p-Rdi1p interaction (Fig. 4.3E).

4.2.4 How does GDI speed up competition? Not acting through the negative feedback

The slow competition in *rsr1Δ/rsr1Δ rdi1Δ/rdi1Δ* cells indicates that the presence of Rdi1p accelerates competition to ensure singularity. How does Rdi1p speed up competition? Since Rdi1p can form a cytoplasmic complex with Cdc42p, one possibility is that Rdi1p keeps excess Cdc42p in the cytoplasm, allowing adequate amount of Cdc42p on the plasma membrane for polarization. In this scenario, more Cdc42p would accumulate on the plasma membrane in the absence of Rdi1p, potentially leading to larger polarization clusters and slow competition. However, the percentage of total Cdc42p or GTP-Cdc42p in the polarized cluster is undistinguishable in *rsr1Δ/rsr1Δ* cells and *rsr1Δ/rsr1Δ rdi1Δ/rdi1Δ* cells (Fig. 4.4A-B). Bem1p-GFP clusters in *rsr1Δ/rsr1Δ rdi1Δ/rdi1Δ* cells are also not obviously brighter and/or bigger than those in *rsr1Δ/rsr1Δ* cells. Our previous results from Cdc42p overexpression experiments further argue against this possibility because Cdc42p overexpressors, which presumably have more Cdc42p on the plasma membrane (and other cellular compartments in general), still resolve multiple clusters rapidly (Fig. 2.12B).

Our previous explanation for rapid competition in Cdc42p overexpressors is that the presence of negative feedback in yeast polarity circuit can buffer the level of GTP-

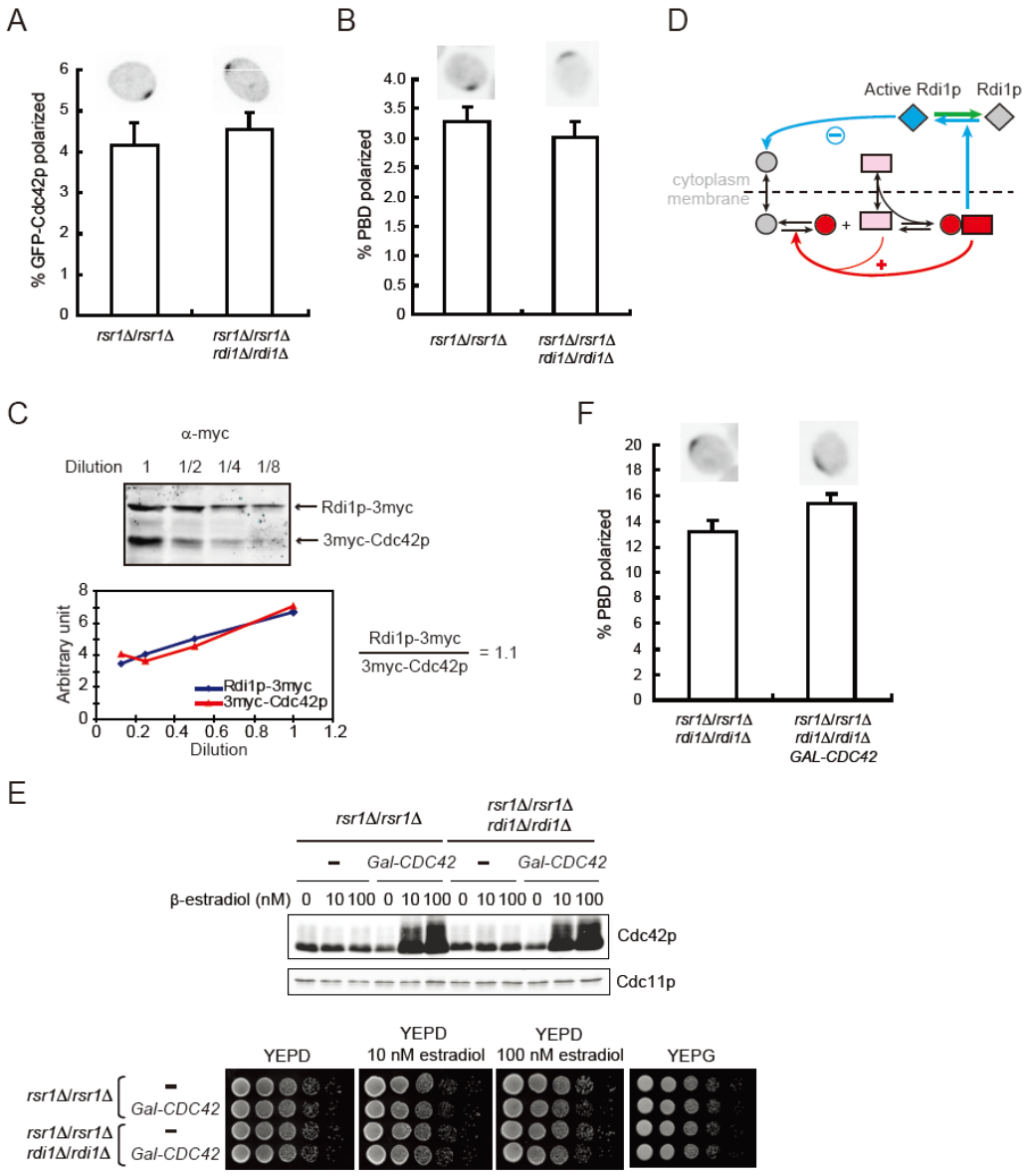

Figure 4.4 GDI is not involved in the negative feedback

(A) The percentages of total Cdc42p in the polarized cluster in *rsr1Δ/rsr1Δ* (DLY13984, n = 21) and *rsr1Δ/rsr1Δ rdi1Δ/rdi1Δ* (DLY14469, n = 25) cells are not significantly different. The bars represents mean ± SEM. **(B)** The percentages of GTP-Cdc42p in the polarized cluster in *rsr1Δ/rsr1Δ* (DLY15879, n = 15) and *rsr1Δ/rsr1Δ rdi1Δ/rdi1Δ* (DLY15782, n = 15) cells are not significantly different.

The bars represents mean ± SEM. **(C)** Quantitative western blot estimated that the molar ratio between endogenous Rdi1p and Cdc42p is around 1:1. A *3myc-CDC42 RDI1-3myc* strain (DLY15851) was used for equal recognition by the α-myc antibody. The protein preparation by TCA was serial diluted for quantification. **(D)** Diagram of the positive feedback model incorporating a hypothetical Rdi1p-mediated negative feedback. Positive feedback and negative feedback are indicated as red and blue arrows, respectively. **(E)** Overexpression of Cdc42p in *rsr1Δ/rsr1Δ* (control: 11971, overexpressor: DLY12127) and *rsr1Δ/rsr1Δ rdi1Δ/rdi1Δ* (control: DLY15514, overexpressor: DLY14418) cells does not affect viability. Upper panel is the western blot showing overexpression of Cdc42p by β-estradiol. Bottom panel is the spot assay on YEPD, β-estradiol-containing YEPD or YEPG plates at 30℃. **(F)** The percentages of GTP-Cdc42p in the polarized cluster in control (DLY16067, n = 15) and Cdc42p overexpression (DLY15567, n = 15) cells are not significantly different. The bars represents mean ± SEM.

Cdc42p in the face of variable polarity factor concentrations. If Rdi1p is taken into account, an alternative explanation is that there are much more Rdi1p molecules than Cdc42p in vivo, allowing cells to sequester excess Cdc42p in the cytoplasm when Cdc42p is overexpressed. Using a strain in which one copy of *RDI* and *CDC42* are tagged with 3myc and expressed under their own promoters, a quantitative western blot analysis estimated that endogenous Rdi1p is present at a 1:1 molar ratio compared to Cdc42p (Fig. 4.4C). This rules out the possibility that Cdc42p is greatly outnumbered by Rdi1p because the similar molar ratio is unable to compensate for the 7-fold Cdc42p overexpression we obtained (Howell et al., 2012).

The slow competition in the absence of Rdi1p raises another hypothesis that Rdi1p is involved in the negative feedback to speed up competition. In this scenario, we assume that GTP-Cdc42p leads to the activation of Rdi1p, which keeps more Cdc42p in the cytoplasmic inactive state, thereby reducing the amount of Cdc42p available for positive feedback (Fig. 4.4D). If Rdi1p is part of the negative feedback loop, its absence would reduce or even abrogate the buffering of GTP-Cdc42p upon Cdc42p overexpression, leading to large GTP-Cdc42p clusters or inability to polarize. However, overexpression of Cdc42p (either via β-estradiol or galactose induction, top panel of Fig. 4.4E) in *rsr1Δ/rsr1Δ rdi1Δ/rdi1Δ* cells did not affect cell viability at 30℃ (bottom panel of Fig. 4.4E). Cdc42p overexpressors had more GTP-Cdc42p polarized in the cluster, but the level was not significantly different from the control strain (Fig. 4.4F), indicating that *rdi1Δ* cells are capable of buffering GTP-Cdc42p in the face of Cdc42p overexpression and that Rdi1p is not required for buffering in the negative feedback.

4.2.5 How does GDI speed up competition? Not through septin recruitment to restrain competition

The septins are cytoskeletal proteins that are recruited by Cdc42p to form a ring at the mother-bud neck (McMurray and Thorner, 2009; Oh and Bi, 2011). In *rsr1Δ/rsr1Δ* cells, septin rings were not recruited to the incipient bud site until Bem1p clusters competition were resolved and/or oscillation was stabilized, which was ~4-5 min after polarization (Fig. 4.5A). Two-color imaging of Bem1p and Cdc3p (a component of septins) showed that similar time delay between Bem1p clustering and septin recruitment was maintained in *rsr1Δ/rsr1Δ rdi1Δ/rdi1Δ* cells (4.5 min on average, Fig. 4.5B). The long coexistence of multiple clusters in *rsr1Δ/rsr1Δ rdi1Δ/rdi1Δ* cells allowed septins to form around long-lasting clusters which were competed away later (Fig. 4.5C). Surprisingly, the septin rings around the losing Bem1p clusters gradually disassembled, hanging around for another 1-3 min after the Bem1p competition was completed. Only the ring around the winning cluster remained and became brighter through time. These findings suggested the signaling from Cdc42p to septin recruitment was not affected by *RDI1* deletion and septin rings underwent dynamic assembly and disassembly before a final polarization site was committed.

Septins has been proposed to act as diffusion barriers to control the exchange of materials between mother and bud in yeast cells (Barral et al., 2000; Luedeke et al., 2005; Shcheprova et al., 2008; Takizawa et al., 2000). In *rdi1Δ* cells, slow growth of clusters allows septins to come in before competition finished. It is possible that the presence of septins could slow down the competition by acting as a barrier to restrain the diffusion of

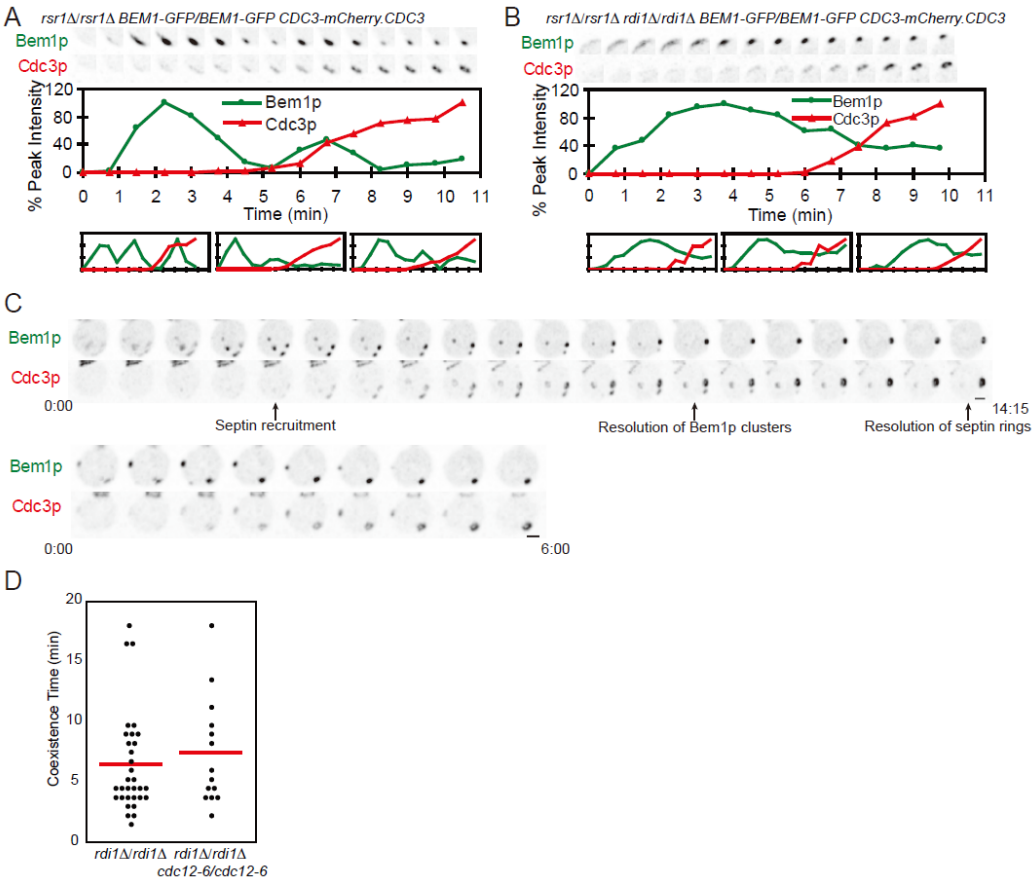

Figure 4.5 Septin recruitment does not slow down competition

(A-B) The timing of septin recruitment is similar in the strains with (A) or without (B) Rdi1p. Top panels are the cropped images of a cell showing Bem1p-GFP and Cdc3-mCherry signals. Middle panels are the quantification of the sum intensity changes. Lower panels are the quantifications of another three cells. **(C)** Two representative cells showing septin recruitment to the long-lasting competing clusters. Septins accumulate around Bem1p clusters as they grow and compete and disassemble few minutes after the losing clusters disappear. **(D)** *rdi1Δ* cells which cannot form septin rings still displayed slow competition. Both control (DLY12577) and *cdc12-6* (DLY15925) strains were filmed at 37℃. Each dot represents one cell. The red line the average time.

polarity factors in the polarized clusters. Alternatively, septins could recruit other downstream factors and thus impede the diffusion of polarity factors out of the clusters. To test whether septin rings slow down competition, we introduced a temperature sensitive septin mutant *cdc12-6* to ask whether the competition time in *rdi1Δ* cells would be shortened when septins were delocalized at 37℃. To make sure the competition dynamics is not altered at higher temperature, we also imaged *rsr1Δ/rsr1Δ rdi1Δ/rdi1Δ* strain at 37℃. Both the control and *rsr1Δ/rsr1Δ rdi1Δ/rdi1Δ cdc12-6/cdc12-6* strains displayed long coexistence time at 37℃, suggesting that septin recruitment did not contribute to restraining competition (Fig. 4.5D).

4.2.6 How does GDI speed up competition? *rdi1Δ* cells may compete for a limiting pool of Cdc42p

Previous FRAP analyses revealed that Cdc42p movement is severely slowed in the absence of Rdi1p. We repeated the same FRAP experiment with our GFP-Cdc42p (8-fold overexpression) and Bem1p-GFP probes. The recovery of GFP-Cdc42p was consistently slower ($t_{1/2}$ ~22 sec), while the recovery of Bem1p-GFP was not affected by *RDI1* deletion ($t_{1/2}$ ~3 sec) (Fig. 4.6A). The slow competition in *rdi1Δ* cells suggests that slow Cdc42p movement could affect competition even though the Bem1p complexes still move rapidly.

We have assumed Bem1p complex as the limiting factor for competition in all our previous mathematical models because Bem1p complex was the species with the lowest abundance. Given that the dynamics of Bem1p complex stay the same in the absence of Rdi1p, we started to question whether Bem1p complex is still the limiting factor in *rdi1Δ*

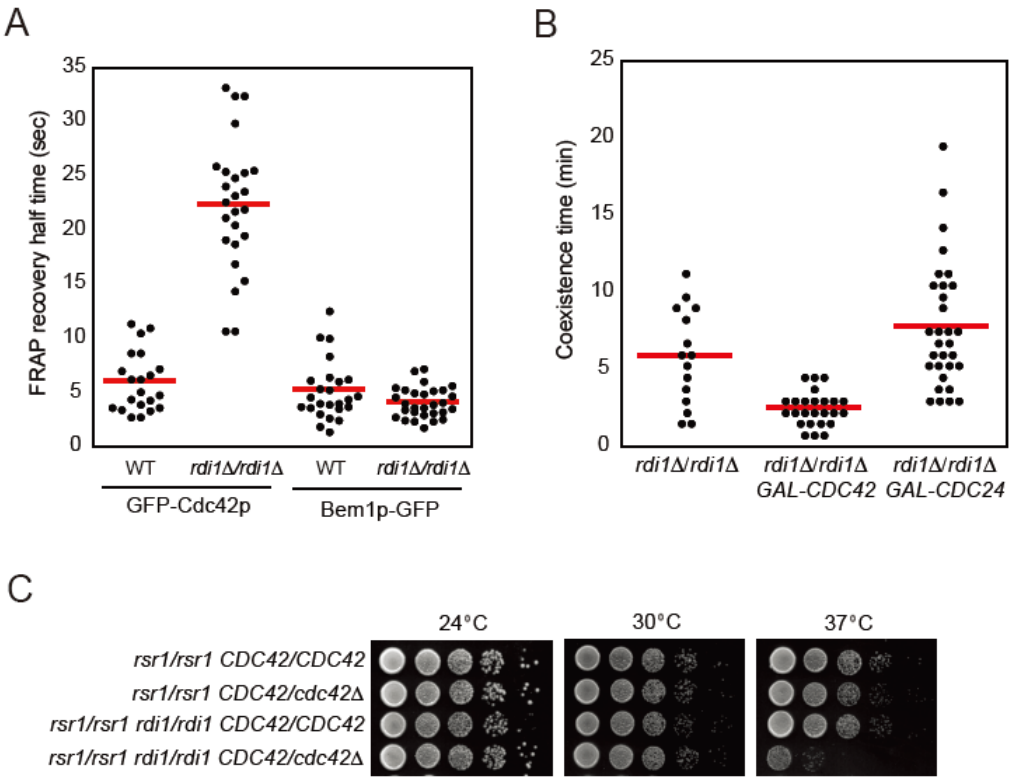

Figure 4.6 *rdi1Δ* cells may compete for a limiting pool of Cdc42p

(A) FRAP recovery half time after photobleaching of GFP-Cdc42p is slowed in *rdi1Δ/rdi1Δ* cells, whereas Bem1p-GFP dynamics is not affected in the absence of Rdi1p. The strains have at least one copy of *RSR1* to avoid oscillation, which interferes with FRAP analysis. Each dot is a single cell. The red line is the averaged time. Strains used from left to right: DLY9201, DLY15121, DLY13920, and DLY14898. **(B)** Coexistence time between Bem1p-GFP clusters in *rsr1Δ/rsr1Δ rdi1Δ/rdi1Δ* control (DLY15514), Cdc42p overexpression (DLY14418), or Cdc24p overexpression strains (DLY15991). Only the overexpression of Cdc42p shortened the coexistence time. **(C)** Deletion of one copy of *CDC42* in *rsr1Δ/rsr1Δ rdi1Δ/rdi1Δ* cells led to decreased cell viability. The spot assay was performed on YEPD plates incubated at indicated temperatures. Strains used from top to bottom: DLY9200, DLY13824, DLY12577, and DLY16447.

cells. In vivo, Cdc42p is present in either the membrane-bound slow-moving pool or cytoplasmic Rdi1p-bound fast-moving pool. Presumably in the absence of Rdi1p, Cdc42p population would shift dramatically to the slow-moving pool. A FCS analysis monitoring the cytoplasmic pool of Cdc42p showed that the percentage of slow-moving pool indeed increased in *rdi1Δ* cells, but there was still a fast-moving pool of Cdc42p present in the cells (Das et al., 2012). If it is the fast-moving Cdc42p that allows competition to happen within a reasonable time in most of *rdi1Δ* cells, the decrease in the amount of this "effective pool" for competition may make Cdc42p become the limiting factor.

If competing for limiting Cdc42p was what led to slow competition in *rdi1Δ* cells, could fast competition be restored by overexpressing Cdc42p? In other words, increasing the amount of Cdc42p may make the Bem1p complexes limiting again and speed up competition. As shown in Fig. 4.4E, overexpressing Cdc42p in *rsr1Δ/rsr1Δ rdi1Δ/rdi1Δ* cells did not affect cell viability, suggesting overexpressors were able to polarize and bud. Strikingly, time-lapse imaging of the overexpressors revealed that the coexistence time between Bem1p clusters were shortened to almost wild-type level (2.5 min on average, Fig. 4.6B). The shortening of coexistence time was not caused by the inducible artificial transcription factor or the β-estradiol treatment because the isogenic control strain with the same treatment still had long cluster coexistence time and generated two buds. The shortened coexistence time was specific to Cdc42p overexpression because Cdc24p (Fig. 4.6B) and Bem1p (data not shown) overexpressors still exhibited slow competition. Interestingly, we found that the initial slow clustering of polarity factors in *rsr1Δ/rsr1Δ rdi1Δ/rdi1Δ* cells was accelerated in some Cdc42p overexpressors. Although the ramp-up

speed was not as fast as that in *rsr1Δ/rsr1Δ* cells, some of them were able to reach the first peak within 3 min and even showed one more cycle of oscillation. Since the β-estradiol induction was heterogeneous from cell to cell (as described in chapter 2), we speculated that those with faster polarization had higher expression level of Cdc42p.

We also tested the effect of Cdc42p amount on competition in a reverse way by deleting one copy of *CDC42* in *rsr1Δ/rsr1Δ rdi1Δ/ rdi1Δ* cells, making Cdc42p even more limiting. Making *CDC42* hemizygous in *rsr1Δ/rsr1Δ* background did not cause any obvious difference in terms of viability and polarization dynamics (Fig. 2.10B and 4.6C); however, *rsr1Δ/rsr1Δ rdi1Δ/rdi1Δ* cells with hemizygous *CDC42* grew much worse than the homozygous strain at 37℃. Even though some of the hemizygous cells managed to polarize at 30℃, ~25% of the cells kept growing bigger without forming a polarized patch within the 1 hr imaging period. Taken together, these data supported our hypothesis that Cdc42p became the limiting factor in competition in the absence of Rdi1p. We suggest that with ample Cdc42p, the Bem1p complex becomes limiting, and that because they readily exchange between membrane and cytoplasm, competition for that limiting pool is more rapid.

4.2.7 How do *rdi1Δ* cells concentrate Cdc42p? Actin-mediated trafficking helps but does not completely account for Cdc42p movement in the absence of Rdi1p

In addition to Rdi1p-mediated Cdc42p trafficking, actin cables has been suggested as an alternative slow pathway to transport Cdc42p on secretory vesicles to the polarization cluster. It has been reported that depolymerization of actin with Latrunculin

B (Lat B) in *rdi1Δ* cells blocked polarization of Cdc42p (Freisinger et al., 2013), suggesting that actin-mediated pathway is the sole alternative pathway to transport Cdc42p in the absence of Rdi1p. Given the different strain backgrounds and GFP-Cdc42p probes used, we first sought to confirm if polymerized actin was required for *rsr1Δ/rsr1Δ rdi1Δ/rdi1Δ* cells to concentrate Cdc42p.

Our FRAP results showed that Lat A treatment reduced the recovery half time of GFP-Cdc42p in *rsr1Δ/rsr1Δ rdi1Δ/rdi1Δ* cells ($t_{1/2}$~ 35 sec, Fig. 4.7A). However, different from the previous study, in which the Cdc42p polar cap dissipated over time in *rdi1Δ* cells treated with LatA (Slaughter et al., 2009), our GFP-Cdc42p was able to recover after photobleaching (Fig. 4.7B). More surprisingly, a small number of *rsr1Δ/rsr1Δ rdi1Δ/rdi1Δ* cells treated with 200 μM Lat A was able to concentrate Cdc42p. Compared to *rsr1Δ/rsr1Δ* cells treated with the same concentration of Lat A, which formed a tight, polarized Cdc42p cluster displaying oscillation, *rsr1Δ/rsr1Δ rdi1Δ/rdi1Δ* cells spent a longer time to gradually concentrate Cdc42p and eventually formed a dimmer cluster without oscillation (Fig. 4.7D).

Although we could detect Cdc42p polarization in Lat A-treated *rsr1Δ/rsr1Δ rdi1Δ/rdi1Δ* cells, only a small number of cells managed to do so. Most cells did not polarize or only exhibited a GFP-Cdc42p "haze" for a long time without forming a clear, tight cluster (exemplified by the first three timeframes in 4.7D). It suggested that in the absence of Rdi1p and polymerized actin, cells do have problem to concentrate Cdc42p. We sought to determine if the polarization of other probes would also be defective in Lat A-treated *rsr1Δ/rsr1Δ rdi1Δ/rdi1Δ* cells. The probes we monitored were Bem1p-GFP and

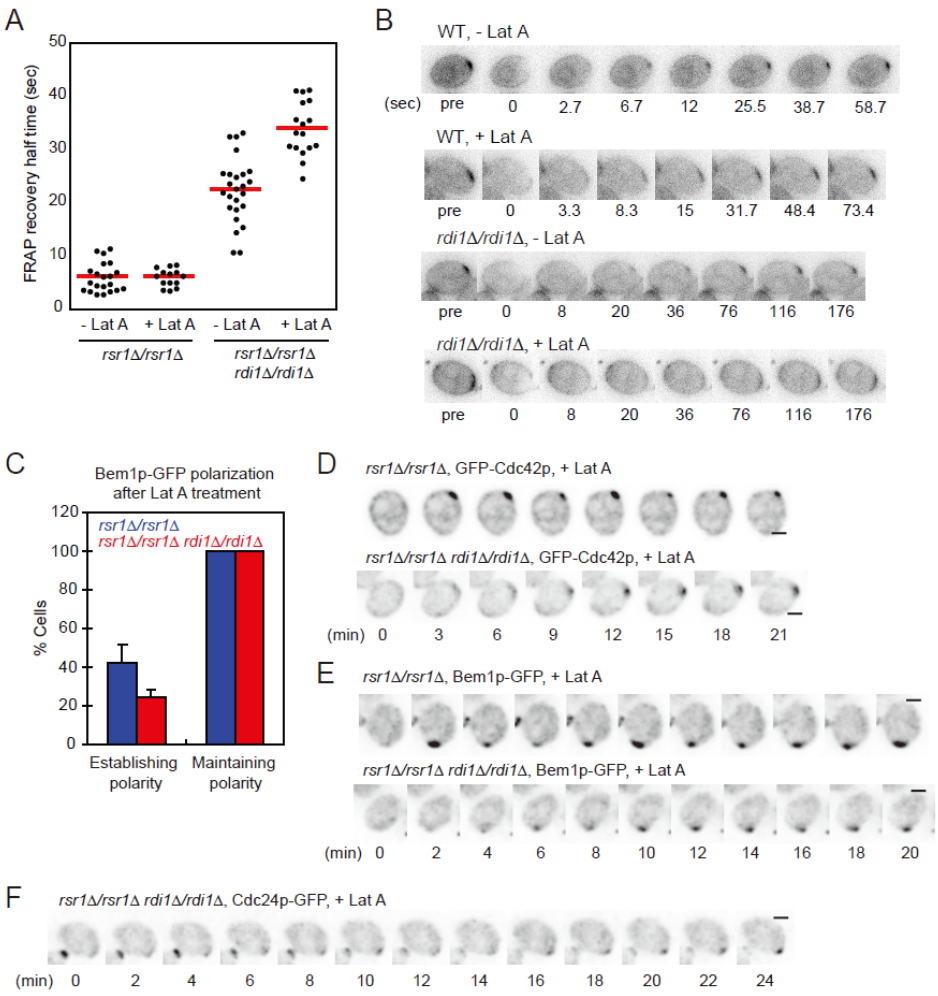

Figure 4.7 *rdi1Δ* cells treated with Lat A can concentrate Cdc42p and polarize

(A) The treatment of Lat A further decreased FRAP recovery half time of GFP-Cdc42p *rsr1Δ/rsr1Δ rdi1Δ/rdi1Δ* cells (DLY14898). **(B)** Four representative cells from (A) (in according orders) recovering GFP-Cdc42p cluster from photobleaching. **(C)** Lat A treatment decreased the ability of *rsr1Δ/rsr1Δ rdi1Δ/rdi1Δ* cells to establish a new polarized cluster, but did not affect the maintenance of a pre-existing one. The bar graph represents the percentage of cells establishing (left) or maintaining (right) a Bem1p-GFP cluster in *rsr1Δ/rsr1Δ* (DLY11320) or *rsr1Δ/rsr1Δ rdi1Δ/rdi1Δ* strains (DLY12577) treated with 200 µM Lat A (mean ± SEM). The effectiveness of Lat A was judged by the absence of actin patches in DLY11320. **(D-E)** Polarization of GFP-Cdc42p (D) or Bem1p-GFP (E) in representative *rsr1Δ/rsr1Δ* (upper panels) or *rsr1Δ/rsr1Δ rdi1Δ/rdi1Δ* (bottom panels) strains treated with Lat A. **(F)** Cdc24p-GFP polarization in *rsr1Δ/rsr1Δ rdi1Δ/rdi1Δ* strain in the presence of Lat A. Scale bars, 2µm

Cdc24p-GFP, both of which were integrated at the endogenous loci and expressed by their own promoters. To get a quantitative view of the difference between *rsr1Δ/rsr1Δ* cells and *rsr1Δ/rsr1Δ rdi1Δ/rdi1Δ* cells treated with Lat A, we scored the number of cells able to establish a new Bem1p-GFP cluster or maintain a preexisting cluster formed before treatment. Latrunculin treatment causes problems on cytokinesis, so we aimed at mother-daughter pairs showing a neck signal before the first 30 min of the filming (assuming they were undergoing cytokinesis) and unbudded cells (assuming they are in G1 phase). About half of Lat A-treated *rsr1Δ/rsr1Δ* cells were able to establish a new Bem1p-GFP cluster which stayed for at least 15 min, whereas only ~25% of *rsr1Δ/rsr1Δ rdi1Δ/rdi1Δ* cells were able to do so (Fig. 4.7C), indicating that cells had a decreased ability in polarity establishment in the absence of Rdi1p and polymerized actin. Intriguingly, both strains were fully capable of maintaining an already polarized cluster for a long time (even more than 1 hr). In most, if not all, of the Lat A-treated *rsr1Δ/rsr1Δ rdi1Δ/rdi1Δ* cells that were able to polarize, Bem1p-GFP and Cdc24p-GFP clustered slowly, but they were able to concentrate and from a clear cluster eventually (Fig. 4.7E-F), which was different from the haze-like behavior of GFP-Cdc42p. The more robust polarization of Bem1p and Cdc24p than Cdc42p in the absence of Rdi1p and polymerized actin raised a possibility that cells could concentrate GTP-Cdc42p without concentrating total Cdc42p. The same Latrunculin experiments looking at the PBD probe will be performed to answer this question.

The other possibility that we were able to observe the polarization of GFP-Cdc42p in our Lat A-treated *rsr1Δ/rsr1Δ rdi1Δ/rdi1Δ* cells is that the GFP-Cdc42p probe we used

is 8-fold overexpressed, which may be higher than those used in previous studies. Overexpression of the probe might enhance the signal and reinforce the functionality of the defective probe, leading to the more robust polarization and concentration of Cdc42p we observed in our strains. We sought to determine if overexpression of wild-type, untagged Cdc42p would also improve polarization in *rsr1Δ/rsr1Δ rdi1Δ/rdi1Δ* cells treated with Lat A. To avoid diluting the fluorescent signal of GFP-Cdc42p at the polarization cluster upon overexpression of untagged Cdc42p, we used Bem1p-GFP probe expressing from its own promoter to observe polarization. We found that Cdc42p overexpression did not increase the percentage of *rdi1Δ* cells polarizing in Lat A compared to the control strain. With the more powerful spinning disk confocal microscopy, we are now able to detect ~45% of *rsr1Δ/rsr1Δ rdi1Δ/rdi1Δ* cells polarizing in Lat A whether they overexpress Cdc42p or not (Fig. 4.8A), as opposed to ~25% of cells imaged with wide-field fluorescent microscopy (Fig. 4.7C). Nonetheless, Cdc42p overexpressors could form brighter clusters (Fig. 4.8B) and sometimes resemble *rsr1Δ/rsr1Δ* cells by exhibiting oscillation or relocation. The only thing that was not improved is that Cdc42p overexpressors clustered polarity factors slowly before reaching the peak. These results suggest that Cdc42p overexpression could potentially enhance polarization and even change polarization dynamics in *rsr1Δ/rsr1Δ rdi1Δ/rdi1Δ* cells treated with Lat A.

4.2.8 How do cells concentrate Cdc42p in the absence of Rdi1p and actin? Abolishing membrane-cytoplasm shuttling of Cdc42p blocks its polarization

It has recently been hypothesized that non-uniform diffusion of Cdc42p on the plasma membrane could result in microdomains that locally concentrate Cdc42p (Slaughter et al., 2013). If non-uniform diffusion accounts for the Rdi1p and actin-independent pathway to concentrate Cdc42p, locking Cdc42p on the membrane should not prohibit its concentration. To achieve this, we fused the first 28 amino acids of Psr1p (which contains one myristoylation and two palmitoylation sites) to the N terminus of GFP-Cdc42p (Psr1-GFP-Cdc42p). Single plane confocal images showed that Psr1-GFP-Cdc42p uniformly localize to the cell cortex (Fig. 4.9A), but we failed to detect any cell with a polarized signal. Psr1-GFP-Cdc42p expressing at endogenous level was unable to complement cells deleted for *CDC42*, whereas mutant Psr1^{C9G,C10G}-GFP-Cdc42p expressing at similar level (lacking palmitoylation sites) (Fig. 4.9B) was able to weakly compliment cells deleted for *CDC42* (Fig. 4.9C). Furthermore, cells overexpressing *PSR1-GFP-CDC42,* but not mutant *psr1^{C9G,C10G}-GFP-CDC42,* was toxic to cells at 37°C. These results suggested that locking GFP-Cdc42p to the membrane is prohibitive to its concentration, not only arguing against the non-uniform diffusion mechanism but also highlighting the importance of shuttling Cdc42p between cytoplasm and membrane for Cdc42p concentration. This again implies that there is an Rdi1p and actin-independent mechanism to transport and concentrate Cdc42p.

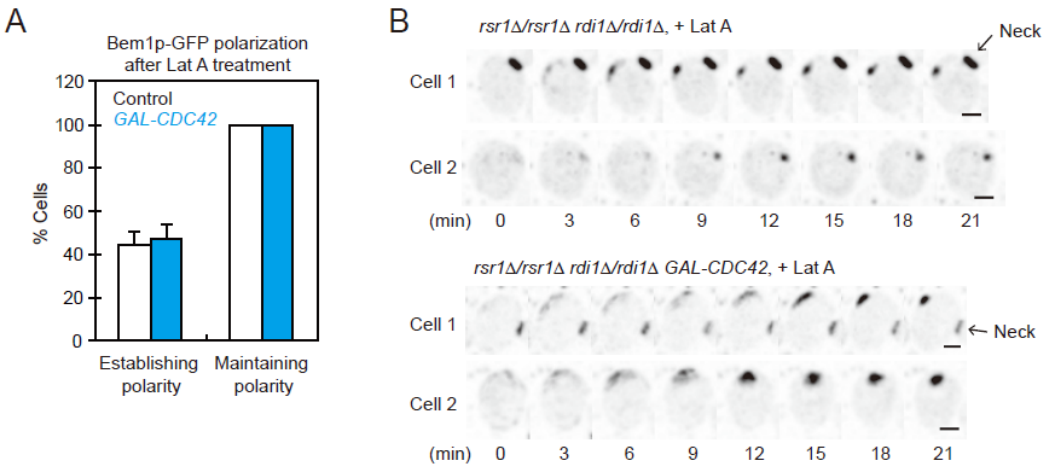

Figure 4.8 Cdc42p overexpression enhances polarization in cells lacking Rdi1p and polymerized actin

(A) The percentage of cells establishing (left) or maintaining (right) a Bem1p-GFP cluster was similar in the *rsr1Δ/rsr1Δ rdi1Δ/rdi1Δ* control (DLY15514) or Cdc42p-overexpressing strains (DLY14418) treated with 200 μM Lat A (mean ± SEM). The effectiveness of Lat A was judged by the absence of actin patches in DLY12120 mixing with the testing strains. **(B)** Bem1p-GFP polarization in the *rsr1Δ/rsr1Δ rdi1Δ/rdi1Δ* control or Cdc42p-overexpressing strains treated with Lat A.

4.3 Discussion

4.3.1 Altered polarization dynamics in the absence of Rdi1p

GDI- and actin-mediated trafficking have been proposed as two independent but redundant pathways for Cdc42p concentration. A recent study reported that the percentage of cells able to polarize Cdc42p after releasing from G1 arrest were not affected in *rdi1Δ* cells (Freisinger et al., 2013), presumably due to the backup of the actin pathway. Using time-lapse imaging to monitor the signal changes of core polarity factors during polarity establishment, here we showed that *rdi1Δ* cells actually displayed very different polarization dynamics from cells with functional Rdi1p. The initial rapid clustering and dispersal of Bem1p-GFP and GFP-Cdc42p and the subsequent oscillatory behaviors observed in *rsr1Δ/rsr1Δ* cells are all gone when *RDI* is deleted. In *rsr1Δ/rsr1Δ rdi1Δ/rdi1Δ* cells, Bem1p and Cdc42p both accumulated slowly at the polarized cluster and their signal intensities either stayed high or dropped to an intermediate level before bud emergence without showing another oscillatory cycle. In chapter 2, we showed that the positive feedback-mediated initial polarization is rapidly antagonized by a delayed negative feedback loop, thereby leading to the oscillatory polarization. Presumably the slow clustering of polarity factors in *rsr1Δ/rsr1Δ rdi1Δ/rdi1Δ* cells allows the delayed negative feedback catch up the action of positive feedback; therefore, the oscillation is greatly diminished or abolished. The $cdc42^{R66A}$ mutant unable to bind Rdi1p also showed slower polarization dynamics, confirming that the altered dynamics is directly due to the

Rdi1p-mediated Cdc42p trafficking instead of indirect effect from disrupting the interaction between Rdi1p and other Rho proteins.

Why does Cdc42p concentrate at the pre-bud site slowly in the absence of Rdi1p? A previous mathematical modeling on yeast polarity predicted that Bem1p complex-mediated positive feedback mechanism is able to generate a GTP-Cdc42p gradient at the pre-bud site, but total Cdc42p cannot be concentrated if the Rdi1p-mediated trafficking is not incorporated in the model (Johnson et al., 2011), indicating that rapid Cdc42p trafficking is important for Cdc42p concentration. Also, Rdi1p-mediated pathway has been suggested as the dominant mechanism for Cdc42p trafficking because its absence dramatically decreased the FRAP recovery half time of GFP-Cdc42p (compared to the minor effect caused by Lat A treatment) (Slaughter et al., 2009). It is possible that slower Cdc42p trafficking in the absence of Rdi1p leads to slower Cdc42p accumulation at the polarization site. However, this idea does not apply to Bem1p. Our FRAP results showed that the movement of Bem1p is not affected in *rdi1Δ* cells even though Bem1p also exhibited slow clustering. Also, the expression level of Bem1p is similar in *rsr1Δ/rsr1Δ* and *rsr1Δ/rsr1Δ rdi1Δ/rdi1Δ* cells (data not shown), from which we assumed the abundance of the Bem1p complex is not dramatically altered in the absence of Rdi1p. These results suggested that although the abundance and the cytoplasmic diffusion rate of the Bem1p complexes remain the same, slowing down Cdc42p trafficking had a dominant effect to decelerate the polarization dynamics of Bem1p (and potentially the other core polarity factors).

4.3.2 Effect of *RDI1* deletion on competition and singularity

The other obvious phenotype in *rsr1Δ/rsr1Δ rdi1Δ/rdi1Δ* cells is the long coexistence between polarization clusters. Two-color imaging showed that the core polarity factors still concentrate and disperse in concert in the absence of Rdi1p when multiple clusters were formed. The characterization of competition phenotype mainly focused on the Bem1p-GFP probe, not only because it formed clear and tight clusters that facilitate visualization and scoring, but also for fair comparison to previous characterization in *RDI1* cells. The averaged coexistence time increased about three-fold in the absence of Rdi1p, and it was contributed by both slower cluster growth and slower competition between clusters. Although the competition was much slower, most *rdi1Δ* cells were able to resolve a winning cluster and generate only one bud. In about 4% of *rsr1Δ/rsr1Δ rdi1Δ/rdi1Δ* cells, the competition did not finish before bud emergence so that the two clusters went on to grow two buds, violating singularity. When two buds formed, the sizes/intensities of the polarized clusters could determine the growth rate of the buds. In some cases, two clusters with uneven sizes/intensities led to the growth of a bigger and a smaller bud. In a small amount of two-budded cells, the competition between the clusters even continued after they were already in separate buds (cell 2 in Fig. 4.3F). The bud stopped growing once the polarized cluster in it was competed away, leaving an abandoned bud on the mother cell. A recent study also reported the detection of multiple GFP-Cdc42p clusters and the formation of two buds in haploid *rdi1Δ* cells (Freisinger et al., 2013). Their results suggested that multiple clusters were stable once they were formed in *rdi1Δ* background because the actin-mediated pathway would

reinforce the clusters by delivering more GTP-Cdc42p to the sites. Our results argued against this hypothesis, showing that the clusters were able to compete and disappear after they were formed.

In addition to yeast bud formation, the involvement of GDI in singularity has been shown in the growth of root hairs in *Arabidopsis thaliana* (Carol et al., 2005). Root hairs are cellular protrusions extending from the root surface that extend the access to inorganic ions in the soil essential to plant growth. In wild-type plants, a root hair cell only produces one root hair whose elongation depends on localized growth at the tip of the hair, which requires localized accumulation of reactive oxygen species (ROS). Mutations in *SCN1*, which encodes a RhoGDI in *A. thaliana*, resulted in the production of ROS at several ectopic foci and thus the initiation of multiple sites of growth along the ouster surface of the root hair cell. The phenotypes in *scn1* mutant are analogous to the multiple polarized clusters and the growth of multiple buds in *rdi1Δ* yeast cells, indicating that GDI is responsible for ensuring the growth to a single site in both yeast and plant.

4.3.3 Septin recruitment does not restrain or stop cluster competition

Two-color filming of Bem1p-GFP and Cdc3p-mCherry showed that in two-budded cells, the septin rings were recruited to both mother-bud necks (data not shown). Septins has been proposed to act as diffusion barriers to control the exchange of materials between mother and bud in yeast cells (Barral et al., 2000; Luedeke et al., 2005; Shcheprova et al., 2008; Takizawa et al., 2000). In some *rdi1Δ* cells, competition keeps going on even after the polarized clusters has entered separate buds, suggesting the septin

rings did not stop polarity factors from diffusing out of the buds. More surprisingly, in some *rsr1Δ/rsr1Δ rdi1Δ/rdi1Δ* cells the septin rings were formed around multiple clusters before the competition was finished. Quantification of the two-color images indicated that the time interval between Bem1p polarization and septin recruitment (~4-5 min) is not affected by *RDI1* deletion. Therefore, the slow clustering and competition of Bem1p clusters in the absence of Rdi1p allowed the formation of multiple septin rings before competition was completed. We showed that the presence of a septin ring around the clusters did not slow down the competition because the disruption of septin ring formation in a *ts* septin mutant did not speed up competition.

Another interesting phonotype we observe was that the septin rings around the losing clusters gradually disassembled after the clusters were competed away. In wild-type cells, septins are recruited to the pre-bud site by GTP-Cdc42p (Cid et al., 2001), assemble into a ring initially, then undergo a conformational change to form a highly-organized collar at the mother-bud neck upon bud emergence, and disassemble following cytokinesis in response of cell cycle cues (McMurray and Thorner, 2009). The disappearing septin rings in *rsr1Δ/rsr1Δ rdi1Δ/rdi1Δ* cells suggests that a polarized GTP-Cdc42p cluster is required to sustain the localization of septins. In addition, septins have not yet formed a highly-organized collar structure before bud emergence and may undergo reversible disassembly more easily at this stage.

4.3.4 Competing for limiting Bem1p or Cdc42p under different conditions

The slow competition in *rsr1Δ/rsr1Δ rdi1Δ/rdi1Δ* cells indicates that the presence of Rdi1p accelerates competition to ensure singularity. How does Rdi1p speed up

competition? We have tested several possibilities and showed that Rdi1p neither acts through the negative feedback nor restricts competition via septin recruitment. We have assumed the Bem1p complex as the limiting factor for competition in our previous studies because the Bem1p complex is the least abundant species among the polarity components. However, as mentioned above, the abundance and the dynamics of the Bem1p complex are not obviously altered in the absence of Rdi1p. If the properties of the Bem1p complex stay the same and the polarized clusters in *rdi1Δ* cells compete for the Bem1p complex, why do the competition dynamics become slower? Is the Bem1p complex still the limiting factor for competition in *rdi1Δ* background? Because the slow movement of Cdc42p seems to coincide with slow competition in the absence of Rdi1p, we hypothesize that Cdc42p becomes the limiting factor in *rdi1Δ* background. Two findings support this hypothesis. First, making the amount of Cdc42p even more limiting by deleting one copy of *CDC42* in *rsr1Δ/rsr1Δ rdi1Δ/rdi1Δ* cells resulted in decreased cell viability at 37℃. Although we did not perform live-cell imaging of this hemizygous strain at 37℃, filming it at 30℃ has already revealed inability to polarize in ~25% of cells (data not shown). On the contrary, cutting down half the amount of Cdc42p in *rsr1Δ/rsr1Δ* cells did not cause obvious alternation in polarization dynamics and viability (Fig. 2.10). These results suggest that cells are more sensitive to the abundance of Cdc42p in the absence of Rdi1p. Second, overexpression of Cdc42p in *rsr1Δ/rsr1Δ rdi1Δ/rdi1Δ* cells speeded up competition to nearly the wild-type level. We suggest that with ample Cdc42p, the Bem1p complex becomes limiting again and thus restored rapid

competition. We seek to use mathematical modeling to simulate the situation we hypothesize here by (1) slowing down the Cdc42p membrane on/off rate to mimic *rdi1Δ* condition, and (2) decreasing Cdc42p concentration to make it limiting. We hope we could recapitulate slow competition in the model.

The overexpression of Cdc42p not only speeded up competition between Bem1p clusters, but also accelerated the FRAP recovery half time of GFP-Cdc42p (data not shown). These phenotype changes are specific to Cdc42p overexpression because Cdc24p or Bem1p overexpression did not lead to the same effect. In addition to the hypothesis of switching Bem1p back as the limiting factor, it is possible that somehow overexpression of Cdc42p activates the actin-mediated or even an unknown Cdc42p trafficking pathway, making Cdc42p moves fast again. Alternatively, some intrinsic property of Cdc42p may directly affect the polarization and competition dynamics when it is overexpressed. It has been reported that Cdc42p could fall off the membrane by itself without the help of Rdi1p in vitro (Johnson et al., 2009). It is possible that in vivo a small cytoplasmic pool of Cdc42p could spontaneously partition between the membrane and cytoplasm and act like GDI-Cdc42p complex. If that is so, there must be a way to stabilize GTP-Cdc42p on the membrane and only allow GDP-Cdc42p to translocate, analogous to the differential affinity of GDI to different nucleotide-bound forms of Cdc42p. Inspired by the study from plant ROP GTPases, transient palmitoylation could be a mechanism to stabilize GTP-Cdc42p on the membrane but allow GDP-Cdc42p to dissociate from the membrane (Sorek et al., 2007; Sorek et al., 2010). Sequence alignment showed that *S. cerevisiae* Cdc42p also has the conserved potential

palmitoylation sites, which provides an appealing model that non-palmitoylated GDP-Cdc42p can dissociate from the membrane and diffuse rapidly in the cytoplasm until it is palmitoylated and stabilized on the membrane upon being converted to GTP-bound form at the polarization site. It is conceivable that this process can be inefficient because without the binding of Rdi1p, a part of the cytoplasmic pool of Cdc42p can be degraded (Boulter et al., 2010) before it is converted to the GTP-bound form and stabilized on the membrane. The spontaneous shuttling may only contribute marginally to Cdc42p trafficking in *rdi1Δ* situation, but there will be a larger cytoplasmic pool of Cdc42p when Cdc42p is overexpressed, which could potentially lead to noticeable changes to Cdc42p trafficking and competition.

4.3.5 Polarization in the absence of Rdi1p and polymerized actin

Cytoplasmic Rdi1p-Cdc42p complexes and targeted delivery of Cdc42p-loaded vesicles along actin cables have been proposed as fast and slow recycling mechanism to concentrate Cdc42p, respectively (Slaughter et al., 2009). A recent study showed that depolymerization of actin with Lat B treatment in *rdi1Δ* or $cdc42^{R66A}$ cells blocked the polarization of a Cdc42p cluster, indicating that these two pathways were the only two mechanisms to concentrate Cdc42p (Freisinger et al., 2013). Surprisingly, utilizing our GFP-Cdc42p probe in our strain background, we were able to detect Cdc42p polarization in a small number of *rdi1Δ* cells treated with Lat A. Actin-mediated vesicle delivery does play a role in concentrating Cdc42p because the majority of Lat A-treated *rdi1Δ* cells did not do anything or formed a haze of GFP-Cdc42p without coalescing into a clear cluster

during 1.5 hr filming. However, few cells were able to form a GFP-Cdc42p cluster even though the intensity of the cluster was dimmer. The inconsistent observation of polarization in the absence of Rdi1p and polymerized actin could be due to different probes used. Our GFP-Cdc42p probe is 8-fold overexpressed, which is probably higher than the one used by Freisinger et al. Higher expression of the fluorescent probe could potentially enhance the polarization signal, facilitating better detection.

The fact that we could only detect weak Cdc42p polarization in a small number of Lat A-treated *rdi1Δ* cells (even with help of GFP-Cdc42p overexpression) but could detect clear polarization of Bem1p and Cdc24p raised that speculation that cells may concentrate GTP-bound Cdc42p without concentrating total Cdc42p to polarize the other core polarity factors in the absence of Rdi1p and actin. We seek to image the polarization of PBD probe in Lat A-treated *rdi1Δ* cells to check whether GTP-Cdc42p is concentrated first. Alternatively, it is possible that cells only need to concentrate total Cdc42p above a certain threshold, which is below the detection limit to most current microscopes, to polarize other factors. In this case, there may be another alternative Cdc42p trafficking pathway to concentrate Cdc42p. To test this possibility, our colleagues have been performing a screening to look for mutants synthetic lethal to *rdi1Δ*.

5. Conclusions and Future Directions

5.1 Conclusions

Symmetry breaking in budding yeast depends on the amplification of stochastic fluctuations by positive feedback, which involves linking a Cdc42p-directed GEF to a Cdc42p effector by the scaffold Bem1p. In principle, positive feedback could lead to the simultaneous growth of several polarized cluster, but yeast cells generate only one front. Some computational models predict that there will be a "winner-takes-all" competition between polarized clusters. In this work, imaging polarity establishment at high resolution revealed that many cells did initially grow more than one cluster of Cdc42p, which subsequently competed with each other to resolve a winning cluster, assuring that cells make only one front. Such competition happens not only in cells breaking symmetry but also in cells with spatial cues. Multicluster intermediates are observed in wild-type yeast cells with intact bud-site-selection machinery, but the locations where they are initiated are biased by the spatial cues. Imaging cells breaking symmetry also revealed oscillatory polarization, suggesting the presence of a delayed negative feedback loop in the yeast polarity circuit. Theoretical studies indicate that negative feedback could buffer the system against fluctuations in polarity protein concentration. In addition to making polarity circuit more robust, negative feedback could speed up competition between polarized clusters, ensuring only one bud forms.

We are trying to understand how competition between clusters occurs. We find that the yeast guanine-nucleotide dissociation inhibitor (GDI), Rdi1p, is needed for rapid competition between clusters. In the absence of Rdi1p the initial clustering of polarity factors is slowed, and competition is also much slower: in some cases cells still have two clusters at the time of bud emergence and they form two buds. We suggest that in the absence of Rdi1p, the clusters compete for a limiting pool of Cdc42p, and that slow exchange of Cdc42p on and off the membrane in *rdi1Δ* cells leads to slow competition. Overexpression of Cdc42p in the *rdi1Δ* background restored rapid competition. We suggest that with ample Cdc42p, other components (e.g. the Bem1p complex) become limiting, and that because these components readily exchange between membrane and cytoplasm, competition for that limiting pool is more rapid.

5.2 Mechanistic basis for negative feedback

In budding yeast cells breaking symmetry, the winning Cdc42p cluster emerging from rapid competition then disperses and reforms in an oscillatory manner. Oscillatory behaviors in biological system usually involve a delayed negative feedback loop. Incorporating a hypothetical negative feedback either through the activation of Cdc42p-directed GAPs or the inhibition of the Bem1p complex recapitulated oscillatory polarization observed in vivo. The mechanism of the negative feedback was unknown when we published the work.

Recently our colleagues Kuo et al. identified a negative feedback mechanism in *S. cerevisiae*. GTP-Cdc42p was known to active PAKs, which then phosphorylate the

Cdc42p-directed GEF, Cdc24p (Bose et al., 2001; Gulli et al., 2000). They showed that Cdc24p phosphorylation reduced its GEF activity in vitro and in vivo. The nonphosphorylatable mutant *CDC24*^{35A} abolished the oscillatory behavior of Bem1p-GFP and led to the accumulation of more GTP-Cdc42p in the polarized cluster in *rsr1Δ/rsr1Δ* cells. These results indicated that Cdc42p phosphorylation acts to reduce polarity factor accumulation at the cortex, and is required for oscillatory polarization. Combined with previous studies, this reveals a negative feedback mechanism involving the following steps: (1) GTP-Cdc42p actives PAKs; (2) activated PAKs phosphorylate Cdc24p to inhibit the GEF activity; (3) decreased GEF activity reduced the level of GTP-Cdc42p. Disruption of this mechanism by a nonphosphorylatable Cdc24p leads to a higher level of GTP-Cdc42p at the polarized cluster, suggesting that negative feedback through Cdc24p phosphorylation is responsible for restraining the positive feedback-mediated growth of polarity clusters.

Previous computational modeling of yeast polarity establishment predicted that negative feedback could buffer the level of GTP-Cdc42p and keep the multiple clusters small in the face of various polarity factor concentrations, thereby ensuring that the competition would happen rapidly to resolve a winning cluster. Although Kuo et al. showed that disrupting the negative feedback via Cdc24p phosphorylation reduced cells' ability to buffer GTP-Cdc42p, the dynamics of competition were not dramatically affected. This observation raises an interesting question: does the buffering of GTP-Cdc42p level necessarily couple to rapid competition? In some *rdi1Δ* cells, we observed the formation of more yet dimmer clusters that competed slowly; however, the percentage

of total Cdc42p and GTP-Cdc42p in the polarized clusters did not seem to be higher in *RDI1* cells. This provides another example that the level of polarity factors in the clusters does not necessarily correlate with the competition time. If that is so, are buffering of GTP-Cdc42p level and rapid competition controlled by different negative feedback mechanisms? Or rapid competition is mediated by other mechanisms irrelevant to negative feedback? We hope our further works on the GDI project would provide other perspective on these questions.

5.3 Does the differential membrane-cytoplasm partitioning between GDP- and GTP-Cdc42p contribute to polarization in the absence of Rdi1p and polymerized actin?

We found that the overexpression of Cdc42p in *rdi1Δ* cells speeded up competition between Bem1p clusters. From this result, we hypothesize that with ample Cdc42p, Bem1p complex becomes the limiting factor again and thus restores rapid competition. Alternatively, we hypothesize that a small pool of GDP-Cdc42p, but not GTP-Cdc42p, could spontaneously partition between the membrane and cytoplasm and act like GDI-Cdc42p complex. One possibility is that transient palmitoylation could be a mechanism to stabilize GTP-Cdc42p on the membrane but allow GDP-Cdc42p to dissociate from the membrane based on the studies on ROP (Rho of Plants) GTPases in *Arabidopsi*s (Sorek et al., 2007; Sorek et al., 2010). When Cdc42p is overexpressed, presumably there would be a larger pool of GDP-Cdc42p undergoing this process and speed up the trafficking of Cdc42p and competition. We have shown that locking Cdc42p

on the membrane by fusing the lipid modification moiety of Psr1p to Cdc42p blocked polarization, indicating that the membrane-cytoplasm shuttling of Cdc42p is required for polarization. If the spontaneous partitioning of GDP-Cdc42p between membrane and cytoplasm does happen in vivo, it could be an alternative mechanism for polarization in the absence of Rdi1p and polymerized actin.

Previous studies in plants suggest that transient S-palmitoylation of ROP6, one of the *Arabidopsis* ROP GTPases, upon its GTP binding and activation contributes to membrane stabilization of ROP6 (Sorek et al., 2007; Sorek et al., 2010). The steady state localization of ROP6 is predominantly on the plasma membrane; the FRAP analysis showed that a constitutively active rop6^{CA} mutant recovers entirely by lateral diffusion after photobleaching, suggesting that GTP-ROP6 tightly anchors to the membrane wherase GDP-ROP6 recovers mainly by exchange. The same FRAP analysis showed that another rop6^{CA} mutant with two palmitoylation sites mutated (C21S and C156S) recovers mainly by exchange, indicating that palmitoylation contributes to membrane anchorage of GTP-ROP6. A similar de/repalmitoylation cycle is also suggested for the rapid redistribution of H-Ras and N-Ras between different cellular compartments (Rocks et al., 2005). Depalmitoylated H-Ras and N-Ras equilibrate between membrane and cytosol (in the range of seconds), allowing rapid exchange between the plasma membrane and the Golgi until their membrane interactions are stablilized by repalmitoylation. Given the fact that palmitoylation is reversible and can be regulated, the finding from the plant ROPs provides an appealing model that non-palmitoylated GDP-Cdc42p can dissociate from the membrane and diffuse rapidly in the cytosol until it is palmitoylted and stablilized on

the membrane upon being converted to GTP-bound form at the polarization site. If the palmitoylation of GTP-Cdc42p is the way to stabilize it on the membrane, then a non-palmitoylatable mutant should make GTP-Cdc42p to have similar mobility as GDP-Cdc42p, which may lead to the failure of Cdc42p polarization. Sequence alignment showed that the two cysteine residues in ROP6 are conserved throughout the Rho family. *S. cerevisiae* Cdc42p also has these two potential palmitoylation sites at C18 and C157. In order to test the importance of this type of specific palmitoylation, these two cysteines will be mutated to generate a non-palmitoylatable mutant.

6. Materials and Methods

6.1 Yeast strains and plasmids

Yeast strains used are listed in Table 6.1. All yeast strains (listed in table 1) are in the YEF473 background (*his3-Δ200 leu2-Δ1 lys2-801 trp1-Δ63 ura3-52*). Standard media and growth conditions were used for plasmid and yeast genetic manipulations (Guthrie and Fink, 1991).

The *rsr1::HIS3* (Schenkman et al., 2002) and *rsr1::TRP1* (Howell et al., 2009) disruptions were previously described. *cdc42::TRP1* was generated by the one-step PCR-based method (Baudin et al., 1993) using ASH58 and ASH59 primers and pRS304 (Sikorski and Hieter, 1989) as template. *rdi1::TRP1* was generated by the same method using ASH45 and AH47 and pRS303 as template.

Strains containing *BEM1-GFP* (Kozubowski et al., 2008), *CDC3-mCherry* (Howell et al., 2009), and *ABP1-mCherry* (Howell et al., 2009) at the corresponding endogenous loci were generated as previously described. *CDC24-GFP*, *BEM1-tdTomato*, and *PBD-tdTomato* were generated using the PCR-based C-terminal tagging method (Longtine et al., 1998). The *CDC24-GFP* PCR primers (CFW1 and CFW3) were designed to create a linker (CTCGAGCTC) between Cdc24p and GFP, and pDLB51 (*pFA6a-GFP-ADH1t-TRP1*) was used as a template. *BEM1-tdTomato* was created using oligos Z588 and Z589 and pDLB3299 (*pFA6a-tdTomato-ADH1t -HIS3MX6*) as template. *PBD-tdTomato* at the *GIC2* locus was generated by inserting the *tdTomato* sequence after

GIC2 nucleotide 624, which creates a truncation of *GIC2* after the Cdc42p-interacting domain fused to *tdTomato*. Primers Z679 and Z680 were used with template pDLB3301 (*pFA6a-tdTomato-ADH1t- kanMX6*) to amplify the *tdTomato* sequence for integration at *GIC2*. Strains containing *GFP-CDC42* were generated by cutting pDLB3457 (*Yip211-P_{CDC42}- GFP-CDC42*) (Bi et al., 2000) at the unique *EcoRV* site to integrate *GFP-CDC42* at the *URA3* locus. Strains containing *myc-GFP-CDC42* were generated by cutting pDLB3261 (*pRS306-P_{CDC42}-MG -CDC42*) (Wedlich-Soldner et al., 2003) at the unique *EcoRV* site to integrate *myc-GFP-CDC42* at the *URA3* locus.

The integrating plasmid containing the new *GFP-linker-CDC42* was constructed in two steps. In the first step, *CDC42* was amplified using oligos Z730/Z731 (both with the linker sequence GCACCACCACGACGACTAGTACACCCA) and template pDLB3457 (*Yip211-P_{CDC42}-GFP-CDC42*) and cloned to the *NotI/SalI* sites of pDLB3457 to remove GFP and add the linker between P_{CDC42} and *CDC42*, generating pDLB3607 (*Yip211-P_{CDC42}-linker-CDC42*). The GFP fragment was released from pDLB3457 and cloned into pDLB3607 by *NotI*, generating pDLB3609 (*Yip211-P_{CDC42}-GFP-linker-CDC42*). Strains containing *GFP-linker-CDC42* were generated by cutting pDLB3609 at the unique *EcoRV* site to integrate *GFP-linker-CDC42* at the *URA3* locus.

The integrating plasmid containing the new *CDC42-mCherry^{SW}* was constructed in two steps. In the first step, a PCR fragment was generated by overlapping PCR using the template pDLB3607 and oligos CFW62/63 and CFW64/65 and cloned into *SpeI/NheI* sites in pDLB3607, generating pDLB4006 [*Yip211-P_{CDC42}-CDC42(SW-linker*)]. CFW63 and CFW64 contain the linker sequence (GGCTCTGGCAGATCTGCATGCTCTCTC

GAGGCGGGCGGC) which has BglII, SphI and XhoI sites in it for further insertion of the mCherry tag. This overlapping PCR reaction added a linker (GSGRSACSLEAGG) after Leu134 of *CDC42*. The mCherry tag was cloned into pDLB4006 by *BglII* and *XhoI*, generating pDLB4017 (*Yip211-*P_{CDC42}*-CDC42-mCherry*^{SW}). Strains containing *CDC42-mCherry*^{SW} were generated by cutting pDLB4017 at the unique *EcoRV* site to integrate *GFP-linker-CDC42* at the *URA3* locus.

Strains overexpressing *CDC42* were constructed by replacing P_{CDC42} with P_{GAL1} using the PCR-based method (Longtine et al., 1998). Primers CFW4 and CFW5 were used with template pDLB2316 (*pFA6a-kanMX6-*P_{GAL1}). Strains overexpressing *CDC24* were constructed by replacing P_{CDC24} with P_{GAL1} using primers ASH35 and ASH36 and template pDLB2318 (*pFA6a-His3MX6-*P_{GAL1}). C-terminal HA-tagging of *CDC24* was done using primers CFW1 and CFW3 and template pDLB2307 (*pFA6a-3HA-kanMX6*). P*GAL1*-dependent expression of *CDC42* or *CDC24-HA* in response to β-estradiol was achieved by integration of the synthetic transcription factor *GAL4DBD-hER-VP16* at *URA3* as previously described (Howell et al., 2009; Takahashi and Pryciak, 2008). Strains overexpressing *CDC24-GFP-CLA4* were constructed by integrating *BamHI*-linearized DLB3605 plasmid [*pRS305-PGAL1- CDC24(ΔPB1)-GFP-CLA4(nt 4-1292)*] at *CLA4* locus.

6.2 Live-cell microscopy

6.2.1 Hydroxyurea treatment

Cells growing in synthetic complete medium at 30℃ were arrested with 200 mM

HU (Sigma) for 3 hr, washed, released into fresh medium for 65 min, harvested, and mounted for live-cell microscopy. Due to the temperature sensitivity of the GFP-Cdc42p (old version)-containing strains, they were grown at 24℃, necessitating a 4 hr HU arrest and 2 hr release.

6.2.2 Latrunculin A and β-estradiol treatment

For Lat A treatment, asynchronous log phase cells were harvested, resuspended in synthetic medium containing 200 μM Lat A (Invitrogen), and mounted on a 2% agarose slab with 200 μM Lat A. Because Lat A treatment led to defective cytokinesis and frequent lysis of cells pretreated with HU, we did not synchronize the cells to be treated with Lat A. The cells were on the slab for at least 15 min prior to imaging.

Expression from the *GAL1* promoter was induced by addition of β-estradiol. For HU-arrested cells, 100 nM β-estradiol was added at the same time as the HU and was maintained in the subsequent media and filming slabs. For Latrunculin A and β-estradiol co-treatment, β-estradiol was added to exponentially growing cells 4 hr before cells were harvested and resuspended in medium with 200 μM Lat A. Cells were then mounted on slabs containing both β-estradiol and Lat A for filming.

6.2.3 Imaging on live cell station (wide-field fluorescent microscope)

Prior to imaging, cells were grown in synthetic medium (MP Biomedicals) with dextrose. Cells were mounted on a slab composed of medium solidified with 2% agarose (Denville Scientific, Inc.). Images were acquired with an Axio Observer.Z1 (Zeiss) with outer environmental chamber (set to 30℃ unless otherwise stated), a X-CITE 120XL

metal halide fluorescence light source, and a 100x/1.46 Plan Apochromat oil-immersion objective controlled by MetaMorph software (Universal Imaging). Images were captured using a QuantEM backthinned EM-CCD camera (Photometrics). The fluorescence light source was used at ~50% maximal output, and a 2% ND filter was placed in the light path. An EM-Gain setting of 750 was used for the EM-CCD camera. Exposures were 250 ms (Bem1p-GFP, Bem1-tdTomato, or Cdc24p-GFP), 150 ms (Abp1p-mCherry), or 100 ms (Cdc3p-mCherry).

6.2.4 Imaging on spinning disk confocal microscope

The growth condition and sample preparation are the same as described above. Comparison of polarization kinetics suggested that imaging in this system was not significantly more phototoxic than with the wide-field system used previously.

Images were acquired with an Andor XD revolution spinning disk confocal microscope (Olympus) with a Yokogawa CSU-X1 5000 r.p.m. disk unit, and a 100x/1.4 UPlanSApo oil-immersion objective controlled by METAMORPH software (Universal Imaging). Images (stacks of 30 images taken at 0.24 μm z-steps for single-color imaging; stacks of 15 images taken at 0.5μm z-steps for two-color imaging) were captured by an iXon3 897 EM-CCD camera with 1.2x auxiliary magnification (Andor Technology). The fluorescence light source was used at 10% maximal output. An EM-Gain setting of 200 was used for the EM-CCD camera. Exposures were 250 ms (Cdc42p-mChrry^{SW}) or 200 ms (Bem1p-GFP, GFP-Cdc42p).

6.3 Deconvolution and image analysis

Images were deconvolved using Huygens Essential software (Scientific Volume Imaging). The classic maximum likelihood estimation and predicted point spread function method were used with a constant background across all images from the same day. A signal-to-noise ratio 10 was used for images taken from the wide-field fluorescence microscopy, whereas a signal-to-noise ratio 3 was used for those taken from spinning disk confocal microscope. The output format was 16-bit, unscaled images to enable comparison of pixel values. To detect polarity foci in different focal planes, maximum intensity projections were constructed and scored visually for the presence of more than one focus.

The coexistence time is the interval between the first frame in which more than one spot was detected and the frame when only one spot was detected. Quantification of Bem1p-GFP intensities used Volocity (Improvision). A threshold was set that would only select the polarized signal, and the summed, polarized intensity was recorded. Changes in intensity are reported as percent of maximum for that cell. Images were processed for presentation using Metamorph and Photoshop (Adobe).

To quantify polarization efficiency, we analyzed 1.5 hr movies of cells released from HU treatment as follows: for each mother-daughter pair that went through cytokinesis in the first 30 min (as indicated by neck localization of Bem1p-GFP), we scored the progeny cells as polarized if and only if Bem1p-GFP polarized within the duration of the movie. For Lat A-treated cells, we also scored single unbudded cells. As some Lat A-treated cells show transient Bem1p-GFP polarization, we only counted cells

as polarized if the polarized signal lasted more than 15 min. Cytokinesis is often defective in Lat A-treated cells, largely accounting for the decrease in the scored efficiency of polarization.

To quantify the frequency of high-amplitude oscillation, we set an arbitrary cutoff such that a cell was not scored unless the summed Bem1p-GFP intensity decreased to below 20% of the first peak before rising again.

6.4 Western blotting

For Western blot analysis, 10^7 cells were collected and total protein was extracted by TCA precipitation as described (Keaton et al., 2008). Electrophoresis and Western blotting were performed as described (Bose et al., 2001). Monoclonal mouse anti-Cdc42p antibodies (Wu and Brennwald, 2010) were used at 1:1000 dilution. Monoclonal mouse anti-HA antibody (Roche Applied Science) was used at a 1:2000 dilution. Polyclonal rabbit anti-Cdc11p antibody (Santa Cruz Biotechnology) was used at a 1:5000 dilution. Fluorophore-conjugated secondary antibodies against mouse (IRDye800 conjugated anti-mouse IgG, Rockland Immunochemicals) or rabbit (Alexa Fluor 680 goat anti-rabbit IgG, Invitrogen) antibodies were used at 1:5000 dilution. Blots were visualized by ODYSSEY imaging system (LI-COR Biosciences).

6.5 Fluorescence recovery after photocleaching (FRAP)

Sample preparation was the same as live-cell imaging. FRAP analysis was performed on unbudded cells with a strong polarized cluster. Cells were photobleached and imaged on an Olympus IX-71 wide-field fluorescent microscope using a 100x/1.40 oil UPLSAPO100X0 1-U2B836 WD objective. The FRAP experiments were performed using the "Design PK Experiment" function in the SoftWoRx 5.0 software (Applied Precision) with 1 iteration of photobleaching at 100% laser power with 100 ms duration and image acquisition at 2% power with 250 ms exposure time using a 488 nm laser. The images were acquired using an Evolve back-thinned EM-CCD camera (Photometrics®). Three single-plane images were taken before photobleaching with a 0.5 sec interval and 23 single-plane post-bleaching images were acquired with adaptive time intervals determined by the software based on the expected recovery half time entered. The averaged background signal intensity was subtracted from the sum intensity from the manually-selected photobleached region using ImageJ. The resulting values were then normalized to the pre-bleaching signal intensity. The data points from each individual cell were fitted to a double-exponential equation ($y = g2 + a1 \times e^{-b1x} + a2 \times e^{-b2x}$) in MATLAB (MathWorks, Inc.) The recovery half time was calculated with the equation $t_{1/2} = \ln 2 / b1$ or b2 (whichever in smaller).

Table 1 Yeast strains

Strain	Relevant genotype	Source
DLY8155	**a**	This study
DLY9069	**a** *BEM1-GFP:LEU2*	Wu 2013
DLY9200	**a**/α *BEM1-GFP:LEU2/ BEM1-GFP:LEU2 rsr1::TRP1/ rsr1::TRP1*	Howell 2009
DLY9201	**a**/α *BEM1-GFP:LEU2/ BEM1-GFP:LEU2*	Wu 2013
DLY9889	**a**/α *BEM1-GFP:LEU2/ BEM1-GFP:LEU2 rsr1::TRP1/ rsr1::TRP1 PBD-RFP:URA3/PBD-RFP:URA3*	Howell 2012
DLY11125	**a**/α *BEM1-GFP:LEU2/ BEM1-GFP:LEU2 rsr1::TRP1/ rsr1::TRP1 rga1::HIS3/rga1::HIS3 rga2::kan^R/rga2::kan^R*	This study
DLY11223	**a**/α *BEM1-GFP:LEU2/ BEM1-GFP:LEU2 rsr1::TRP1/ rsr1::TRP1 rga1::HIS3/rga1::HIS3*	This study
DLY11224	**a**/α *BEM1-GFP:LEU2/ BEM1-GFP:LEU2 rsr1::TRP1/ rsr1::TRP1 rga2::kan^R/rga2::kan^R*	This study
DLY11225	**a**/α *BEM1-GFP:LEU2/ BEM1-GFP:LEU2 rsr1::TRP1/ rsr1::TRP1 bem3::TRP1/bem3::TRP1*	This study
DLY11320	**a**/α *BEM1-GFP:LEU2/ BEM1-GFP:LEU2 rsr1::TRP1/ rsr1::TRP1 ABP1-mCherry:kan^R/ABP1-mCherry:kan^R*	Howell 2012
DLY11780	**a**/α *BEM1-GFP:LEU2/ BEM1-GFP:LEU2 rsr1::TRP1/ rsr1::TRP1 SPC42-mCherry ::kan^R/SPC42*	Wu 2013
DLY11971	**a**/α *BEM1-GFP:LEU2/ BEM1-GFP:LEU2 rsr1::TRP1/ rsr1::TRP1 P_{ADH1}-GAL4DBD-hER-VP16:URA3/ura3*	Howell 2012
DLY12127	**a**/α *BEM1-GFP:LEU2/ BEM1-GFP:LEU2 rsr1::TRP1/ rsr1::TRP1 P_{ADH1}-GAL4DBD-hER-VP16:URA3/ura3 kan^R:P_{GAL1}-CDC42/CDC42*	Howell 2012
DLY12207	**a** *rsr1::TRP1 BEM1-GFP:LEU2 kan^R:P_{GAL1}-CDC42 P_{ADH1}-GAL4DBD-hER-VP16:URA3*	This study
DLY12577	**a**/α *BEM1-GFP:LEU2/ BEM1-GFP:LEU2 rsr1::HIS3/ rsr1::HIS3 rdi1::TRP1/rdi1::TRP1*	This study
DLY12658	**a**/α *cdc42::TRP1/CDC42*	This study
DLY12831	**a**/α *cdc42::TRP1/CDC42 P_{CDC42}-MG-CDC42:URA3/ura3*	Howell 2012
DLY12833	**a**/α *cdc42::TRP1/CDC42 P_{CDC42}-GFP-CDC42:URA3/ura3*	This study
DLY12844	**a** *cdc42::TRP1 P_{CDC42}-GFP-CDC42:URA3*	This study

DLY12938	**a**/α *rsr1::HIS3/rsr1::HIS3 rdi1::TRP1/rdi1::TRP1 CDC24-GFP::TRP1/CDC24-GFP::TRP1*	This study
DLY13096	**a**/α *rsr1::HIS3/rsr1::HIS3 CDC24-GFP:TRP1/ CDC24-GFP:TRP1 BEM1-tdTomato:HIS3MX6/ BEM1-tdTomato:HIS3MX6*	Howell 2012
DLY13098	**a**/α *BEM1-GFP:LEU2/ BEM1-GFP:LEU2 rsr1::TRP1/ rsr1::TRP1 CDC3-mCherry:LEU2/CDC3*	Howell 2012
DLY13157	**a**/α *BEM1-GFP:LEU2/ BEM1-GFP:LEU2 rsr1::TRP1/ rsr1::TRP1 PBD-tdTomato:kan^R/GIC2*	Howell 2012
DLY13158	**a**/α *BEM1-tdTomato:HIS3MX6/BEM1 rsr1::TRP1/ rsr1::TRP1 P_{CDC42}-GFP-CDC42:URA3/ura3 cdc42::TRP1/CDC42*	Howell 2012
DLY13164	**a**/α *rsr1::TRP1/rsr1::TRP1 PBD-tdTomato:kan^R/GIC2 P_{CDC42}-GFP-CDC42:URA3/ura3 cdc42::TRP1/CDC42*	Howell 2012
DLY13355	**a**/α *BEM1-GFP:LEU2/ BEM1-GFP:LEU2 rsr1::TRP1/ rsr1::TRP1 P_{ADH1}-GAL4DBD-hER-VP16:URA3/ura3 HIS3MX6:P_{GAL1}-CDC24-HA:kan^R /CDC24*	Howell 2012
DLY13824	**a**/α *BEM1-GFP:LEU2/ BEM1-GFP:LEU2 rsr1::TRP1/ rsr1::TRP1 cdc42::TRP1/CDC42*	Howell 2012
DLY13859	**a**/α *rsr1::TRP1/rsr1::TRP1 cdc42::TRP1/CDC42 P_{CDC42}-GFP-CDC42:URA3/ura3*	Howell 2012
DLY13861	**a**/α *BEM1-tdTomato:HIS3MX6/BEM1 rsr1::TRP1/ rsr1::TRP1 P_{ADH1}-GAL4DBD-hER-VP16:URA3/ura3 P_{GAL1}-CDC24(ΔPB1)-GFP-CLA4::LEU2/CLA4*	Howell 2012
DLY13878	**a**/α *cdc42::TRP1/CDC42 P_{CDC42}-GFP-linker-CDC42:URA3/ura3* (8x expression)	This study
DLY13891	**a** *cdc42::TRP1 P_{CDC42}-GFP-linker-CDC42:URA3* (8x expression)	This study
DLY13920	**a**/α *rsr1::HIS3/RSR1 cdc42::TRP1/CDC42 P_{CDC42}-GFP-linker-CDC42:URA3/ura3* (8x expression)	This study
DLY13961	**a**/α *BEM1-GFP:LEU2/ BEM1-GFP:LEU2 rsr1::TRP1/ rsr1::TRP1 P_{ADH1}-GAL4DBD-hER-VP16:URA3/ura3 kan^R:P_{GAL1}-CDC42/CDC42 rga1::HIS3/rga1::HIS3*	This study
DLY14009	**a**/α *BEM1-GFP:LEU2/ BEM1-GFP:LEU2 rsr1::TRP1/ rsr1::TRP1 P_{ADH1}-GAL4DBD-hER-VP16:URA3/ura3 kan^R:P_{GAL1}-CDC42/CDC42 rga2::HIS3/rga2::HIS3*	This study
DLY14010	**a**/α *BEM1-GFP:LEU2/ BEM1-GFP:LEU2 rsr1::TRP1/ rsr1::TRP1 P_{ADH1}-GAL4DBD-hER-VP16:URA3/ura3 kan^R:P_{GAL1}-CDC42/CDC42 bem3::HIS3/bem3::HIS3*	This study
DLY14112	**a** *rsr1::TRP1 P_{ADH1}-GAL4DBD-hER-VP16:URA3*	Howell 2012

	PBD-tdTomato:kan^R	
DLY14117	**a** *rsr1::TRP1 BEM1-GFP:LEU2 kan^R:P$_{GAL1}$-CDC42 P$_{ADH1}$-GAL4DBD-hER-VP16:URA3 PBD-tdTomato:kan^R*	Howell 2012
DLY14123	**a**/α *BEM1-tdTomato:HIS3MX6/BEM1 rsr1::TRP1/ rsr1::TRP1 P$_{ADH1}$-GAL4DBD-hER-VP16:URA3/ura3 P$_{GAL1}$-CDC24(ΔPB1)-GFP-CLA4::LEU2/CLA4 kan^R:P$_{GAL1}$-CDC42/CDC42*	Howell 2012
DLY14418	**a**/α *rsr1::TRP1/ rsr1::TRP1 rdi1::TRP1/rdi1::TRP1 BEM1-GFP:LEU2/ BEM1-GFP:LEU2 P$_{ADH1}$-GAL4DBD-hER-VP16:URA3/ura3 kan^R:P$_{GAL1}$-CDC42/CDC42*	This study
DLY14469	**a**/α *rsr1::HIS3/ rsr1::HIS3 rdi1::TRP1/rdi1::TRP1 cdc42::TRP1/CDC42 GFP-CDC42:URA3/ura3*	This study
DLY14535	**a**/α *rsr1::TRP1/ rsr1::TRP1 rdi1::TRP1/rdi1::TRP1 BEM1-GFP:LEU2/ BEM1-GFP:LEU2 CDC3-mCherry:LEU2/CDC3*	This study
DLY14742	**a** *P$_{ADH1}$-GAL4DBD-hER-VP16:TRP1*	This study
DLY14898	**a**/α *rsr1::HIS3/RSR1 rdi1::TRP1/rdi1::TRP1 cdc42::TRP1/CDC42 P$_{CDC42}$-GFP-linker-CDC42:URA3/ura3* (8x expression)	This study
DLY15015	**a**/α *P$_{CDC42}$-GFP-linker-CDC42/CDC42*	This study
DLY15016	**a** *P$_{CDC42}$-GFP-linker-CDC42*	This study
DLY15121	**a**/α *Bem1-GFP:LEU2/ BEM1-GFP:LEU2 rdi1::TRP1/rdi1::TRP1*	This study
DLY15125	**a**/α *BEM1-GFP:LEU2/ BEM1-GFP:LEU2 rga1::HIS3/rga1::HIS3*	Wu 2013
DLY15135	**a** *P$_{ADH1}$-GAL4DBD-hER-VP16:TRP1 P$_{GAL1}$-PSR1(1-28 a.a.)-GFP::LEU2*	This study
DLY15137	**a** *P$_{ADH1}$-GAL4DBD-hER-VP16:TRP1 P$_{GAL1}$-PSR1(1-28 a.a.)-GFP-CDC42::URA3*	This study
DLY15514	**a**/α *BEM1-GFP:LEU2/ BEM1-GFP:LEU2 rsr1::TRP1/ rsr1::TRP1 rdi1::TRP1/rdi1::TRP1 P$_{ADH1}$-GAL4DBD-hER-VP16:URA3/ura3*	This study
DLY15572	**a**/α *BEM1-GFP:LEU2/ BEM1-GFP:LEU2 rsr1::TRP1/ rsr1::TRP1 cdc42^{R66A}/cdc42^{R66A}*	This study
DLY15782	**a**/α *rsr1::HIS3/rsr1::HIS3 rdi1::TRP1/rdi1::TRP1 BEM1-GFP:LEU2/ BEM1-GFP:LEU2 PBD-tdTomato:kan^R/GIC2*	This study
DLY15851	**a**/α *rsr1::TRP1/ rsr1::TRP1 RDI1-3myc:HIS/RDI1*	This study

	pRS303-P_{CDC42}-3myc-CDC42:CDC42/CDC42	
DLY15879	**a**/α *rsr1::HIS3/ rsr1::HIS3 BEM1-GFP:LEU2/ BEM1-GFP:LEU2 PBD-tdTomato:kan^R/GIC2*	This study
DLY15925	**a**/α *rsr1::HIS3/ rsr1::HIS3 rdi1::TRP1/rdi1::TRP1 BEM1-GFP:LEU2/ BEM1-GFP:LEU2 cdc12-6/cdc12-6*	This study
DLY15991	**a**/α *BEM1-GFP:LEU2/ BEM1-GFP:LEU2 rsr1::TRP1/ rsr1::TRP1 rdi1::TRP1/rdi1::TRP1 P_{ADH1}-GAL4DBD-hER-VP16:URA3/ura3 HIS3MX6:P_{GAL1}-CDC24-HA:kan^R /CDC24*	This study
DLY16447	**a**/α *BEM1-GFP:LEU2/ BEM1-GFP:LEU2 rsr1::HIS3/ rsr1::HIS3 rdi1::TRP1/rdi1::TRP1 cdc42::TRP1/CDC42*	This study
DLY16487	**a**/α *cdc42::TRP1/CDC42 P_{CDC42}-GFP-linker-CDC42:URA3/ura3* (3x overexpression)	This study
DLY16730	**a** *cdc42::TRP1 P_{CDC42}-GFP-linker-CDC42:URA3* (3x expression)	This study
DLY16813	**a** *P_{ADH1}-GAL4DBD-hER-VP16:TRP1 P_{GAL1}-PSR1(1-28 a.a.)(C9G, C10G)-GFP-CDC42::URA3*	This study
DLY16847	**a**/α *cdc42::TRP1/CDC42 P_{CDC42}-CDC42-mCherry^{SW}:URA3/ura3*	This study
DLY16855	**a** *cdc42::TRP1 P_{CDC42})-CDC42-mCherry^{SW}:URA3*	This study
DLY17109	**a**/α *rsr1::HIS3/ rsr1::HIS3 rdi1::TRP1/rdi1::TRP1 BEM1-GFP:LEU2/ BEM1-GFP:LEU2 cdc42::TRP1/CDC42 P_{CDC42}-CDC42-mCherry^{SW}:URA3/ura3*	This study
DLY17110	**a**/α *rsr1::HIS3/ rsr1::HIS3 BEM1-GFP:LEU2/ BEM1-GFP:LEU2 cdc42::TRP1/CDC42 P_{CDC42}-CDC42-mCherry^{SW}:URA3/ura3*	This study

7. Mathematical modeling

7.1 Modeling negative feedback

7.1.1 Modeling oscillatory polarization with negative feedback

(1) Positive feedback only

This model is similar to the one developed by Goryachev (Goryachev and Pokhilko, 2008; Howell et al., 2009), with the simplifying assumption that the role of the GDI, which binds GDP-Cdc42p and allows it to exchange between membrane and cytoplasm (Johnson et al., 2009), can be incorporated in the rate constants for GDP-Cdc42p exchange between membrane and cytoplasm. Other model assumptions include:

(i) GDP-Cdc42p can exchange between the plasma membrane and cytoplasm. The membrane-bound and cytoplasmic forms are labeled as Cdc42D and $Cdc42I_c$, respectively. GTP-Cdc42p (Cdc42T) is always associated with the plasma membrane.

(ii) The Bem1p complex can exchange between cytoplasm (indicated as $Bem1GEF_c$) and membrane (indicated as $Bem1GEF_m$). Either form can bind to GTP-Cdc42p on the membrane, generating a complex indicated as Bem1GEFCdc42T.

(iii) The GEF activity of the Bem1p complex increases 2-fold when it binds GTP-Cdc42p (Howell et al., 2009).

(iv) GAP activity is spatially uniform and is incorporated in the first-order hydrolysis rate constant k_{2r}.

(v) The GEF and GAP are not saturated by substrate (GDP-Cdc42p or GTP-Cdc42p respectively).

(vi) The cell dimensions, total Cdc42p, and total Bem1p complex are all constant. The ratio of membrane volume to cytoplasmic volume is indicated by .

(vii) All membrane-bound species have the same diffusion coefficient, D_m, and all cytosolic species the same diffusion coefficient, D_c, with $D_c >> D_m$.

Model parameter values are listed in the Table 2 below. This model is described by the following reaction-diffusion equations:

$$\frac{\partial Cdc42I_c}{\partial t} = D_c \nabla^2 Cdc42I_c + \eta(-k_1 Cdc42I_c + k_{1r} Cdc42D)$$

$$\frac{\partial Cdc42D}{\partial t} = D_m \nabla^2 Cdc42D + k_1 Cdc42I_c - k_{1r} Cdc42D$$
$$-Cdc42D(k_2 Bem1GEF_m + k_{2p} Bem1GEFCdc42T) + k_{2r} Cdc42T$$

$$\frac{\partial Cdc42T}{\partial t} = D_m \nabla^2 Cdc42T + Cdc42D(k_2 Bem1GEF_m + k_{2p} Bem1GEFCdc42T) - k_{2r} Cdc42T$$
$$-(k_4 Bem1GEF_c + k_5 Bem1GEF_m) Cdc42T + k_{5r} Bem1GEFCdc42T$$

$$\frac{\partial Bem1GEFCdc42T}{\partial t} = D_m \nabla^2 Bem1GEFCdc42T + (k_4 Bem1GEF_c + k_5 Bem1GEF_m) Cdc42T$$
$$-k_{5r} Bem1GEFCdc42T$$

$$\frac{\partial Bem1GEF_c}{\partial t} = D_c \nabla^2 Bem1GEF_c + \eta(-k_3 Bem1GEF_c + k_{3r} Bem1GEF_m - k_4 Bem1GEF_c \cdot Cdc42T)$$

$$\frac{\partial Bem1GEF_m}{\partial t} = D_m \nabla^2 Bem1GEF_m + k_3 Bem1GEF_c - k_{3r} Bem1GEF_m$$
$$-k_5 Bem1GEF_m \cdot Cdc42T + k_{5r} Bem1GEFCdc42T$$

(2) Negative feedback via GAP activation

We assume that GTP-Cdc42p activates a cytoplasmic GAP, perhaps by phosphorylation of the GAP by the PAK Cla4p (Cla4p is a Cdc42p effector and part of the Bem1p complex) (Fig S3). The total GAP concentration is assumed to be 1 μM. The two states of the GAP are denoted as GAP_c (basal GAP activity) and GAP^*_c (high GAP activity). Active GAP is γ-fold more active than basal GAP. We imagine that a PAK bound to one molecule of GTP-Cdc42p would phosphorylate a GAP molecule transiently bound to a neighboring molecule of GTP-Cdc42p, so the GAP activation rate would be proportional to the product Bem1GEFCdc42T x Cdc42T x GAP_c. GAP inactivation is assumed to occur in the cytoplasm at a constant rate k_7. Model parameter values are listed in the Table below. This model is described by the following equations:

$$\frac{\partial Cdc42I_c}{\partial t} = D_c\nabla^2 Cdc42I_c + \eta(-k_1 Cdc42I_c + k_{1r} Cdc42D)$$

$$\frac{\partial Cdc42D}{\partial t} = D_m\nabla^2 Cdc42D + k_1 Cdc42I_c - k_{1r} Cdc42D$$
$$-Cdc42D(k_2 Bem1GEF_m + k_{2p} Bem1GEFCdc42T) + k_{2r}(GAP_c + \gamma GAP_c^*)Cdc42T$$

$$\frac{\partial Cdc42T}{\partial t} = D_m\nabla^2 Cdc42T + Cdc42D(k_2 Bem1GEF_m + k_{2p} Bem1GEFCdc42T) - k_{2r}(GAP_c + \gamma GAP_c^*)Cdc42T$$
$$-(k_4 Bem1GEF_c + k_5 Bem1GEF_m)Cdc42T + (k_{4r} + k_{5r})Bem1GEFCdc42T$$

$$\frac{\partial Bem1GEFCdc42T}{\partial t} = D_m\nabla^2 Bem1GEFCdc42T + (k_4 Bem1GEF_c + k_5 Bem1GEF_m)Cdc42T$$
$$-(k_{4r} + k_{5r})Bem1GEFCdc42T$$

$$\frac{\partial Bem1GEF_c}{\partial t} = D_c\nabla^2 Bem1GEF_c + \eta(-k_3 Bem1GEF_c + k_{3r} Bem1GEF_m$$
$$-k_4 Bem1GEF_c \cdot Cdc42T + k_{4r} Bem1GEFCdc42T)$$

$$\frac{\partial Bem1GEF_m}{\partial t} = D_m \nabla^2 Bem1GEF_m + k_3 Bem1GEF_c - k_{3r} Bem1GEF_m$$
$$- k_5 Bem1GEF_m \cdot Cdc42T + k_{5r} Bem1GEFCdc42T$$

$$\frac{\partial GAP_c}{\partial t} = D_c \nabla^2 GAP_c - \eta \cdot k_6 Bem1GEFCdc42T \cdot Cdc42T \cdot GAP_c + k_7 GAP_c^*$$

$$\frac{\partial GAP_c^*}{\partial t} = D_c \nabla^2 GAP_c^* + \eta \cdot k_6 Bem1GEFCdc42T \cdot Cdc42T \cdot GAP_c - k_7 GAP_c^*$$

(3) Negative feedback via disruption of the Bem1p complex

We assume that GTP-Cdc42p initiates a feedback loop that leads to the modification of the Bem1GEFCdc42T complex. Upon dissociation this yields Cdc42T and a modified Bem1GEF* that cannot rebind Cdc42T until its modification has been reversed by a spatially uniform cytoplasmic process characterized by the first-order rate constant k_7. One possible mechanism for this negative feedback loop would be that the PAK Cla4p in one Bem1GEFCdc42T phosphorylates Bem1p complex components in a neighboring Bem1GEFCdc42T, changing their affinity for each other or for GTP-Cdc42p. In this scenario, the rate at which Bem1GEFCdc42T is modified is proportional to the square of the Bem1GEFCdc42T concentration. To keep additional assumptions to a minimum, we assumed that although the modified Bem1p complex cannot re-associate with GTP-Cdc42p, it retains basal GEF activity and transitions between the membrane and cytoplasm at the same rates as the unmodified complex. Model parameter values are listed in the Table below. This model is described by the following equations:

$$\frac{\partial Cdc42I_c}{\partial t} = D_c \nabla^2 Cdc42I_c + \eta(-k_1 Cdc42I_c + k_{1r} Cdc42D)$$

$$\frac{\partial Cdc42D}{\partial t} = D_m \nabla^2 Cdc42D + k_1 Cdc42I_c - k_{1r} Cdc42D - Cdc42D(k_2(Bem1GEF_m + Bem1GEF_m^*) + k_{2p}(Bem1GEFCdc42T + Bem1GEF^* Cdc42T)) + k_{2r} Cdc42T$$

$$\frac{\partial Cdc42T}{\partial t} = D_m \nabla^2 Cdc42T + Cdc42D(k_2(Bem1GEF_m + Bem1GEF_m^*) + k_{2p}(Bem1GEFCdc42T + Bem1GEF^* Cdc42T)) - k_{2r} Cdc42T - (k_4 Bem1GEF_c + k_5 Bem1GEF_m) Cdc42T + k_{5r} Bem1GEFCdc42T + k_{5r} Bem1GEF^* Cdc42T$$

$$\frac{\partial Bem1GEFCdc42T}{\partial t} = D_m \nabla^2 Bem1GEFCdc42T + (k_4 Bem1GEF_c + k_5 Bem1GEF_m) Cdc42T - k_{5r} Bem1GEFCdc42T - k_6 Bem1GEFCdc42T^2$$

$$\frac{\partial Bem1GEF^* Cdc42T}{\partial t} = D_m \nabla^2 Bem1GEF^* Cdc42T + k_6 Bem1GEFCdc42T^2 - k_{5r} Bem1GEF^* Cdc42T$$

$$\frac{\partial Bem1GEF_c}{\partial t} = D_c \nabla^2 Bem1GEF_c + \eta(-k_3 Bem1GEF_c + k_{3r} Bem1GEF_m - k_4 Bem1GEF_c \cdot Cdc42T) + k_7 Bem1GEF_c^*$$

$$\frac{\partial Bem1GEF_m}{\partial t} = D_m \nabla^2 Bem1GEF_m + k_3 Bem1GEF_c - k_{3r} Bem1GEF_m - k_5 Bem1GEF_m \cdot Cdc42T + k_{5r} Bem1GEFCdc42T$$

$$\frac{\partial Bem1GEF_m^*}{\partial t} = D_m \nabla^2 Bem1GEF_m^* + k_{5r} Bem1GEF^* Cdc42T - k_{3r} Bem1GEF_m^* + k_3 Bem1GEF_c^*$$

$$\frac{\partial Bem1GEF_c^*}{\partial t} = D_c \nabla^2 Bem1GEF_c^* + \eta(k_{3r} Bem1GEF_m^* - k_3 Bem1GEF_c^*) - k_7 Bem1GEF_c^*$$

(4) Parameter values

Model parameter values for all models are listed in the Table below. Here we provide a brief description of how the model 1 parameter values were estimated. The GDI-related rate constants (simplified to k1 and k1r in this work) were estimated based on real-time FRET measurements reporting interaction kinetics of recombinant human Cdc42p and GDI with insect cell membranes in vitro (Nomanbhoy et al., 1999).

The GEF- and GAP-regulated rate constants for GDP/GTP exchange and GTP hydrolysis by Cdc42p (k2, k2p, and k2r) were estimated based on in vitro rates of GDP release and GTP hydrolysis by recombinant yeast Cdc42p upon incubation with crude yeast lysates from synchronized cells (Howell et al., 2009).

Because we do not have specific data on the weak interaction of Bem1p complexes with the membrane, the relevant rate constants (k3 and k3r) were estimated based on similar PX-domain/membrane interactions in the literature (Goryachev and Pokhilko, 2008).

The binding/dissociation of the Bem1p complex to/from GTP-Cdc42p is a simplification of a more complex situation in which reversible binding reactions occur between GTP-Cdc42p and PAK, between PAK and Bem1p, and between Bem1p and Cdc24p. Because the SH3-mediated PAK-Bem1p interaction is likely to be the most labile of these, the relevant rate constants (k4, k5, and k5r) are estimated based on other SH3 interactions in the literature (Howell et al., 2009).

The membrane diffusion constant was estimated based on FRAP analysis of GFP-

tagged prenylated reporters in latrunculin-treated cells (to eliminate endocytosis) (Marco et al., 2007).

Although the general ballpark values of these parameters are as realistic as we are able to estimate, the modeling results in this paper should be treated as qualitative rather than quantitative. Because the mechanism of negative feedback is unknown, the negative feedback parameters (k6 and k7) are purely speculative.

Table 2 Parameter values for modeling negative feedback

	Model (1)	**Model (2)**	**Model (3)**	**Reference (Model 1)**
k_1	0.9 s^{-1}	1 s^{-1}	0.9 s^{-1}	This work
k_{1r}	0.15 s^{-1}	0.125 s^{-1}	0.15 s^{-1}	This work
k_2	0.16 $M^{-1}s^{-1}$	0.2 $M^{-1}s^{-1}$	0.16 $M^{-1}s^{-1}$	(Howell et al., 2009)
k_{2p}	0.35 $M^{-1}s^{-1}$	0.6 $M^{-1}s^{-1}$	0.35 $M^{-1}s^{-1}$	(Howell et al., 2009)
k_{2r}	0.32 s^{-1}	0.3 s^{-1}	0.32 s^{-1}	(Howell et al., 2009)
k_3	10 s^{-1}	10 s^{-1}	10 s^{-1}	(Goryachev and Pokhilko, 2008)
k_{3r}	10 s^{-1}	10 s^{-1}	10 s^{-1}	(Goryachev and Pokhilko, 2008)
k_4	10 $M^{-1}s^{-1}$	7.5 $M^{-1}s^{-1}$	10 $M^{-1}s^{-1}$	(Goryachev and Pokhilko, 2008)
k_{4r}	-	2.5 s^{-1}	-	This work
k_5	10 $M^{-1}s^{-1}$	10 $M^{-1}s^{-1}$	10 $M^{-1}s^{-1}$	(Goryachev and Pokhilko,

				2008)
k_{5r}	10 s^{-1}	10 s^{-1}	10 s^{-1}	(Howell et al., 2009)
k_6	-	0.2 $M^{-2}s^{-1}$	0.05 $M^{-1}s^{-1}$	This work
k_7	-	0.00475 s^{-1}	0.0022 s^{-1}	This work
	-	10	-	This work
	0.01	0.01	0.01	(Goryachev and Pokhilko, 2008)
D_c	10 m^2s^{-1}	10 m^2s^{-1}	10 m^2s^{-1}	(Goryachev and Pokhilko, 2008)
D_m	0.036 m^2s^{-1}	0.036 m^2s^{-1}	0.036 m^2s^{-1}	(Marco et al., 2007)
Total Cdc42p	5 M	5 M	5 M	(Goryachev and Pokhilko, 2008)
Total Bem1p complex	0.017 M	0.017 M	0.017 M	(Goryachev and Pokhilko, 2008)
Total GAP	-	1 M	-	This work

7.1.2 Bifurcation diagram

We examined the dynamical behavior of models (1), (2) and (3) in the plane of total Cdc42p and Bem1p complex concentration. The range of concentration is chosen from 0 to 10-fold of the concentrations from previous studies (see Table 2 for 1x values: model 1).

There are 8 types of spatiotemporal behavior based on the number of fixed points

and their stability with respect to spatial perturbations (two of them do not appear in the parameters used for Figure 2.7 and 2.8):

(i) Monostable: The spatially homogeneous steady state has only one fixed point and it is stable to all perturbations (white regions in all bifurcation diagrams).

(ii) Bistable 1: Three spatially homogeneous fixed points exist, two of which are stable (blue regions in Fig. 2.8B and E). The fixed point with low GTP-Cdc42p is stable to all local perturbations, whereas the fixed point with high GTP-Cdc42p is stable to spatially homogenous perturbations but Turing unstable to spatial perturbations.

(iii) Turing unstable: Only one fixed point exists, which is stable with regard to spatially uniform perturbations, but unstable given any small spatial perturbation (red regions in all bifurcation diagrams: points 3 and 4, Fig. 2.7C). In this region away from the lower boundary, all models produce stable polarity site(s), which do not oscillate. The majority of polarization occurs in this region. At the lower boundary of this region, close to the region with mixed Turing and Hopf instability (see below), models (2) and (3) show damped oscillatory polarization (point 3, Fig. 2.7C). This type of behavior does not occur in model (1), and occurs in a relatively narrow region of parameter space for models (2) and (3).

(iv) Subcritical Turing unstable: For this case, only one uniform stable fixed point exists. However, it becomes unstable under sufficiently large spatial perturbations (the gray regions in all bifurcation diagrams).

(v) Excitable: Three spatially homogeneous fixed points exist, but only one is

stable. The stable fixed point is an unstable spiral: large enough homogenous perturbations can excite transient homogeneous increases in the level of active Cdc42p (cyan regions in Fig. 2.7C and 2.8B-E). Spatially localized perturbations can induce transient polarization. Excitable behavior does not occur in model (1).

(vi) Turing and Hopf unstable: Only one fixed point exists, which is Hopf unstable and Turing unstable (green regions in Fig. 2.7C and Fig. 2.8B-E). This type of behavior does not occur in model (1). In this region, the typical dynamics is alternating polarization and several rounds of uniform oscillation (points 1 and 2, Fig. 2.7C). A spatially localized perturbation initiates formation of a polarized distribution of GTP-Cdc42p. Negative feedback then destabilizes polarization. As GTP-Cdc42p levels fall, the negative feedback is reduced, but remains sufficient to repress polarization. Thus, GTP-Cdc42p increases uniformly and then oscillates. After several such oscillations, the strength of negative feedback drops below threshold, enabling the positive feedback to accumulate GTP-Cdc42 locally. During polarization of GTP-Cdc42, the negative feedback increases again, starting another round of uniform oscillations. However, noise converts the uniform oscillations to oscillatory clustering.

Using appropriate parameter values, there are two other types of behavior:

(vii) Bistable 0: Three fixed points exist for spatially homogeneous concentrations, two of which are stable with different levels of active Cdc42p. Both fixed points are stable to spatial perturbations.

(viii) Hopf unstable: Only one fixed point exists that is unstable to all

perturbations. The long-term behavior of the system is uniform oscillations of active Cdc42p.

The stability of (i), (ii), (iii), (v), (vii) and (viii) were assessed by numerically determining the steady state and calculating the eigenvalues for the linearized reaction equations in 1D. The Turing instability in (iii) and (vi) was determined by linear stability analysis (Murray, 2003). The boundary of region (iv) was determined by numerical simulations. All three models show similar behaviors in planes of other parameter values.

7.1.3 Competition and equalization of two polarity foci

We used model (1) (positive feedback only) and model (3) (with negative feedback) to examine how negative feedback affects competition between polarized foci. Simulations were done on a 1D line ($L=5\pi\mu m$) with periodic boundary conditions, representing a cell perimeter.

To simulate competition between two unequal GTP-Cdc42p foci, we evolved a symmetric two-peak solution for the points in parameter space shown in Fig. 2.12. This was done by transiently including a spatial dependence of the rate constant k_3 for Bem1 binding to the membrane. Specifically, we took $k_3(\theta)$ to consist of two identical Gaussian distributions centered at $\pi/2$ and $3\pi/2$. After the spatial dependence of k_3 was removed and the two peaks had reached steady state, we adjusted the profile of GTP-Cdc42p from a 50:50 ratio between the peaks to various other ratios (55:45, 60:40, 70:30, 80:20 or 90:10) keeping total Cdc42p constant. The shared points (white circles in Fig. 2.12) are limited to low Bem1p complex concentrations because model (1) could not sustain a two-

peak distribution with larger amounts of Bem1p complex: once the spatial dependence of k_3 was withdrawn, the peaks flattened out to a homogeneous distribution that was unstable to spatial perturbation.

The competition simulations for each point started with the two-peak profiles adjusted as described above. We defined the duration of competition as the time taken to reach a state in which the peak GTP-Cdc42p concentration in the larger focus was 10-fold that of the smaller focus.

Whereas all points tested for model (1) (positive feedback only) displayed competition, in model (3) (with negative feedback) there was a transition from competition to conditional equalization as the total amounts of Cdc42p and the Bem1p complex were increased. By conditional equalization we mean that the two peaks became equal in size if the initial difference was less than a certain threshold. As the total Cdc42p and Bem1p complex amounts were increased further, two different peaks would equalize regardless of their relative size (Fig. 2.12E).

To examine how this behavior impacts a biologically realistic situation, we asked how many peaks would form if simulations were initiated with a variety of initial conditions. In the competition region, only one peak formed no matter what initial conditions were used. In the conditional equalization region, different initial conditions led to either one or two peaks. In the equalization region, two peaks of GTP-Cdc42p were established independent of the initial conditions.

7.2 Modeling bud-site selection

To ask how the presence landmark-localized Rsr1-GEF complexes would impact the dynamics of polarization, we turned to computational modeling. To provide context for the model, we provide a brief historical synopsis below.

7.2.1 Background on model development

The model used here evolved from one first formulated by Goryachev and Pokhilko in 2008 (Goryachev and Pokhilko, 2008). That model used mass action kinetics to describe the known biochemical interactions and activities of three molecular species: Cdc42p, a GDI, and a Bem1p-GEF complex. There was also an implicit GAP activity. The model contained positive feedback, but no negative feedback.

Some model parameters (representing Bem1p-GEF and implicit GAP activities, as well as interaction rate constants) were subsequently adjusted using in vitro biochemical data as a guide (Howell et al., 2009). For example, the total GEF activity measured in yeast lysates was used to constrain product of two model parameters: GEF abundance and GEF specific activity. Thus, the model is based on documented biochemistry, but several individual parameters (as opposed to their product) remain poorly constrained.

That model was then elaborated to include negative feedback modeled in 7.1 (Howell et al., 2012), based on the observed oscillatory dynamics of polarization. The mechanism of negative feedback remains to be established. Two hypothetical mechanisms (acting by positive regulation of a GAP or by negative regulation of the Bem1-GEF complex) were considered and yielded qualitatively similar behavior. Here

we chose to use the simpler of the models, involving Bem1p-GEF regulation. We note that because the mechanism remains speculative, the negative feedback parameters are also speculative and not constrained by data.

Two other features of the negative feedback model are noteworthy. First, the action of the GDI in the model was simplified. The 2008 model included a GDI able to bind GDP-Cdc42p and extract it reversibly from the membrane to the cytoplasm. In the negative feedback model there is an implicit GDI represented by allowing GDP-Cdc42p to spontaneously exchange between membrane and cytoplasm. Second, the model added a Gaussian noise term to the Bem1p-GEF species. Both the implicit GDI and the Bem1p-GEF noise were retained in our model.

A subsequent study obtained a better-constrained value for the abundance of Cdc42p (1 μM) (Das et al., 2012), which we have adopted in the current model. In addition, we manually tuned some of the other parameters so that the model would reproduce three features extracted from imaging data: (i) the measured shape of the Cdc42p peak (peak width at half height, 1.9 μm (Layton et al., 2011)); (ii) Cdc42p dynamics in the peak (FRAP recovery half-time, 3.5 s (Slaughter et al., 2009)); and our estimate of the amount of Cdc42p in the peak (proportion of the total Cdc42p, 4.6%). All parameter values are listed in Table 3.

In our model we also made the GAP explicit, rather than implicit. The parameter-adjusted model was used to represent *rsr1* mutant cells, in which landmark proteins do not affect Cdc42p behavior. Unique to this study is the addition of the Rsr1p-GEF and the

Rga1p-GAP.

Previous work indicated that the Cdc42p-directed GEF, Cdc24p, was present in both cytoplasmic and local cortical pools that exchanged rapidly (Wedlich-Soldner et al., 2004). The cytoplasmic pool was in significant excess compared to the localized pool, which presumably represents the sum of Bem1p-bound and Rsr1p-bound GEF. Because the GEF is in excess, we assume here that Rsr1p- and Bem1p-bound pools of GEF are not in competition with each other. This allowed us to simplify the model, using only two GEF species (Rsr1p-GEF and Bem1p-GEF) and ignoring the excess cytoplasmic GEF. Bem1p-GEF behaves as in the previous models. The new Rsr1p-GEF is represented as an immobile GEF located at the sites demarcated by landmarks (a ring in haploids and two circular patches at the cell poles in diploids).

The localization of Rga1p at a circular patch at the cytokinesis site was determined experimentally (Tong et al., 2007). Thus, we modeled Rga1p-GAP as an immobile GAP located at that site. The Rsr1p-GEF and Rga1p-GAP activities were set as described below: there are no available data to constrain these values, except that the Rga1p-GAP must be strong enough to exclude polarization within the previous division site (Tong et al., 2007).

7.2.2 Model description

Molecular species:

- The Bem1p complex including GEF and PAK is modelled as a single entity that can exchange between cytoplasm (denoted BemGEFc) and membrane (BemGEF), subject

to Gaussian noise. BemGEF promotes conversion of GDP-Cdc42p to GTP-Cdc42p at the membrane.

- GDP-Cdc42 exchanges between membrane (Cdc42D) and cytoplasm (Cdc42Dc). In cells, this is assisted by the GDI, but we model the exchange as occurring without assistance for simplicity.
- GTP-Cdc42p is only present at the membrane, where it can bind the Bem1 complex to generate a new species (BemGEF42) with increased GEF activity.
- A GAP (generic and uniformly active, representing at least 4 distinct GAPs present in yeast) exchanges between membrane (GAP) and cytoplasm (GAPc). GAP promotes conversion of GTP-Cdc42p to GDP-Cdc42p at the membrane.

Positive Feedback:

- Binding of BemGEF to Cdc42T increases local GEF activity in regions with higher Cdc42T, generating more local Cdc42T via positive feedback.

Negative Feedback:

- BemGEF42 promotes the modification of nearby BemGEF42, generating BemGEF42*. Dissociation yields Cdc42T and BemGEF*.
- BemGEF* retains GEF activity, but is unable to rebind Cdc42T. Partitioning to the cytoplasm yields BemGEFc*.
- BemGEFc* is unable to re-associate with the membrane, and accumulates as an inert species, depleting the cellular pool of active GEF at the membrane. It reverts to the unmodified BemGEFc via a first-order reaction.

Spatial Cues:

Rsr1p-GEF and Rga1p-GAP are localized proteins with the following properties:

- Rsr1p-GEF (denoted RsrGEF) and Rga1p-GAP (RgaGAP) are immobile at the membrane, within pre-defined areas.
- RgaGAP (when present) is at twice the RsrGEF concentration.
- The GEF activity of RsrGEF is equal to that of BemGEF, but the total amount of RsrGEF is either 2.5% or 0.025% of the total BemGEF.
- The GAP activity of RsrGAP is equal to that of the generic GAP.

Diploid:

- Two circular RsrGEF patches, diameter 2.2 μm, are present at opposite ends of the simulated cell surface.
- A circular RgaGAP patch, diameter 2 μm, is centered within one of the RsrGEF patches.

Haploid:

- A hollow ring of RsrGEF is present, with inner diameter 2 μm and outer diameter 2.2 μm.
- A circular RgaGAP patch, diameter 2 μm, is located within the ring.

General:

- All species on the membrane have the same diffusion coefficient, apart from the non-diffusing RsrGEF and RgaGAP.

- The cytoplasm is well mixed, approximating fast diffusion.
- Cell size is constant.
- Proteins can interconvert between different forms (e.g. membrane versus cytoplasmic) but are neither made nor degraded. Thus, for proteins that exist in several forms, the total mass is conserved.

The dynamics of the species discussed above were modeled by solving the reaction diffusion equations below on a discretized square surface with periodic boundary conditions, generating a torus. This is a simplification of the true plasma membrane geometry (the surface of an ovoid). The equations governing the concentrations of all species are as follows:

$$\frac{\partial}{\partial t}Cdc42T = D_m\Delta Cdc42T + f_1Cdc42D - (f_2 + f_3)Cdc42T + k_{4b}(BemGEF42 + BemGEF42^*)$$

$$\frac{\partial}{\partial t}Cdc42D = D_m\Delta Cdc42D + f_2Cdc42T - f_1Cdc42D - k_{5b}Cdc42D + k_{5a}Cdc42Dc$$

$$\frac{\partial}{\partial t}Cdc42Dc = D_c\Delta Cdc42Dc + \eta(k_{5b}Cdc42D - k_{5a}Cdc42Dc)$$

$$\frac{\partial}{\partial t}BemGEF42 = D_m\Delta BemGEF42 + f_3Cdc42T - (k_{4b} + k_8BemGEF42)\cdot BemGEF42$$

$$\frac{\partial}{\partial t}BemGEF42^* = D_m\Delta BemGEF42^* + k_8BemGEF42\cdot BemGEF42 - k_{4b}BemGEF42^*$$

$$\frac{\partial}{\partial t}BemGEF = D_m\Delta BemGEF + f_4 + k_{4b}BemGEF42 - k_{4a}Cdc42T\cdot BemGEF - \sqrt{s}\xi(t)$$

$$\frac{\partial}{\partial t}BemGEFc = D_c\Delta BemGEFc + \eta\left(\sqrt{s}\xi(t) - f_4 - k_7Cdc42T\cdot BemGEFc\right) + k_9BemGEFc^*$$

$$\frac{\partial}{\partial t}BemGEF^* = D_m\Delta BemGEF^* + f_4^* + k_{4b}BemGEF42^*$$

$$\frac{\partial}{\partial t}BemGEFc^* = D_c\Delta BemGEFc^* - \eta(f_4^* + k_9BemGEFc^*)$$

$$\frac{\partial}{\partial t}GAP = D_m\Delta GAP + k_{1a}GAPc - k_{1b}GAP$$

$$\frac{\partial}{\partial t}GAPc = D_c\Delta GAPc + \eta(k_{1b}GAP - k_{1a}GAPc)$$

Where,

$$f_1 = k_{2a}(BemGEF + BemGEF^* + RsrGEF) + k_3(BemGEF42 + BemGEF42^*)$$
$$f_2 = k_{2b}(GAP + RgaGAP)$$
$$f_3 = k_{4a}BemGEF + k_7BemGEFc$$
$$f_4 = k_{1a}BemGEFc - k_{1b}BemGEF$$
$$f_4^* = k_{1a}BemGEFc^* - k_{1b}BemGEF^*$$

Table 3 Parameter values for modeling bud-site selection

Description	Parameter	Value	Units
BemGEFc → BemGEF BemGEFc* → BemGEF* GAPc → GAP	k_{1a}	10	s^{-1}
BemGEF → BemGEFc BemGEF* → BemGEFc* GAP → GAPc	k_{1b}	10	s^{-1}
BemGEF + Cdc42D → Cdc42T BemGEF* + Cdc42D → Cdc42T RsrGEF + Cdc42D → Cdc42T	k_{2a}	0.16	$\mu M^{-1}s^{-1}$
BemGEF42 + Cdc42D → Cdc42T BemGEF42* + Cdc42D → Cdc42T	k_3	0.35	$\mu M^{-1}s^{-1}$
GAP + Cdc42T → Cdc42D RgaGAP + Cdc42T → Cdc42D	k_{2b}	0.35	$\mu M^{-1}s^{-1}$
BemGEFc + Cdc42T → BemGEF42	k_7	10	$\mu M^{-1}s^{-1}$
BemGEF + Cdc42T → BemGEF42	k_{4a}	10	$\mu M^{-1}s^{-1}$
BemGEF42 → BemGEF + Cdc42T BemGEF42* → BemGEF* + Cdc42T	k_{4b}	10	s^{-1}
Cdc42Dc → Cdc42D	k_{5a}	36	s^{-1}
Cdc42D → Cdc42Dc	k_{5b}	0.65	s^{-1}
*BemGEF*42 + *BemGEF*42 → *BemGEF*42* + *BemGEF*42*	k_8	0.05	$\mu M^{-1}s^{-1}$
*BemGEFc** → *BemGEFc*	k_9	0.0022	s^{-1}
Diffusion coefficient on the membrane	D_m	0.0025	$\mu m^2 s^{-1}$
Total [Cdc42]		1	μM
Total [BemGEF]		0.068	μM
Total [GAP]		1	μM
Total [RsrGEF]		$[1.7x10^{-5}, 1.7x10^{-3}]$	μM
Total [RgaGAP]		$[3.4x10^{-5}, 3.4x10^{-3}]$	μM

References

Abo, A., Pick, E., Hall, A., Totty, N., Teahan, C.G., and Segal, A.W. (1991). Activation of the NADPH oxidase involves the small GTP-binding protein p21rac1. Nature *353*, 668-670.

Adamo, J.E., Moskow, J.J., Gladfelter, A.S., Viterbo, D., Lew, D.J., and Brennwald, P.J. (2001). Yeast Cdc42 functions at a late step in exocytosis, specifically during polarized growth of the emerging bud. The Journal of cell biology *155*, 581-592.

Adams, A.E.M., Johnson, D.I., Longnecker, R.M., Sloat, B.F., and Pringle, J.R. (1990). *CDC42* and *CDC43*, two additional genes involved in budding and the establishment of cell polarity in the yeast *Saccharomyces cerevisiae*. J Cell Biol *111*, 131-142.

Adams, A.E.M., and Pringle, J.R. (1984). Relationship of actin and tubulin distribution to bud growth in wild-type and morphogenetic-mutant *Saccharomyces cerevisiae*. J Cell Biol *98*, 934-945.

Allen, W.E., Zicha, D., Ridley, A.J., and Jones, G.E. (1998). A role for Cdc42 in macrophage chemotaxis. The Journal of cell biology *141*, 1147-1157.

Altschuler, S.J., Angenent, S.B., Wang, Y., and Wu, L.F. (2008). On the spontaneous emergence of cell polarity. Nature *454*, 886-889.

Ayscough, K.R., Eby, J.J., Lila, T., Dewar, H., Kozminski, K.G., and Drubin, D.G. (1999). Sla1p is a functionally modular component of the yeast cortical actin cytoskeleton required for correct localization of both Rho1p-GTPase and Sla2p, a protein with talin homology. Molecular biology of the cell *10*, 1061-1075.

Ayscough, K.R., Stryker, J., Pokala, N., Sanders, M., Crews, P., and Drubin, D.G. (1997). High rates of actin filament turnover in budding yeast and roles for actin in establishment and maintenance of cell polarity revealed using the actin inhibitor latrunculin-A. J Cell Biol *137*, 399-416.

Benard, V., Bohl, B.P., and Bokoch, G.M. (1999). Characterization of rac and cdc42 activation in chemoattractant-stimulated human neutrophils using a novel assay for active GTPases. The Journal of biological chemistry *274*, 13198-13204.

Bender, A. (1993). Genetic evidence for the roles of the bud-site-selection genes BUD5 and BUD2 in control of the Rsr1p (Bud1p) GTPase in yeast. Proceedings of the National Academy of Sciences of the United States of America *90*, 9926-9929.

Bender, A., and Pringle, J.R. (1989). Multicopy suppression of the cdc24 budding defect in yeast by CDC42 and three newly identified genes including the ras-related gene RSR1. Proc Natl Acad Sci USA *86*, 9976-9980.

Bender, A., and Pringle, J.R. (1991). Use of a screen for synthetic lethal and multicopy suppressee mutants to identify two new genes involved in morphogenesis in *Saccharomyces cerevisiae*. Mol Cell Biol *11*, 1295-1305.

Bender, L., Shuen Lo, H., Lee, H., Kokojan, V., Peterson, J., and Bender, A. (1996). Associations among PH and SH3 domain-containing proteins and Rho-type GTPases in yeast. J Cell Biol *133*, 879-894.

Bi, E., Chiavetta, J.B., Chen, H., Chen, G.C., Chan, C.S., and Pringle, J.R. (2000). Identification of novel, evolutionarily conserved Cdc42p-interacting proteins and of redundant pathways linking Cdc24p and Cdc42p to actin polarization in yeast. Molecular biology of the cell *11*, 773-793.

Bi, E., and Park, H.O. (2012). Cell polarization and cytokinesis in budding yeast. Genetics *191*, 347-387.

Bose, I., Irazoqui, J.E., Moskow, J.J., Bardes, E.S., Zyla, T.R., and Lew, D.J. (2001). Assembly of scaffold-mediated complexes containing Cdc42p, the exchange factor Cdc24p, and the effector Cla4p required for cell cycle-regulated phosphorylation of Cdc24p. The Journal of biological chemistry *276*, 7176-7186.

Boulter, E., Garcia-Mata, R., Guilluy, C., Dubash, A., Rossi, G., Brennwald, P.J., and Burridge, K. (2010). Regulation of Rho GTPase crosstalk, degradation and activity by RhoGDI1. Nature cell biology *12*, 477-483.

Brown, J.L., Jaquenoud, M., Gulli, M.P., Chant, J., and Peter, M. (1997). Novel Cdc42-binding proteins Gic1 and Gic2 control cell polarity in yeast. Genes Dev *11*, 2972-2982.

Carlton, P.M., Boulanger, J., Kervrann, C., Sibarita, J.B., Salamero, J., Gordon-Messer, S., Bressan, D., Haber, J.E., Haase, S., Shao, L.*, et al.* (2010). Fast live simultaneous multiwavelength four-dimensional optical microscopy. Proceedings of the National Academy of Sciences of the United States of America *107*, 16016-16022.

Castellano, F., Montcourrier, P., Guillemot, J.C., Gouin, E., Machesky, L., Cossart, P., and Chavrier, P. (1999). Inducible recruitment of Cdc42 or WASP to a cell-surface receptor triggers actin polymerization and filopodium formation. Curr Biol *9*, 351-360.

Caviston, J.P., Tcheperegine, S.E., and Bi, E. (2002). Singularity in budding: a role for the evolutionarily conserved small GTPase Cdc42p. Proceedings of the National Academy of Sciences of the United States of America *99*, 12185-12190.

Chant, J., Corrado, K., Pringle, J.R., and Herskowitz, I. (1991). Yeast BUD5, encoding a putative GDP-GTP exchange factor, is necessary for bud site selection and interacts with bud formation gene BEM1. Cell *65*, 1213-1224.

Chant, J., and Herskowitz, I. (1991). Genetic control of bud site selection in yeast by a set of gene products that constitute a morphogenetic pathway. Cell *65*, 1203-1212.

Chant, J., and Pringle, J.R. (1995). Patterns of bud-site selection in the yeast *Saccharomyces cerevisiae*. J Cell Biol *129*, 751-765.

Chen, G.C., Kim, Y.J., and Chan, C.S. (1997). The Cdc42 GTPase-associated proteins Gic1 and Gic2 are required for polarized cell growth in Saccharomyces cerevisiae. Genes Dev *11*, 2958-2971.

Chen, H., Kuo, C.C., Kang, H., Howell, A.S., Zyla, T.R., Jin, M., and Lew, D.J. (2012). Cdc42p regulation of the yeast formin Bni1p mediated by the effector Gic2p. Molecular biology of the cell *23*, 3814-3826.

Cheong, R., and Levchenko, A. (2010). Oscillatory signaling processes: the how, the why and the where. Curr Opin Genet Dev *20*, 665-669.

Cid, V.J., Adamikova, L., Sanchez, M., Molina, M., and Nombela, C. (2001). Cell cycle control of septin ring dynamics in the budding yeast. Microbiology *147*, 1437-1450.

Cvrckova, F., De Virgilio, C., Manser, E., Pringle, J.R., and Nasmyth, K. (1995). Ste20-like protein kinases are required for normal localization of cell growth and for cytokinesis in budding yeast. Genes Dev *9*, 1817-1830.

Devreotes, P.N., and Zigmond, S.H. (1988). Chemotaxis in eukaryotic cells: a focus on leukocytes and Dictyostelium. Annual review of cell biology *4*, 649-686.

Di-Poi, N., Faure, J., Grizot, S., Molnar, G., Pick, E., and Dagher, M.C. (2001). Mechanism of NADPH oxidase activation by the Rac/Rho-GDI complex. Biochemistry *40*, 10014-10022.

Dobbelaere, J., Gentry, M.S., Hallberg, R.L., and Barral, Y. (2003). Phosphorylation-Dependent Regulation of Septin Dynamics during the Cell Cycle. Developmental cell *4*, 345-357.

Endo, M., Shirouzu, M., and Yokoyama, S. (2003). The Cdc42 binding and scaffolding activities of the fission yeast adaptor protein Scd2. The Journal of biological chemistry *278*, 843-852.

Engqvist-Goldstein, A.E., and Drubin, D.G. (2003). Actin assembly and endocytosis: from yeast to mammals. Annu Rev Cell Dev Biol *19*, 287-332.

Etienne-Manneville, S. (2004). Cdc42 - the centre of polarity. Journal of cell science *117*, 1291-1300.

Etienne-Manneville, S., and Hall, A. (2002). Rho GTPases in cell biology. Nature *420*, 629-635.

Etienne-Manneville, S., and Hall, A. (2003). Cell polarity: Par6, aPKC and cytoskeletal crosstalk. Current opinion in cell biology *15*, 67-72.

Feijo, J.A., Sainhas, J., Holdaway-Clarke, T., Cordeiro, M.S., Kunkel, J.G., and Hepler, P.K. (2001). Cellular oscillations and the regulation of growth: the pollen tube paradigm. Bioessays *23*, 86-94.

Feng, Q., Albeck, J.G., Cerione, R.A., and Yang, W. (2002). Regulation of the Cool/Pix proteins: key binding partners of the Cdc42/Rac targets, the p21-activated kinases. The Journal of biological chemistry *277*, 5644-5650.

Finger, F.P., and Novick, P. (1998). Spatial regulation of exocytosis: lessons from yeast. The Journal of cell biology *142*, 609-612.

Freisinger, T., Klunder, B., Johnson, J., Muller, N., Pichler, G., Beck, G., Costanzo, M., Boone, C., Cerione, R.A., Frey, E.*, et al.* (2013). Establishment of a robust single axis of cell polarity by coupling multiple positive feedback loops. Nat Commun *4*, 1807.

Fukumoto, Y., Kaibuchi, K., Hori, Y., Fujioka, H., Araki, S., Ueda, T., Kikuchi, A., and Takai, Y. (1990). Molecular cloning and characterization of a novel type of regulatory protein (GDI) for the rho proteins, ras p21-like small GTP-binding proteins. Oncogene *5*, 1321-1328.

Garcia-Mata, R., Boulter, E., and Burridge, K. (2011). The 'invisible hand': regulation of RHO GTPases by RHOGDIs. Nat Rev Mol Cell Biol *12*, 493-504.

Garrard, S.M., Capaldo, C.T., Gao, L., Rosen, M.K., Macara, I.G., and Tomchick, D.R. (2003). Structure of Cdc42 in a complex with the GTPase-binding domain of the cell polarity protein, Par6. The EMBO journal *22*, 1125-1133.

Gierer, A., and Meinhardt, H. (1972). A theory of biological pattern formation. Kybernetik *12*, 30-39.

Gladfelter, A.S., Bose, I., Zyla, T.R., Bardes, E.S., and Lew, D.J. (2002). Septin ring assembly involves cycles of GTP loading and hydrolysis by Cdc42p. The Journal of cell biology *156*, 315-326.

Gladfelter, A.S., Pringle, J.R., and Lew, D.J. (2001). The septin cortex at the yeast mother-bud neck. Curr Opin Microbiol *4*, 681-689.

Goryachev, A.B., and Pokhilko, A.V. (2008). Dynamics of Cdc42 network embodies a Turing-type mechanism of yeast cell polarity. FEBS letters *582*, 1437-1443.

Gotta, M., Abraham, M.C., and Ahringer, J. (2001). CDC-42 controls early cell polarity and spindle orientation in C. elegans. Curr Biol *11*, 482-488.

Grill, S.W., Gonczy, P., Stelzer, E.H., and Hyman, A.A. (2001). Polarity controls forces governing asymmetric spindle positioning in the Caenorhabditis elegans embryo. Nature *409*, 630-633.

Gulli, M.P., Jaquenoud, M., Shimada, Y., Niederhauser, G., Wiget, P., and Peter, M. (2000). Phosphorylation of the Cdc42 exchange factor Cdc24 by the PAK-like kinase Cla4 may regulate polarized growth in yeast. Mol Cell *6*, 1155-1167.

Hall, A. (1998). Rho GTPases and the actin cytoskeleton. Science (New York, NY *279*, 509-514.

Halme, A., Michelitch, M., Mitchell, E.L., and Chant, J. (1996). Bud10p directs axial cell polarization in budding yeast and resembles a transmembrane receptor. Curr Biol *6*, 570-579.

Hancock, J.F., and Hall, A. (1993). A novel role for RhoGDI as an inhibitor of GAP proteins. The EMBO journal *12*, 1915-1921.

Harkins, H.A., Page, N., Schenkman, L.R., De Virgilio, C., Shaw, S., Bussey, H., and Pringle, J.R. (2001). Bud8p and Bud9p, proteins that may mark the sites for bipolar budding in yeast. Molecular biology of the cell *12*, 2497-2518.

Hart, M.J., Maru, Y., Leonard, D., Witte, O.N., Evans, T., and Cerione, R.A. (1992). A GDP dissociation inhibitor that serves as a GTPase inhibitor for the Ras-like protein CDC42Hs. Science (New York, NY *258*, 812-815.

Hartwell, L., and Unger, M. (1977). Unequal division in *Saccharomyces cerevisiae* and its implications for the control of cell division. J Cell Biol *75*, 422-435.

Hartwell, L.H., Culotti, J., Pringle, J.R., and Reid, B.J. (1974). Genetic control of the cell division cycle in yeast. Science (New York, NY *183*, 46-51.

Hawkins, P.T., Anderson, K.E., Davidson, K., and Stephens, L.R. (2006). Signalling through Class I PI3Ks in mammalian cells. Biochem Soc Trans *34*, 647-662.

Hepler, P.K., Vidali, L., and Cheung, A.Y. (2001). Polarized cell growth in higher plants. Annu Rev Cell Dev Biol *17*, 159-187.

Holly, S.P., and Blumer, K.J. (1999). PAK-Family Kinases Regulate Cell and Actin Polarization throughout the Cell Cycle of Saccharomyces cerevisiae. The Journal of cell biology *147*, 845-856.

Howell, A.S., Savage, N.S., Johnson, S.A., Bose, I., Wagner, A.W., Zyla, T.R., Nijhout, H.F., Reed, M.C., Goryachev, A.B., and Lew, D.J. (2009). Singularity in polarization: rewiring yeast cells to make two buds. Cell *139*, 731-743.

Hung, T.J., and Kemphues, K.J. (1999). PAR-6 is a conserved PDZ domain-containing protein that colocalizes with PAR-3 in Caenorhabditis elegans embryos. Development (Cambridge, England) *126*, 127-135.

Iglesias, P.A., and Devreotes, P.N. (2008). Navigating through models of chemotaxis. Current opinion in cell biology *20*, 35-40.

Irazoqui, J.E., Gladfelter, A.S., and Lew, D.J. (2003). Scaffold-mediated symmetry breaking by Cdc42p. Nature cell biology *5*, 1062-1070.

Irazoqui, J.E., Howell, A.S., Theesfeld, C.L., and Lew, D.J. (2005). Opposing roles for actin in Cdc42p polarization. Molecular biology of the cell *16*, 1296-1304.

Ito, T., Matsui, Y., Ago, T., Ota, K., and Sumimoto, H. (2001). Novel modular domain PB1 recognizes PC motif to mediate functional protein-protein interactions. The EMBO journal *20*, 3938-3946.

Iwase, M., Luo, J., Nagaraj, S., Longtine, M., Kim, H.B., Haarer, B.K., Caruso, C., Tong, Z., Pringle, J.R., and Bi, E. (2006). Role of a Cdc42p effector pathway in recruitment of the yeast septins to the presumptive bud site. Molecular biology of the cell *17*, 1110-1125.

Johnson, J.L., Erickson, J.W., and Cerione, R.A. (2009). New insights into how the Rho guanine nucleotide dissociation inhibitor regulates the interaction of Cdc42 with membranes. The Journal of biological chemistry *284*, 23860-23871.

Johnston, G.C., Prendergast, J.A., and Singer, R.A. (1991). The Saccharomyces cerevisiae MYO2 gene encodes an essential myosin for vectorial transport of vesicles. The Journal of cell biology *113*, 539-551.

Johnston, G.C., Pringle, J.P., and Hartwell, L.H. (1977). Coordination of growth with cell division in the yeast *S. cerevisiae*. Exp Cell Res *105*, 75-98.

Kaksonen, M., Sun, Y., and Drubin, D.G. (2003). A pathway for association of receptors, adaptors, and actin during endocytic internalization. Cell *115*, 475-487.

Kang, P.J., Angerman, E., Nakashima, K., Pringle, J.R., and Park, H.O. (2004). Interactions among Rax1p, Rax2p, Bud8p, and Bud9p in marking cortical sites for bipolar bud-site selection in yeast. Molecular biology of the cell *15*, 5145-5157.

Kay, A.J., and Hunter, C.P. (2001). CDC-42 regulates PAR protein localization and function to control cellular and embryonic polarity in C. elegans. Curr Biol *11*, 474-481.

Kilmartin, J.V., and Adams, A.E.M. (1984). Structural rearrangements of tubulin and actin during the cell cycle of the yeast *Saccharomyces*. J Cell Biol *98*, 922-933.

Kim, H.B., Haarer, B.K., and Pringle, J.R. (1991). Cellular morphogenesis in the *Saccharomyces cerevisiae* cell cycle: localization of the *CDC3* gene product and the timing of events at the budding site. J Cell Biol *112*, 535-544.

Knaus, M., Pelli-Gulli, M.P., van Drogen, F., Springer, S., Jaquenoud, M., and Peter, M. (2007). Phosphorylation of Bem2p and Bem3p may contribute to local activation of Cdc42p at bud emergence. The EMBO journal *26*, 4501-4513.

Kozminski, K.G., Beven, L., Angerman, E., Tong, A.H., Boone, C., and Park, H.O. (2003). Interaction between a Ras and a Rho GTPase couples selection of a growth site to the development of cell polarity in yeast. Molecular biology of the cell *14*, 4958-4970.

Kozubowski, L., Larson, J.R., and Tatchell, K. (2005). Role of the septin ring in the asymmetric localization of proteins at the mother-bud neck in Saccharomyces cerevisiae. Molecular biology of the cell *16*, 3455-3466.

Kozubowski, L., Saito, K., Johnson, J.M., Howell, A.S., Zyla, T.R., and Lew, D.J. (2008). Symmetry-Breaking Polarization Driven by a Cdc42p GEF-PAK Complex. Curr Biol *18*, 1719-1726.

Layton, A.T., Savage, N.S., Howell, A.S., Carroll, S.Y., Drubin, D.G., and Lew, D.J. (2011). Modeling vesicle traffic reveals unexpected consequences for Cdc42p-mediated polarity establishment. Curr Biol *21*, 184-194.

Leonard, D., Hart, M.J., Platko, J.V., Eva, A., Henzel, W., Evans, T., and Cerione, R.A. (1992). The identification and characterization of a GDP-dissociation inhibitor (GDI) for the CDC42Hs protein. The Journal of biological chemistry *267*, 22860-22868.

Lew, D.J., and Reed, S.I. (1993). Morphogenesis in the yeast cell cycle: regulation by Cdc28 and cyclins. J Cell Biol *120*, 1305-1320.

Lillie, S.H., and Brown, S.S. (1994). Immunofluorescence localization of the unconventional myosin, Myo2p, and the putative kinesin-related protein, Smy1p, to the same regions of polarized growth in *Saccharomyces cerevisiae*. J Cell Biol *125*, 825-842.

Lin, Q., Fuji, R.N., Yang, W., and Cerione, R.A. (2003). RhoGDI is required for Cdc42-mediated cellular transformation. Curr Biol *13*, 1469-1479.

Lin, R., Bagrodia, S., Cerione, R., and Manor, D. (1997). A novel Cdc42Hs mutant induces cellular transformation. Curr Biol *7*, 794-797.

Louvion, J.F., Havaux-Copf, B., and Picard, D. (1993). Fusion of GAL4-VP16 to a steroid-binding domain provides a tool for gratuitous induction of galactose-responsive genes in yeast. Gene *131*, 129-134.

Marco, E., Wedlich-Soldner, R., Li, R., Altschuler, S.J., and Wu, L.F. (2007). Endocytosis optimizes the dynamic localization of membrane proteins that regulate cortical polarity. Cell *129*, 411-422.

Marquitz, A.R., Harrison, J.C., Bose, I., Zyla, T.R., McMillan, J.N., and Lew, D.J. (2002). The Rho-GAP Bem2p plays a GAP-independent role in the morphogenesis checkpoint. The EMBO journal *21*, 4012-4025.

Masuda, T., Tanaka, K., Nonaka, H., Yamochi, W., Maeda, A., and Takai, Y. (1994). Molecular cloning and characterization of yeast rho GDP dissociation inhibitor. The Journal of biological chemistry *269*, 19713-19718.

Matsui, Y., Matsui, R., Akada, R., and Toh-e, A. (1996). Yeast src homology region 3 domain-binding proteins involved in bud formation. The Journal of cell biology *133*, 865-878.

McMurray, M.A., and Thorner, J. (2009). Septins: molecular partitioning and the generation of cellular asymmetry. Cell Div *4*, 18.

Miura, Y., Kikuchi, A., Musha, T., Kuroda, S., Yaku, H., Sasaki, T., and Takai, Y. (1993). Regulation of morphology by rho p21 and its inhibitory GDP/GTP exchange protein (rho GDI) in Swiss 3T3 cells. The Journal of biological chemistry *268*, 510-515.

Mulholland, J., Wesp, A., Riezman, H., and Botstein, D. (1997). Yeast actin cytoskeleton mutants accumulate a new class of Golgi-derived secretary vesicle. Molecular biology of the cell *8*, 1481-1499.

Munemitsu, S., Innis, M.A., Clark, R., McCormick, F., Ullrich, A., and Polakis, P. (1990). Molecular cloning and expression of a G25K cDNA, the human homolog of the yeast cell cycle gene CDC42. Molecular and cellular biology *10*, 5977-5982.

Nern, A., and Arkowitz, R.A. (2000). Nucleocytoplasmic shuttling of the Cdc42p exchange factor Cdc24p. The Journal of cell biology *148*, 1115-1122.

Nobes, C.D., and Hall, A. (1999). Rho GTPases control polarity, protrusion, and adhesion during cell movement. The Journal of cell biology *144*, 1235-1244.

Nomanbhoy, T.K., and Cerione, R. (1996). Characterization of the interaction between RhoGDI and Cdc42Hs using fluorescence spectroscopy. The Journal of biological chemistry *271*, 10004-10009.

Nomanbhoy, T.K., Erickson, J.W., and Cerione, R.A. (1999). Kinetics of Cdc42 membrane extraction by Rho-GDI monitored by real-time fluorescence resonance energy transfer. Biochemistry *38*, 1744-1750.

Novak, B., and Tyson, J.J. (2008). Design principles of biochemical oscillators. Nat Rev Mol Cell Biol *9*, 981-991.

Novick, P., and Botstein, D. (1985). Phenotypic analysis of temperature-sensitive yeast actin mutants. Cell *40*, 405-416.

Oh, Y., and Bi, E. (2011). Septin structure and function in yeast and beyond. Trends Cell Biol *21*, 141-148.

Onsum, M.D., and Rao, C.V. (2009). Calling heads from tails: the role of mathematical modeling in understanding cell polarization. Current opinion in cell biology *21*, 74-81.

Ozbudak, E.M., Becskei, A., and van Oudenaarden, A. (2005). A System of Counteracting Feedback Loops Regulates Cdc42p Activity during Spontaneous Cell Polarization. Developmental cell *9*, 565-571.

Parent, C.A., and Devreotes, P.N. (1999). A cell's sense of direction. Science (New York, NY *284*, 765-770.

Park, H.O., and Bi, E. (2007). Central roles of small GTPases in the development of cell polarity in yeast and beyond. Microbiol Mol Biol Rev *71*, 48-96.

Park, H.O., Bi, E., Pringle, J.R., and Herskowitz, I. (1997). Two active states of the Ras-related Bud1/Rsr1 protein bind to different effectors to determine yeast cell polarity. Proceedings of the National Academy of Sciences of the United States of America *94*, 4463-4468.

Park, H.O., Chant, J., and Herskowitz, I. (1993). BUD2 encodes a GTPase-activating protein for Bud1/Rsr1 necessary for proper bud-site selection in yeast. Nature *365*, 269-274.

Peter, M., Neiman, A.M., Park, H.-O., van Lohuizen, M., and Herskowitz, I. (1996). Functional analysis of the interaction between the small GTP binding protein Cdc42 and the Ste20 protein kinase in yeast. EMBO J *15*, 7046-7059.

Peterson, J., Zheng, Y., Bender, L., Myers, A., Cerione, R., and Bender, A. (1994). Interactions between the bud emergence proteins Bem1p and Bem2p and Rho- type GTPases in yeast. The Journal of cell biology *127*, 1395-1406.

Pollard, T.D., and Borisy, G.G. (2003). Cellular motility driven by assembly and disassembly of actin filaments. Cell *112*, 453-465.

Postma, M., Roelofs, J., Goedhart, J., Gadella, T.W., Visser, A.J., and Van Haastert, P.J. (2003). Uniform cAMP stimulation of Dictyostelium cells induces localized patches of signal transduction and pseudopodia. Molecular biology of the cell *14*, 5019-5027.

Pruyne, D., Legesse-Miller, A., Gao, L., Dong, Y., and Bretscher, A. (2004). Mechanisms of polarized growth and organelle segregation in yeast. Annu Rev Cell Dev Biol *20*, 559-591.

Pruyne, D.W., Schott, D.H., and Bretscher, A. (1998). Tropomyosin-containing actin cables direct the Myo2p-dependent polarized delivery of secretory vesicles in budding yeast [In Process Citation]. The Journal of cell biology *143*, 1931-1945.

Richman, T.J., and Johnson, D.I. (2000). Saccharomyces cerevisiae cdc42p GTPase is involved in preventing the recurrence of bud emergence during the cell cycle [In Process Citation]. Molecular and cellular biology *20*, 8548-8559.

Richman, T.J., Sawyer, M.M., and Johnson, D.I. (2002). Saccharomyces cerevisiae Cdc42p localizes to cellular membranes and clusters at sites of polarized growth. Eukaryot Cell *1*, 458-468.

Rocks, O., Peyker, A., Kahms, M., Verveer, P.J., Koerner, C., Lumbierres, M., Kuhlmann, J., Waldmann, H., Wittinghofer, A., and Bastiaens, P.I. (2005). An acylation cycle regulates localization and activity of palmitoylated Ras isoforms. Science (New York, NY *307*, 1746-1752.

Savage, N.S., Layton, A.T., and Lew, D.J. (2012). Mechanistic mathematical model of polarity in yeast. Molecular biology of the cell *23*, 1998-2013.

Schiller, M.R., Chakrabarti, K., King, G.F., Schiller, N.I., Eipper, B.A., and Maciejewski, M.W. (2006). Regulation of RhoGEF activity by intramolecular and intermolecular SH3 domain interactions. The Journal of biological chemistry *281*, 18774-18786.

Schott, D., Ho, J., Pruyne, D., and Bretscher, A. (1999). The COOH-Terminal Domain of Myo2p, a Yeast Myosin V, Has a Direct Role in Secretory Vesicle Targeting. The Journal of cell biology *147*, 791-808.

Servant, G., Weiner, O.D., Herzmark, P., Balla, T., Sedat, J.W., and Bourne, H.R. (2000). Polarization of chemoattractant receptor signaling during neutrophil chemotaxis. Science (New York, NY *287*, 1037-1040.

Shimada, Y., Gulli, M.P., and Peter, M. (2000). Nuclear sequestration of the exchange factor Cdc24 by Far1 regulates cell polarity during yeast mating. Nature cell biology *2*, 117-124.

Shinjo, K., Koland, J.G., Hart, M.J., Narasimhan, V., Johnson, D.I., Evans, T., and Cerione, R.A. (1990). Molecular cloning of the gene for the human placental GTP-binding protein Gp (G25K): identification of this GTP-binding protein as the human homolog of the yeast cell-division-cycle protein CDC42. Proceedings of the National Academy of Sciences of the United States of America *87*, 9853-9857.

Slaughter, B.D., Das, A., Schwartz, J.W., Rubinstein, B., and Li, R. (2009a). Dual modes of cdc42 recycling fine-tune polarized morphogenesis. Developmental cell *17*, 823-835.

Slaughter, B.D., Smith, S.E., and Li, R. (2009b). Symmetry breaking in the life cycle of the budding yeast. Cold Spring Harb Perspect Biol *1*, a003384.

Slaughter, B.D., Unruh, J.R., Das, A., Smith, S.E., Rubinstein, B., and Li, R. (2013). Non-uniform membrane diffusion enables steady-state cell polarization via vesicular trafficking. Nat Commun *4*, 1380.

Sloat, B.F., Adams, A.E.M., and Pringle, J.R. (1981). Roles of the *CDC24* gene product in cellular morphogenesis during the *Saccharomyces cerevisiae* cell cycle. J Cell Biol *89*, 395-405.

Sloat, B.F., and Pringle, J.R. (1978). A mutant of yeast defective in cellular morphogenesis. Science (New York, NY *200*, 1171-1173.

Smith, G.R., Givan, S.A., Cullen, P., and Sprague, G.F., Jr. (2002). GTPase-activating proteins for Cdc42. Eukaryot Cell *1*, 469-480.

Smith, S.E., Rubinstein, B., Mendes Pinto, I., Slaughter, B.D., Unruh, J.R., and Li, R. (2013). Independence of symmetry breaking on Bem1-mediated autocatalytic activation of Cdc42. The Journal of cell biology *202*, 1091-1106.

Sorek, N., Poraty, L., Sternberg, H., Bar, E., Lewinsohn, E., and Yalovsky, S. (2007). Activation status-coupled transient S acylation determines membrane partitioning of a plant Rho-related GTPase. Molecular and cellular biology *27*, 2144-2154.

Sorek, N., Segev, O., Gutman, O., Bar, E., Richter, S., Poraty, L., Hirsch, J.A., Henis, Y.I., Lewinsohn, E., Jurgens, G.*, et al.* (2010). An S-acylation switch of conserved G

domain cysteines is required for polarity signaling by ROP GTPases. Curr Biol *20*, 914-920.

Srinivasan, S., Wang, F., Glavas, S., Ott, A., Hofmann, F., Aktories, K., Kalman, D., and Bourne, H.R. (2003). Rac and Cdc42 play distinct roles in regulating PI(3,4,5)P3 and polarity during neutrophil chemotaxis. The Journal of cell biology *160*, 375-385.

Stevenson, B.J., Ferguson, B., De Virgilio, C., Bi, E., Pringle, J.R., Ammerer, G., and Sprague, G.F., Jr. (1995). Mutation of *RGA1*, which encodes a putative GTPase-activating protein for the polarity-establishment protein Cdc42p, activates the pheromone- response pathway in the yeast *Saccharomyces cerevisiae*. Genes Dev *9*, 2949-2963.

Takahashi, S., and Pryciak, P.M. (2008). Membrane localization of scaffold proteins promotes graded signaling in the yeast MAP kinase cascade. Curr Biol *18*, 1184-1191.

Takaishi, K., Kikuchi, A., Kuroda, S., Kotani, K., Sasaki, T., and Takai, Y. (1993). Involvement of rho p21 and its inhibitory GDP/GTP exchange protein (rho GDI) in cell motility. Molecular and cellular biology *13*, 72-79.

Takizawa, P.A., DeRisi, J.L., Wilhelm, J.E., and Vale, R.D. (2000). Plasma membrane compartmentalization in yeast by messenger RNA transport and a septin diffusion barrier. Science (New York, NY *290*, 341-344.

Tolias, K.F., Couvillon, A.D., Cantley, L.C., and Carpenter, C.L. (1998). Characterization of a Rac1- and RhoGDI-associated lipid kinase signaling complex. Molecular and cellular biology *18*, 762-770.

Tong, Z., Gao, X.D., Howell, A.S., Bose, I., Lew, D.J., and Bi, E. (2007). Adjacent positioning of cellular structures enabled by a Cdc42 GTPase-activating protein-mediated zone of inhibition. The Journal of cell biology *179*, 1375-1384.

Turing, A. (1952). The Chemical Basis of Morphogenesis. Philos Trans R Soc Lond B Biol Sci *237*, 37-72.

Ueda, T., Kikuchi, A., Ohga, N., Yamamoto, J., and Takai, Y. (1990). Purification and characterization from bovine brain cytosol of a novel regulatory protein inhibiting the dissociation of GDP from and the subsequent binding of GTP to rhoB p20, a ras p21-like GTP-binding protein. The Journal of biological chemistry *265*, 9373-9380.

Valdez-Taubas, J., and Pelham, H.R. (2003). Slow diffusion of proteins in the yeast plasma membrane allows polarity to be maintained by endocytic cycling. Curr Biol *13*, 1636-1640.

Versele, M., and Thorner, J. (2004). Septin collar formation in budding yeast requires GTP binding and direct phosphorylation by the PAK, Cla4. The Journal of cell biology *164*, 701-715.

Walch-Solimena, C., Collins, R.N., and Novick, P.J. (1997). Sec2p mediates nucleotide exchange on Sec4p and is involved in polarized delivery of post-Golgi vesicles. The Journal of cell biology *137*, 1495-1509.

Wang, F., Herzmark, P., Weiner, O.D., Srinivasan, S., Servant, G., and Bourne, H.R. (2002). Lipid products of PI(3)Ks maintain persistent cell polarity and directed motility in neutrophils. Nat Cell Biol *4*, 513-518.

Wedlich-Soldner, R., Altschuler, S., Wu, L., and Li, R. (2003). Spontaneous cell polarization through actomyosin-based delivery of the Cdc42 GTPase. Science (New York, NY *299*, 1231-1235.

Wedlich-Soldner, R., and Li, R. (2003). Spontaneous cell polarization: undermining determinism. Nature cell biology *5*, 267-270.

Wedlich-Soldner, R., Wai, S.C., Schmidt, T., and Li, R. (2004). Robust cell polarity is a dynamic state established by coupling transport and GTPase signaling. The Journal of cell biology *166*, 889-900.

Weiner, O.D., Neilsen, P.O., Prestwich, G.D., Kirschner, M.W., Cantley, L.C., and Bourne, H.R. (2002). A PtdInsP(3)- and Rho GTPase-mediated positive feedback loop regulates neutrophil polarity. Nature cell biology *4*, 509-513.

Weiss, E.L., Bishop, A.C., Shokat, K.M., and Drubin, D.G. (2000). Chemical genetic analysis of the budding-yeast p21-activated kinase Cla4p. Nat Cell Biol *2*, 677-685.

Winters, M.J., and Pryciak, P.M. (2005). Interaction with the SH3 domain protein Bem1 regulates signaling by the Saccharomyces cerevisiae p21-activated kinase Ste20. Molecular and cellular biology *25*, 2177-2190.

Yamaguchi, Y., Ota, K., and Ito, T. (2007). A novel Cdc42-interacting domain of the yeast polarity establishment protein Bem1. Implications for modulation of mating pheromone signaling. The Journal of biological chemistry *282*, 29-38.

Yamamoto, T., Mochida, J., Kadota, J., Takeda, M., Bi, E., and Tanaka, K. (2010). Initial polarized bud growth by endocytic recycling in the absence of actin cable-dependent vesicle transport in yeast. Molecular biology of the cell *21*, 1237-1252.

Yan, A., Xu, G., and Yang, Z.B. (2009). Calcium participates in feedback regulation of the oscillating ROP1 Rho GTPase in pollen tubes. Proceedings of the National Academy of Sciences of the United States of America *106*, 22002-22007.

Zahner, J.E., Harkins, H.A., and Pringle, J.R. (1996). Genetic analysis of the bipolar pattern of bud site selection in the yeast Saccharomyces cerevisiae. Molecular and cellular biology *16*, 1857-1870.

Zheng, Y., Bender, A., and Cerione, R.A. (1995). Interactions among proteins involved in bud-site selection and bud-site assembly in Saccharomyces cerevisiae. The Journal of biological chemistry *270*, 626-630.

Zheng, Y., Cerione, R., and Bender, A. (1994). Control of the yeast bud-site assembly GTPase Cdc42. Catalysis of guanine nucleotide exchange by Cdc24 and stimulation of GTPase activity by Bem3. The Journal of biological chemistry *269*, 2369-2372.

Ziman, M., Chuang, J.S., and Schekman, R.W. (1996). Chs1p and Chs3p, two proteins involved in chitin synthesis, populate a compartment of the Saccharomyces cerevisiae endocytic pathway. Molecular biology of the cell *7*, 1909-1919.

Ziman, M., and Johnson, D.I. (1994). Genetic evidence for a functional interaction between *Saccharomyces cerevisiae CDC24* and *CDC42*. Yeast (Chichester, England) *10*, 463-474.

Ziman, M., O'Brien, J.M., Ouellette, L.A., Church, W.R., and Johnson, D.I. (1991). Mutational analysis of *CDC42*Sc, a *Saccharomyces cerevisiae* gene that encodes a putative GTP-binding protein involved in the control of cell polarity. Mol Cell Biol *11*, 3537-3544.

Ziman, M., Preuss, D., Mulholland, J., O'Brien, J.M., Botstein, D., and Johnson, D.I. (1993). Subcellular localization of Cdc42p, a *Saccharomyces cerevisiae* GTP- binding protein involved in the control of cell polarity. Molecular biology of the cell *4*, 1307-1316.

Biography

Chi-Fang Wu

Born on June 10, 1982 in Tainan, Taiwan

Education:

Ph.D. Genetics and Genomics, Duke University, 2013

M.S. Pharmaceutical Sciences, National Yang Ming University, Taipei, Taiwan, 2006

B.S. Biological Sciences, National Chiao Tung University, Hsinchu, Taiwan, 2004

Honors:

- Fitzgerald Academic Achievement Award, Department of Pharmacology and Cancer Biology, Duke University, 2013
- Duke University Graduate School Travel Fellowship, 2010, 2011, 2012
- Poster Award, Departmental Retreat of Pharmacology and Cancer Biology, Duke University, 2008
- Poster Award, 21st Joint Annual Conference of Biomedical Sciences, Taipei, 2006
- Scholarship of Student Exchange Program, National Chiao Tung University, 2003-2004

Publications:

- **Chi-Fang Wu**, Natasha S. Savage, and Daniel J. Lew. Interaction between bud-site-selection and polarity-establishment machineries in budding yeast. (2013) *Phil. Trans. R. Soc. B* 368(1629):20130006.
- Benjamin D. Atkins, Satoshi Yoshida, Koji Saito, **Chi-Fang Wu**, Daniel J. Lew, David Pellman. Inhibition of Cdc42 during mitotic exit is required for cytokinesis. (2013) *J. Cell Biol.* 202(2):231-40.
- **Chi-Fang Wu** and Daniel J. Lew. (2013) Beyond symmetry-breaking: competition and negative feedback in GTPase regulation. *Trends Cell Biol.* 23(10):476-83.
- Audrey S. Howell*, Meng Jin*, **Chi-Fang Wu***, Trevin R. Zyla, Timothy C. Elston, and Daniel J. Lew. (2012) Negative Feedback Enhances Robustness in the Yeast Polarity Establishment Circuit. *Cell* 149(2):322-333. * co-first authors
- Yi-Ching Hsieh, Pei-Jung Tu, Ying-Yuan Lee, Chun-Chen Kuo, Yi-Chien Lin, **Chi-Fang Wu**, Jing-Jer Lin (2007) The U3 small nucleolar ribonucleoprotein component Imp4p is a novel telomere-associated protein. *Biochem. J.*,408(3):387-393.